AD-A162 257 PASSIVELY DAMPED JOINTS FOR ADVANCED SPACE STRUCTURES 1/2
(U) MCDONNELL DOUGLAS ASTRONAUTICS CO-HB HUNTINGTON
BEACH CA R W TRUDELL ET AL. 30 JUN 84 MDC-H1178
UNCLASSIFIED AFOSR-TR-85-1078 F49620-83-C-0117 F/G 13/5 NL

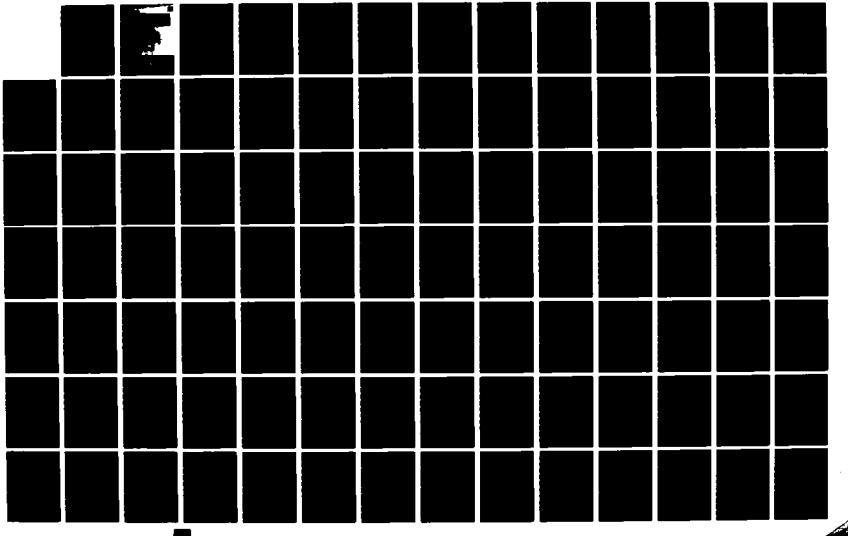

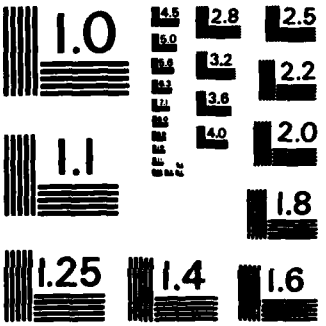

MICROCOPY RESOLUTION TEST CHART
NATIONAL BUREAU OF STANDARDS - 1963 - A

(2)

PASSIVELY DAMPED JOINTS FOR ADVANCED SPACE STRUCTURES

ANNUAL TECHNICAL REPORT

June 1984

MDC H1178

MCDONNELL DOUGLAS ASTRONAUTICS COMPANY

MCDONNELL DOUGLAS CORPORATION

PASSIVELY DAMPED JOINTS FOR ADVANCED SPACE STRUCTURES

ANNUAL TECHNICAL REPORT

June 1984

MDC H1178

Prepared by

R. W. Trudell
C. E. Blevins

Approved by:

G. E. Kahre, Branch Chief
Vibration, Shock & Acoustics
Design & Technology
Engineering Division

J. E. Barrett, Director
Design Engineering - Design Integration
Design & Technology
Engineering Division

AIR FORCE OFFICE OF SCIENTIFIC RESEARCH
BOLLING AFB, WASHINGTON, DC

MCDONNELL DOUGLAS ASTRONAUTICS COMPANY-HUNTINGTON BEACH
5301 Bolsa Avenue Huntington Beach, California 92647 (714) 896-3311

UNCLASSIFIED

SECURITY CLASSIFICATION OF THIS PAGE

REPORT DOCUMENTATION PAGE

a. REPORT SECURITY CLASSIFICATION: UNCLASSIFIED	1b. RESTRICTIVE MARKINGS: None
2a. SECURITY CLASSIFICATION AUTHORITY: F49620-83-C-0117	3. DISTRIBUTION/AVAILABILITY OF REPORT: Approved for public release; distribution unlimited. Public
2b. DECLASSIFICATION/DOWNGRADING SCHEDULE: N/A	
4. PERFORMING ORGANIZATION REPORT NUMBER(S): MDC H1178	5. MONITORING ORGANIZATION REPORT NUMBER(S): AFOSR-TR- 85-1078
6a. NAME OF PERFORMING ORGANIZATION: McDonnell Douglas Astronautics Company; 6b. OFFICE SYMBOL (If applicable):	7a. NAME OF MONITORING ORGANIZATION: Air Force Office of Scientific Research (AFOSR)
6c. ADDRESS (City, State and ZIP Code): 5301 Bolsa Ave. Huntington Beach, CA 92647	7b. ADDRESS (City, State and ZIP Code): Bolling AFB Washington, DC
8a. NAME OF FUNDING/SPONSORING ORGANIZATION: AFOSR; 8b. OFFICE SYMBOL (If applicable): AFOSR/NA	9. PROCUREMENT INSTRUMENT IDENTIFICATION NUMBER: F49620-83-C-0117
8c. ADDRESS (City, State and ZIP Code): Bolling AFB, Washington, DC	10. SOURCE OF FUNDING NOS. — PROGRAM ELEMENT NO.: 61102F; PROJECT NO.: 2302; TASK NO.: B1; WORK UNIT NO.:
11. TITLE (Include Security Classification): PASSIVELY DAMPED JOINTS FOR ADVANCED SPACE STRUCTURES (U)	
12. PERSONAL AUTHOR(S): Trudell, Richard W. Blevins, Creed E.	
13a. TYPE OF REPORT: Annual; 13b. TIME COVERED: FROM 15 May 83 TO 13 Jun 84; 14. DATE OF REPORT (Yr., Mo., Day): 1984 Jun 30; 15. PAGE COUNT: 170	
16. SUPPLEMENTARY NOTATION	
17. COSATI CODES — FIELD / GROUP / SUB. GR.	18. SUBJECT TERMS (Continue on reverse if necessary and identify by block number): Passive, Damping, Joints, Space, Structures

19. ABSTRACT (Continue on reverse if necessary and identify by block number)

This annual report contains a description of the significant technical accomplishments (including:) of the subject research during the first contract year. These include: (1) the development of a viscoelastic materials selection guide for this research activity; (2) the development of an analytic statics model of the joint specimens; (3) the design, fabrication and preliminary testing of 15 viscoelastic joint specimens; (4) the procurement, fabrication and assembly of most of the test equipment for the test program at the Georgia Institute of Technology as well as the development of data reduction computer programs; and (5) the development and successful demonstration of a transient pulse method for evaluating energy losses in joints.

20. DISTRIBUTION/AVAILABILITY OF ABSTRACT: UNCLASSIFIED/UNLIMITED ☒ SAME AS RPT. ☐ DTIC USERS ☐	21. ABSTRACT SECURITY CLASSIFICATION: UNCLASSIFIED
22a. NAME OF RESPONSIBLE INDIVIDUAL: Dr A. K. Amos	22b. TELEPHONE NUMBER (Include Area Code): 202/767-4937; 22c. OFFICE SYMBOL: AFOSR/NA

DD FORM 1473, 83 APR — EDITION OF 1 JAN 73 IS OBSOLETE.

UNCLASSIFIED

SECURITY CLASSIFICATION OF THIS PAGE

PREFACE

The work reported herein was performed under Air Force Office of Scientific Research contract number F49620-83-C-0117. This report documents the results of activities during the first contract year and was prepared in satisfaction of Contract Data Requirements List Item 0002AB. The Air Force Project Manager for this effort is Dr. Anthony Amos. The research is supported by technical specialists (see Section 3) at McDonnell Douglas Astronautics Co. and Georgia Institute of Technology.

CONTENTS

FIGURES

Section 1
INTRODUCTION AND SCOPE

Mission requirements for future space structures dictate that many will be extremely large by today's standards. The missions for these large structures raise fundamental questions about controllability and general vibration control. Many missions require that extremely tight orientation tolerances and low vibration levels be maintained. A key element of any vibration control approach is passive damping. The enhancement of structural damping causes several favorable synergisms such as improved vibration isolator performance and more robust control systems with fewer modes to control (Reference 1). Past practice in the damping field has been limited to add-on approaches. Numerous examples of this approach are contained in the literature in the form of case histories of constrained-layer viscoelastic damping treatments applied over large areas and viscous dampers applied to problem components. While generally successful, some penalties are usually attendant because of the add-on nature of the approach. This research is directed at methods to make the joints, which must inevitably exist in large structures, damping elements that form an integral part of the structural design. This designed-in approach provides the opportunity to minimize the penalties while maximizing the damping benefit. An example of such an approach for a space experiment platform is shown pictorially in Figure 1-1. In this case, a simple extensional damper in each strut of the platform truss structure constitutes a well integrated approach to damping enhancement (Reference 2).

The basis for utilization of the joints for damping is the hypothesis that a favorable tradeoff results when structural stiffness is exchanged for increased structural damping. The need to accept reduced structural stiffness arises from the requirement to make the joints somewhat flexible so that a reasonable portion of the total strain energy in the structure is resident in the joints. This strain energy is then available for dissipation in the joint materials selected expressly for this purpose. This approach seems particularly useful for increasing the damping of low loss factor structures (on the order of 0.005 or less) to the order of 0.1 as is illustrated in Figure 1-2. The reduction

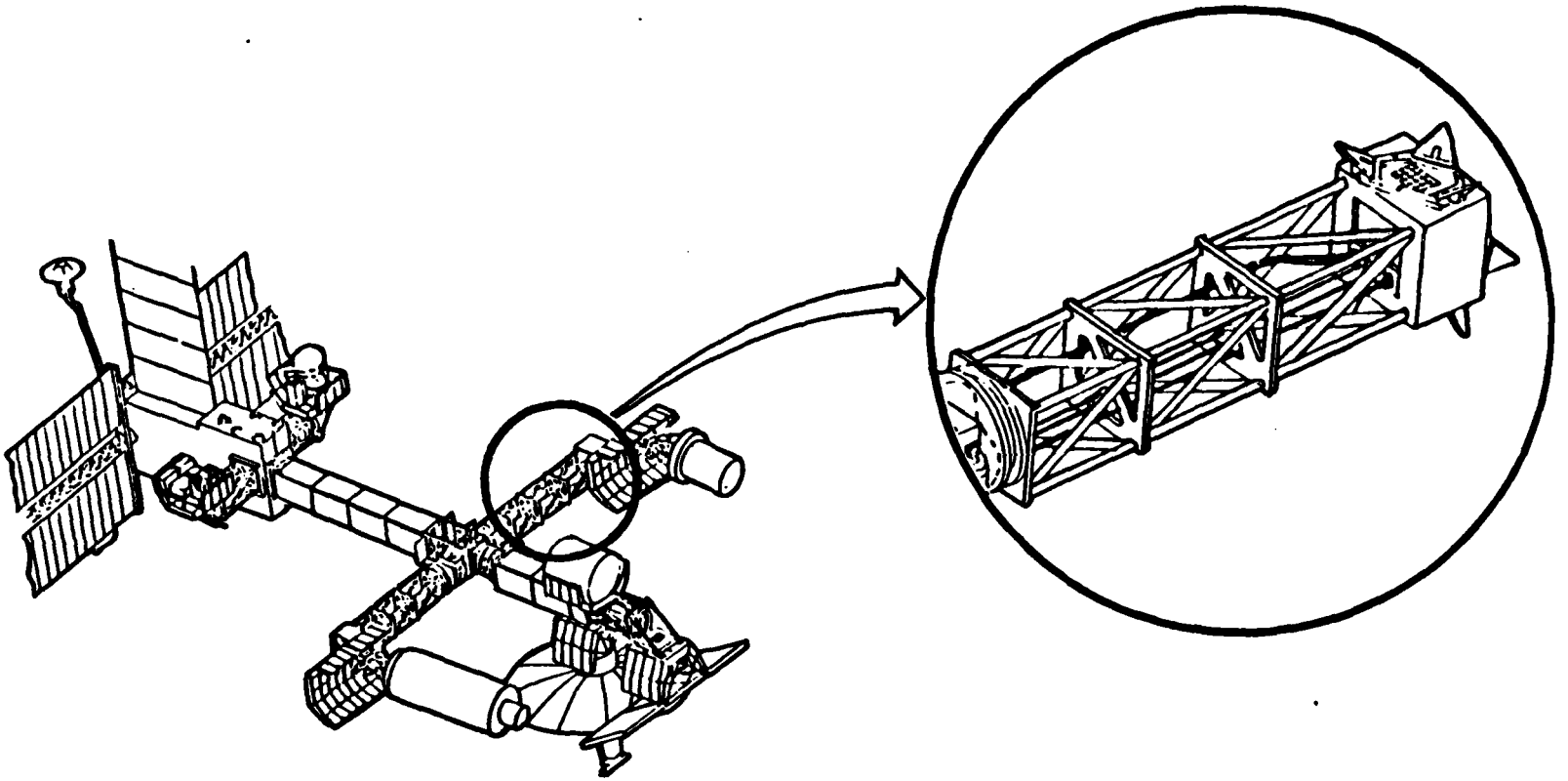

Figure 1-1. Viscoelastic Damper Built Into Each Strut

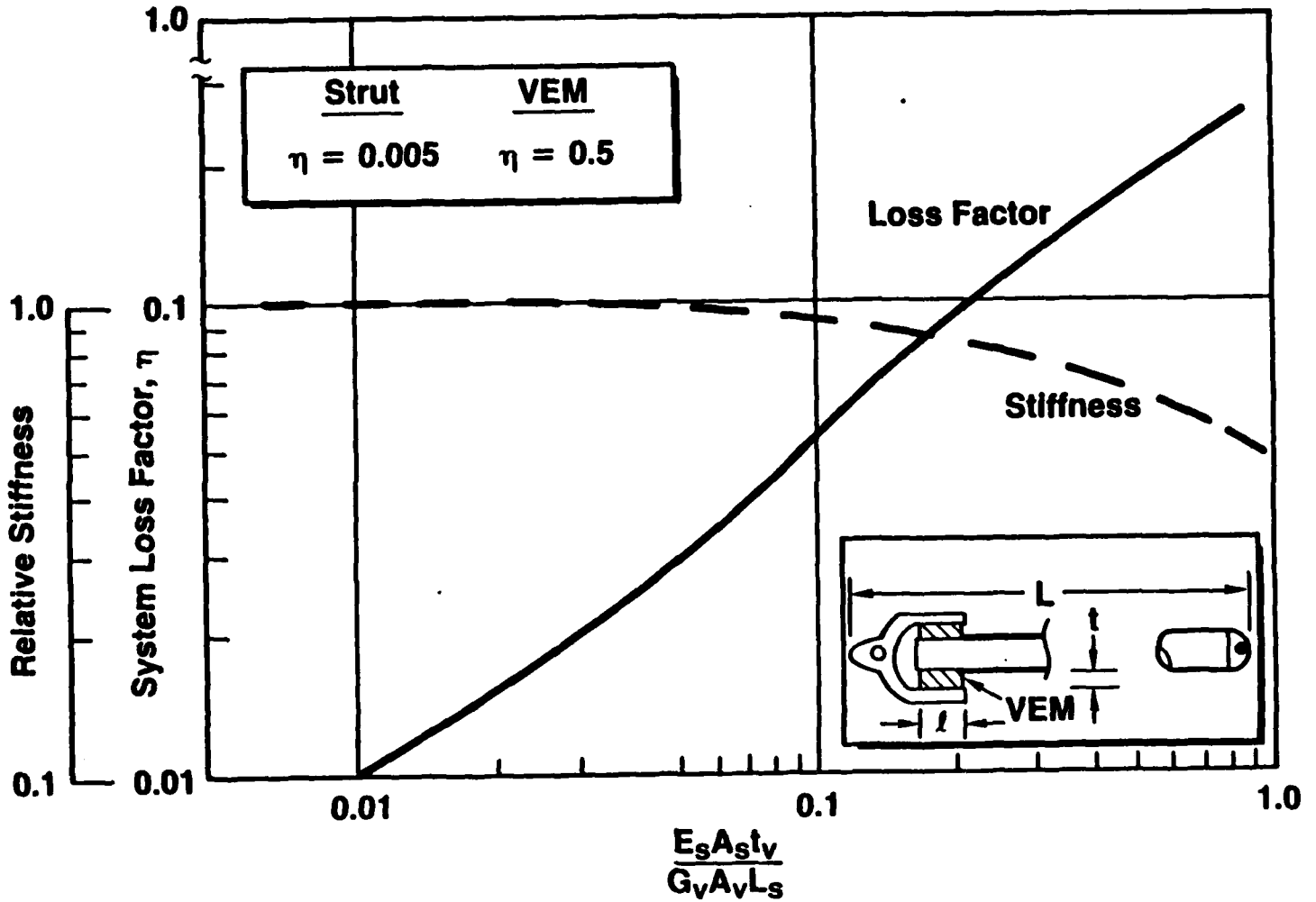

Figure 1-2. Viscoelastic Materials Effectiveness of Damping Treatment on Strut Extensional Damping

in stiffness is only on the order of 10%, which reduces the platform frequencies by only 5%.

The benefits of such a change are illustrated in Figures 1-3 and 1-4, which show the effects of a uniformly distributed damping change on transfer function magnitude and phase. The magnitude effect is the most well known because damping has been consistently applied to reduce resonant stresses and loads. The phase effect, though academically well known, has not been so widely applied.

The reduction of the rate of change of the phase versus frequency is a key element to increasing control system robustness by reducing sensitivity to plant estimation errors. Even if active control of the vibration response of large structures is not an objective, because of slew rate requirements, the control systems for large structures will inevitably have many resonant modes in the control bandwidth. The sheer size and weight of some experiment platforms, such as the example of Figures 1-3 and 1-4, generate resonances within the control bandwidth of the experiments mounted on them. The smoother phase response of the damped structure reduces the sensitivity of both the experiment control systems and the platform control systems to plant estimation errors, whether made a priori or adaptively.

In the platform case illustrated, the damping approach involved only the platform truss structure and not the payloads or solar panels. This fact violates the presumption of uniform damping in the data shown in Figures 1-3 and 1-4. The results of a non-proportional damping analysis, which accounts for the uneven distribution of dampers, are summarized in Figures 1-5, 1-6 and 1-7. Figure 1-5 shows that many modes have the low damping associated with the untreated portions of the structure, and the magnitude of the frequency response shown in Figure 1-6 shows some peaks that are not effectively reduced. The phase response shown in Figure 1-7, however, shows that the smoothing trend is well maintained with only small perturbations introduced at localized frequencies. These examples serve to show that locally placed damping in the struts of the platform truss will achieve practical and useful results.

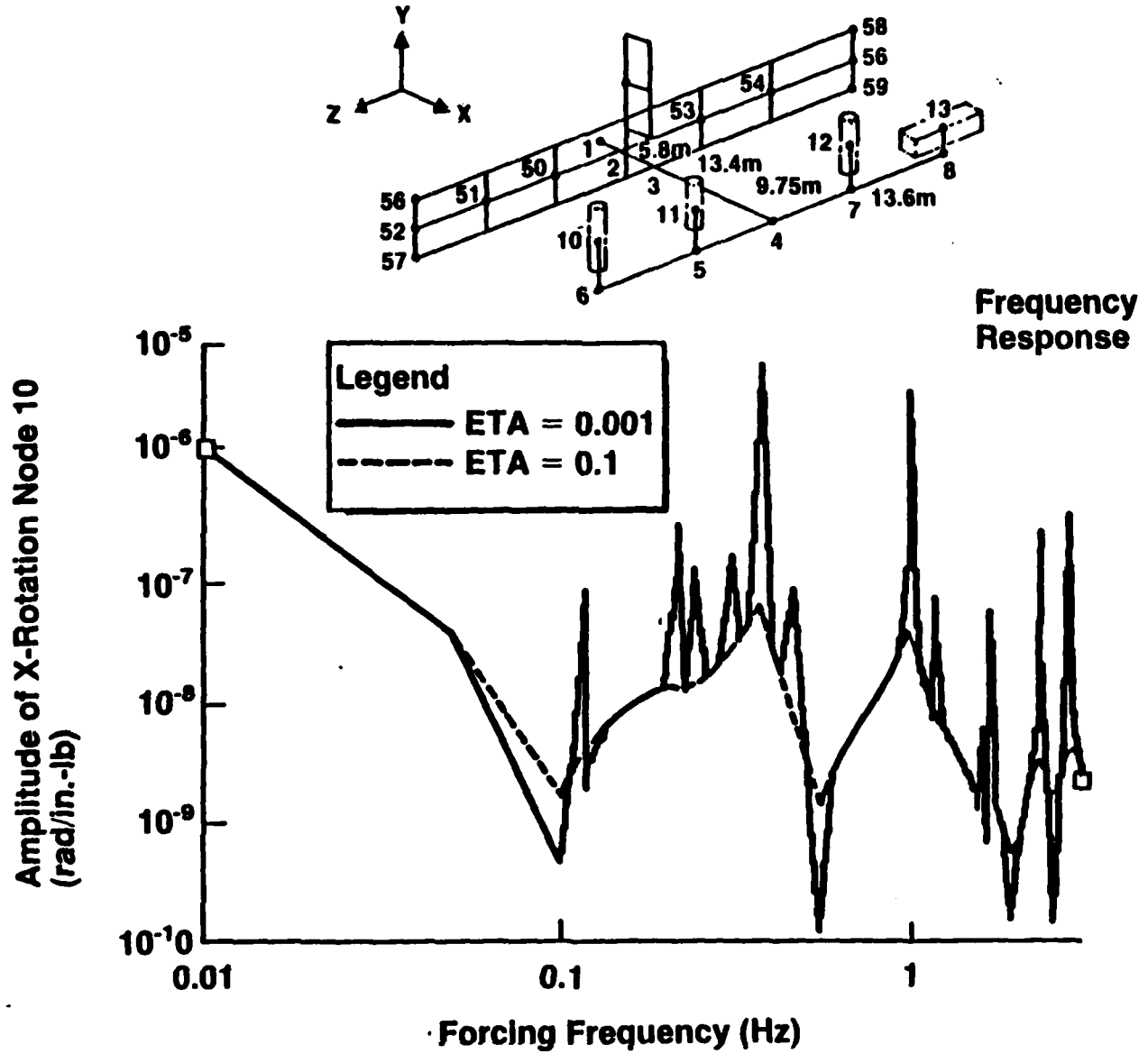

Figure 1-3. Long T-Bar Configuration Amplitude Response of Node 10 From a Unit Torque

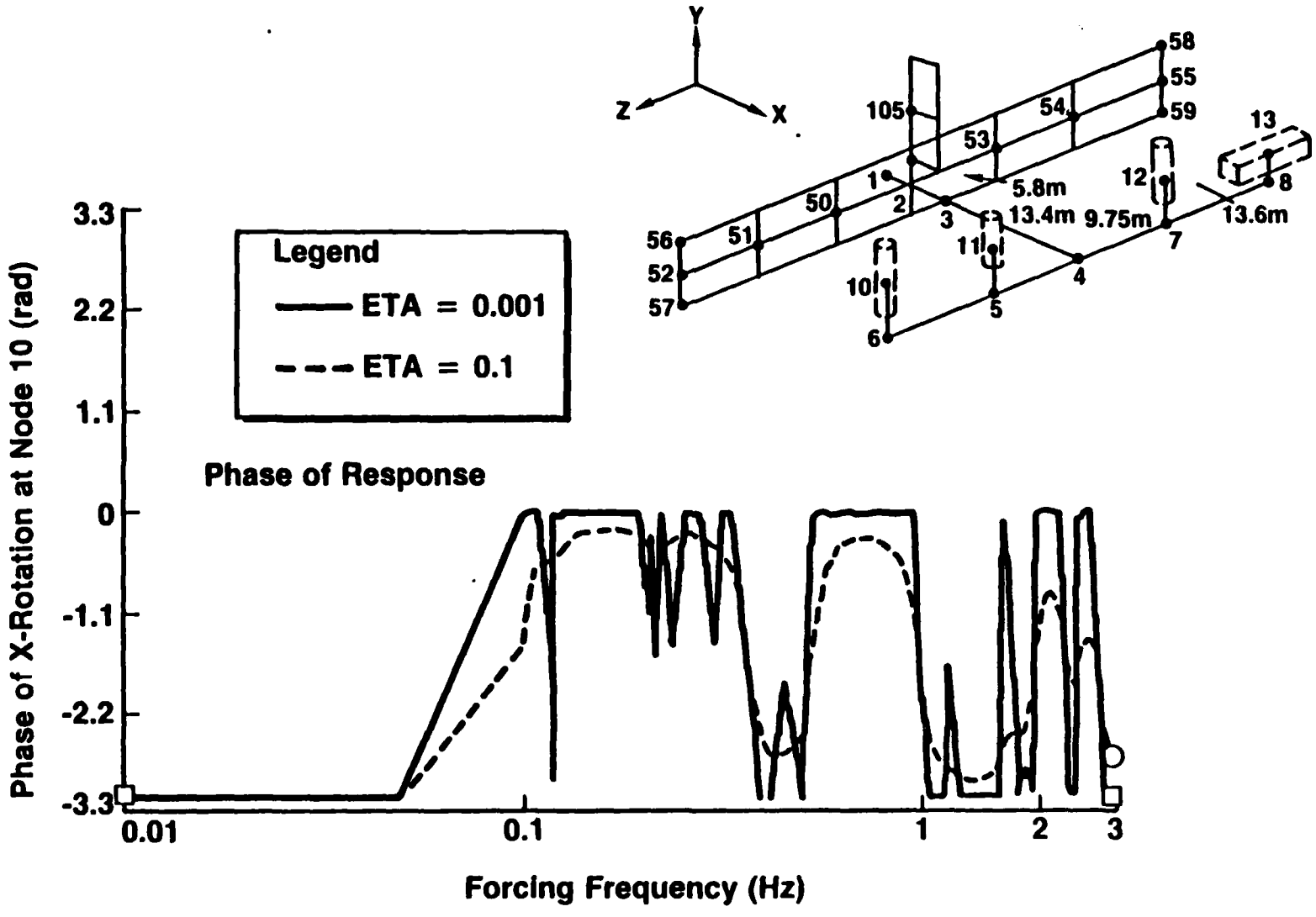

Figure 1-4. Long T-Bar Configuration Phase Response of Node 10 From a Unit Torque

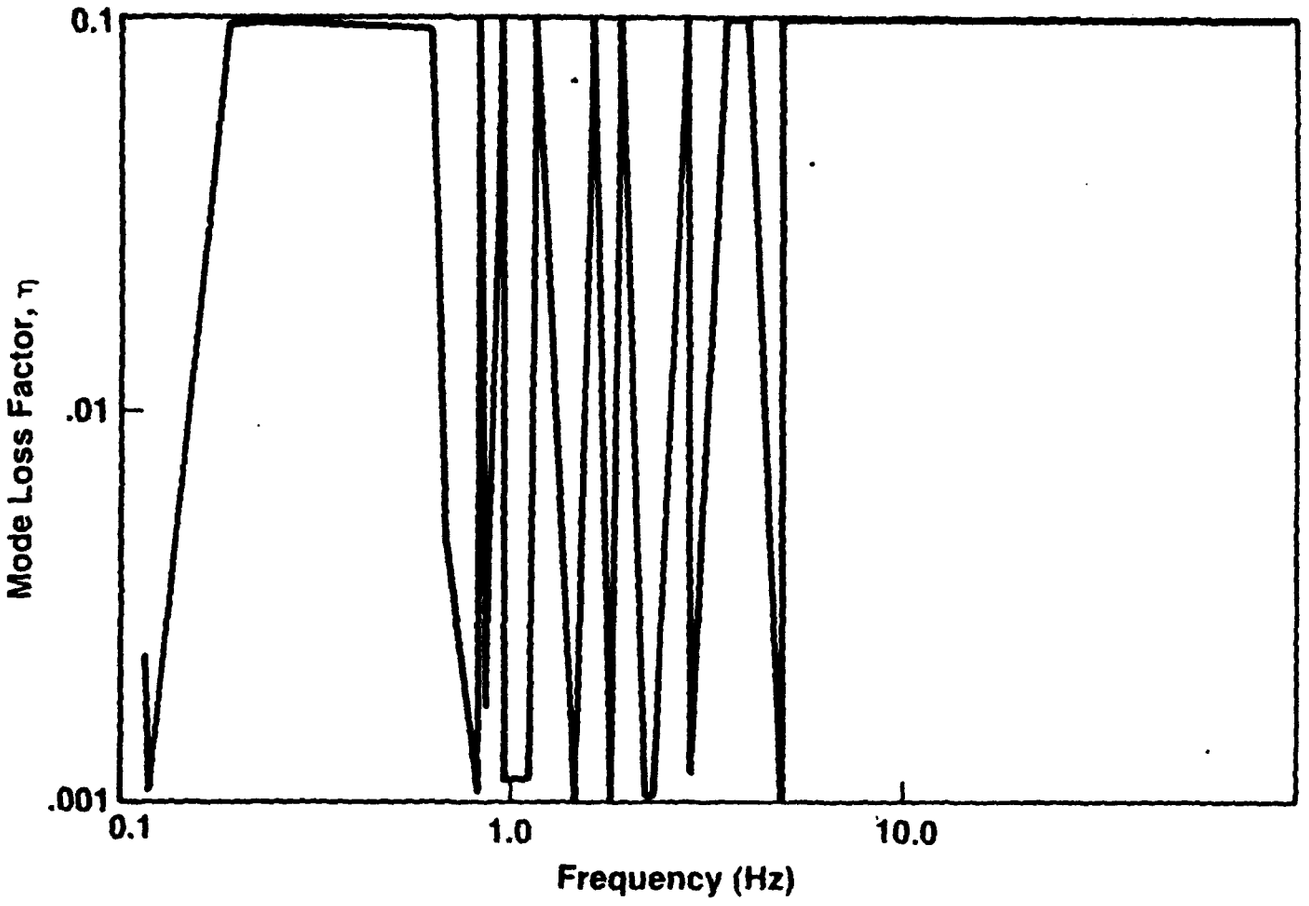

Figure 1-5. Effect of Truss Member Dampers on System Damping - Short T-Bar

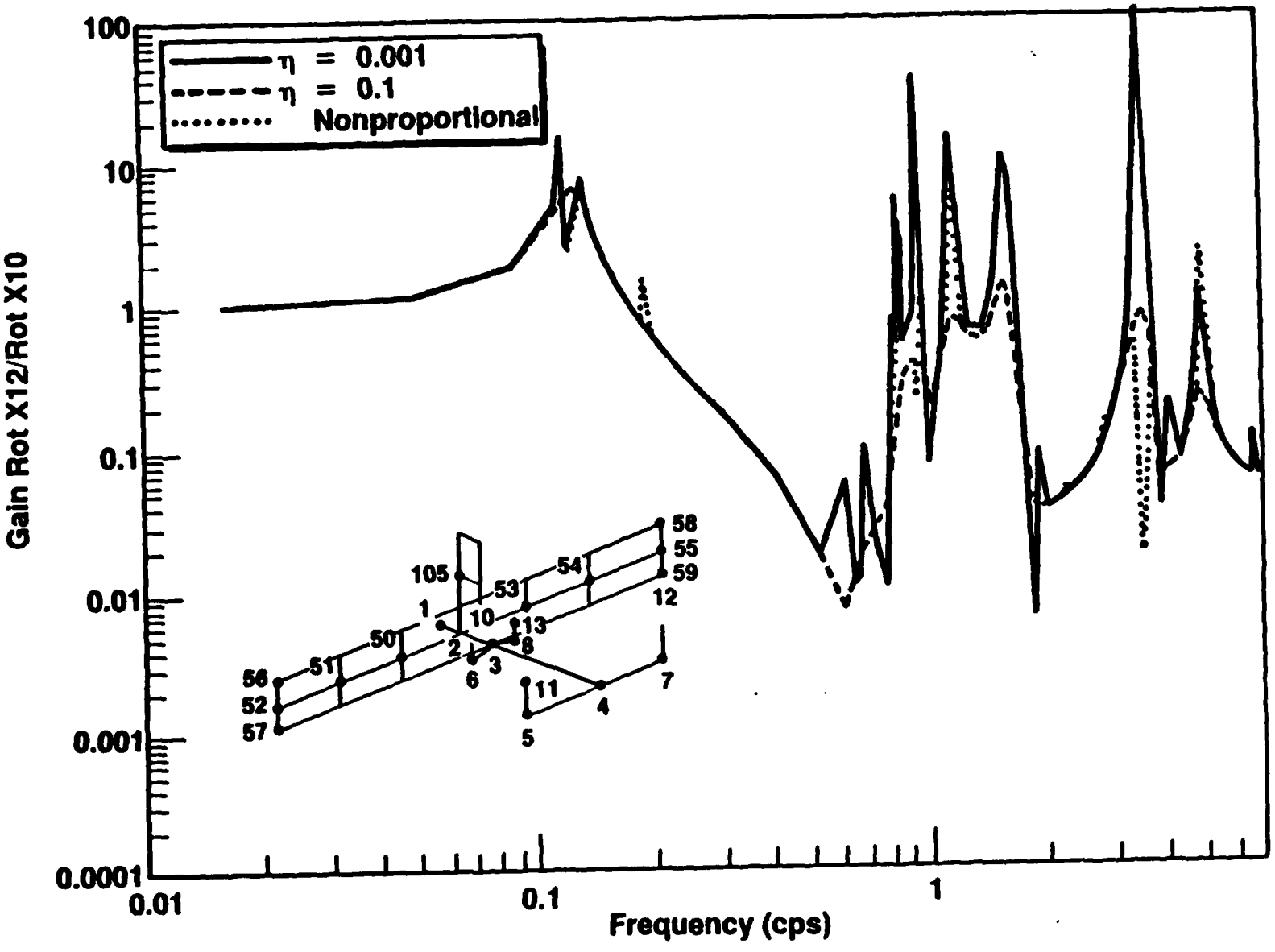

Figure 1-6. Short T-Bar Configuration Transfer Function ROT X12/ROT X10

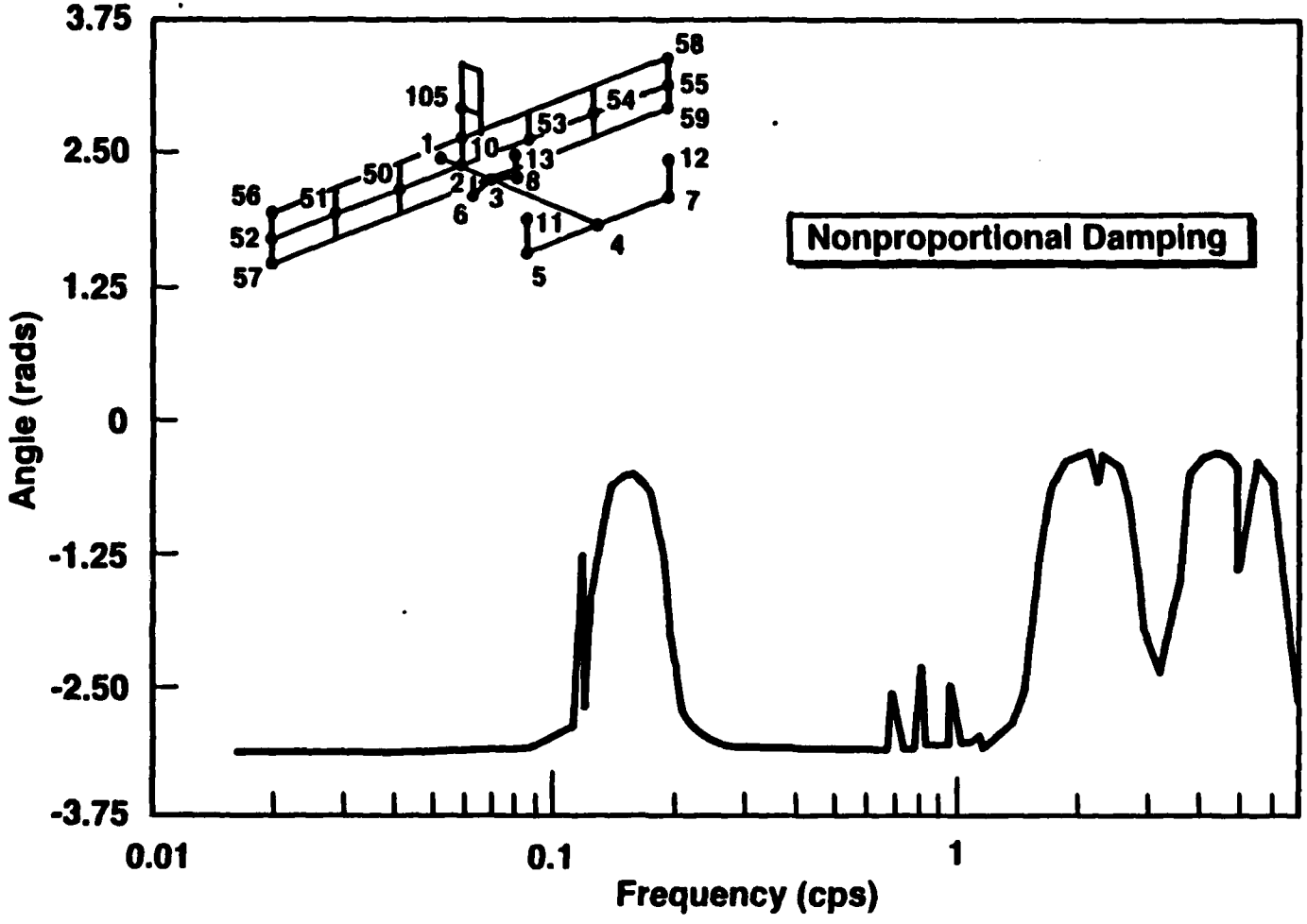

Figure 1-7. Short T-Bar Configuration Phase - ROT X10

The Air Force Office of Scientific Research has contracted with the McDonnell Douglas Astronautics Company (MDAC) to perform research on generic damped joints for the purpose of improving the damping of large advanced space structures.

MDAC has executed a subcontract with the Georgia Institute of Technology (GIT) to test and evaluate the joints developed at MDAC. Under the terms of the prime contract, the MDAC/GIT team are to perform the following tasks over a two-year period:

a. Development of structural joint concepts which incorporate viscoelastic materials as vibration energy dissipation media.

b. Analytical modeling and assessment of the performance characteristics of such concepts.

c. Validation of analytical methods developed and joint performance predictions through a carefully planned and executed experimental program.

d. Iteration on joint designs for enhanced damping characteristics.

e. Experimental evaluation of the joint designs.

The schedule adopted at the beginning of this program is shown in Figures 1-8 and 1-9.

This annual technical report and its appendices summarize the progress made during the first year of the contract.

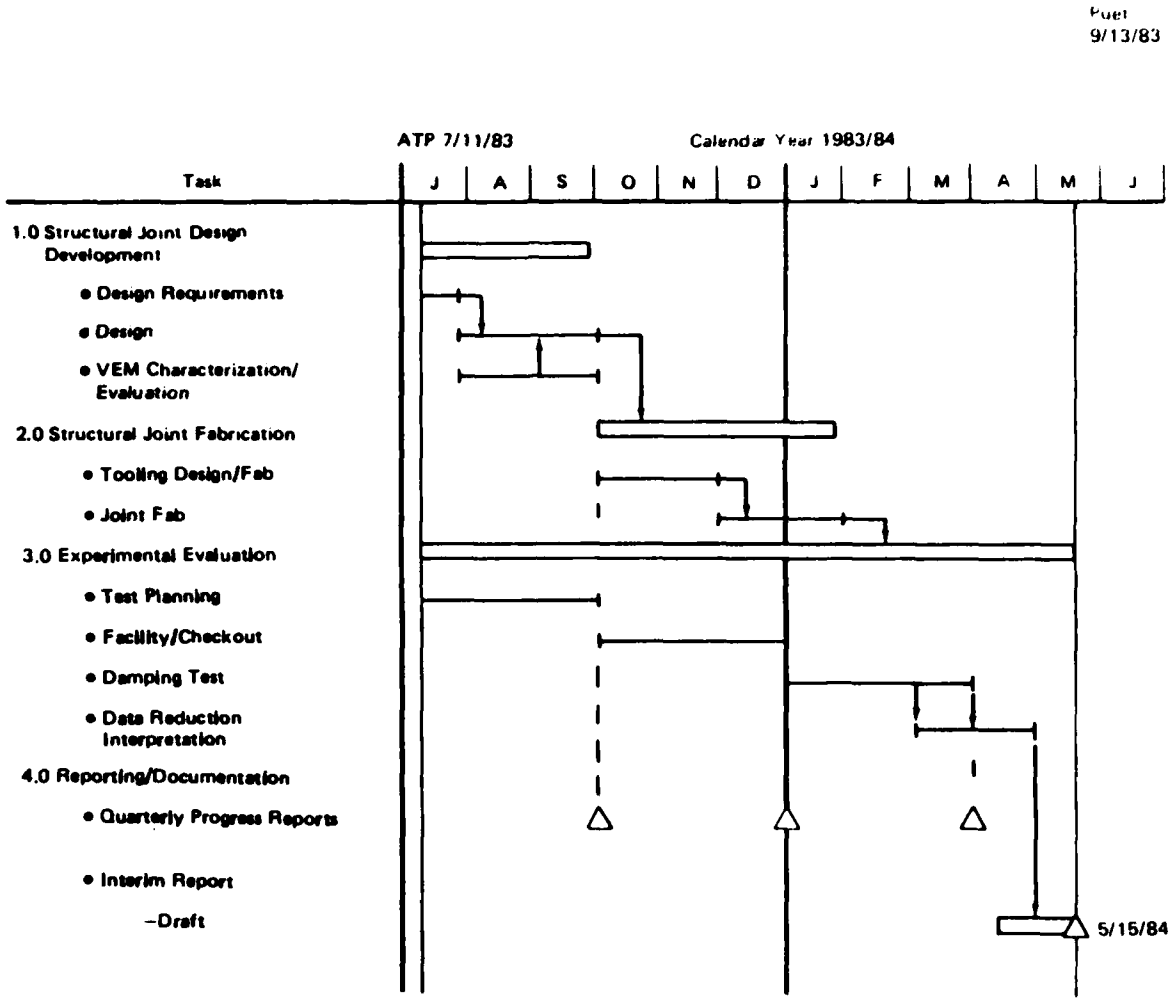

Figure 1-8. Passively Damped Joining Concepts for Advanced Space Structures - Program Schedule - Year 1

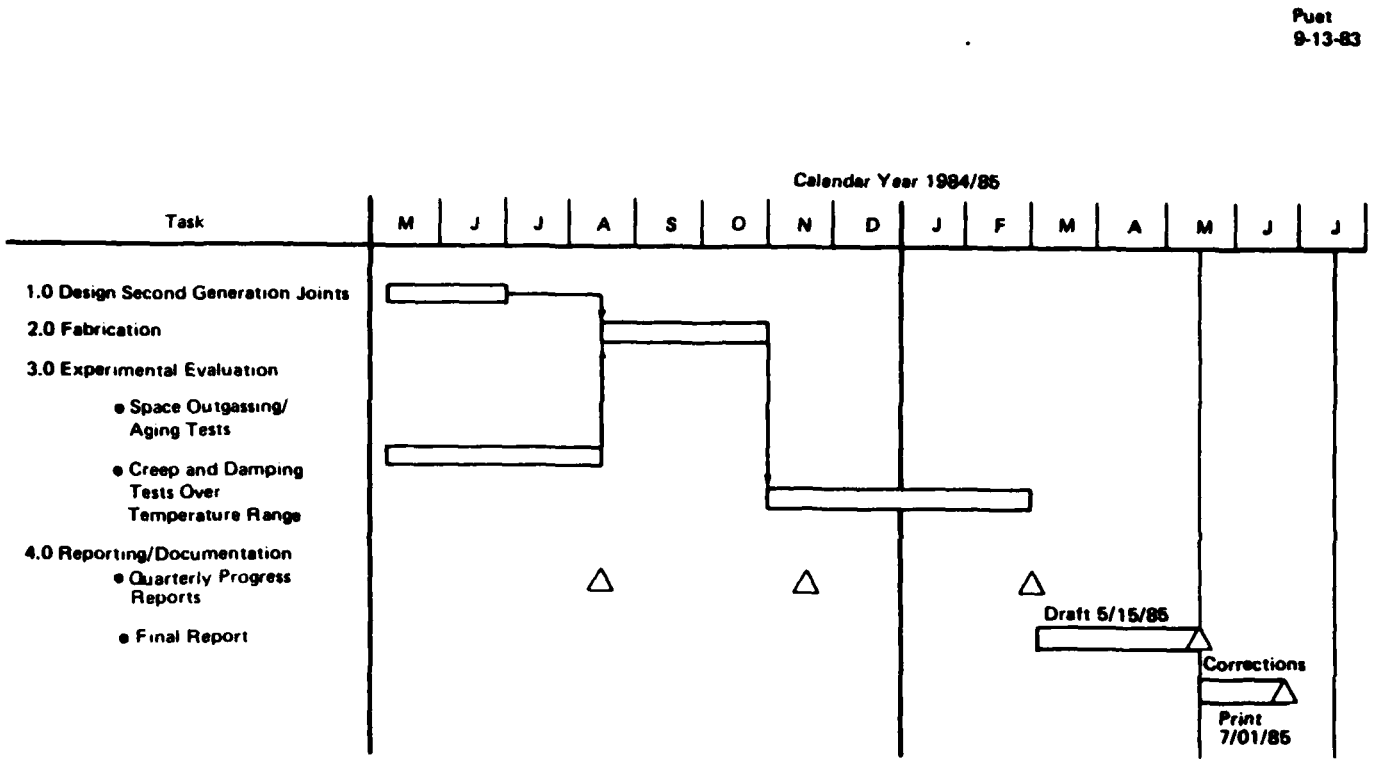

Figure 1-9. Passively Damped Joining Concepts for Advanced Space Structures - Program Schedule - Year 2

Section 2
TECHNICAL PROGRESS SUMMARY

The thrust of this research is the characterization and modeling of generic joints for the damping of structures. An example of one type of joint being studied is shown in Figure 2-1. This joint is a symmetric lap joint that also incorporates a return-to-zero feature. The damping is achieved by the shearing of the viscoelastic material that results when an axial force is applied to the joint. The unidirectional glass shown limits the maximum flexibility of the joint at elevated temperatures and also results in a restoring force to provide the return-to-zero function. Test specimens are being fabricated for evaluation of both the concept and suitable materials.

The major accomplishments in the first year of activity include:

1. The development of a viscoelastic materials selection guide for this research activity.

2. The development of an analytic statics model of the joint specimens.

3. The design, fabrication and preliminary testing of 15 viscoelastic joint specimens.

4. The procurement, fabrication and assembly of most of the test equipment for the test program at the Georgia Institute of Technology as well as the development of data reduction computer programs.

5. The development and successful demonstration of a transient pulse method for evaluating energy losses in joints.

The status of the current year tasks is given in Figure 2-2. The experiment is somewhat behind schedule because of a problem with delivery of the piezoelectric displacement transducer required for testing. The vendor had

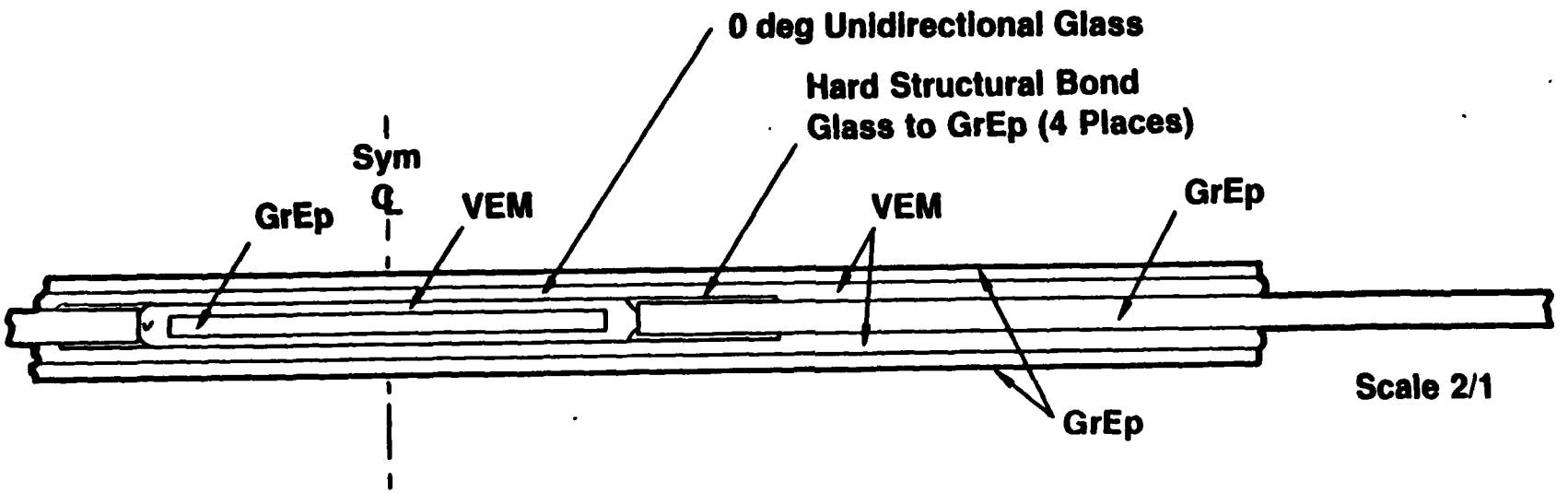

Figure 2-1. Structural Damping Joint Configuration

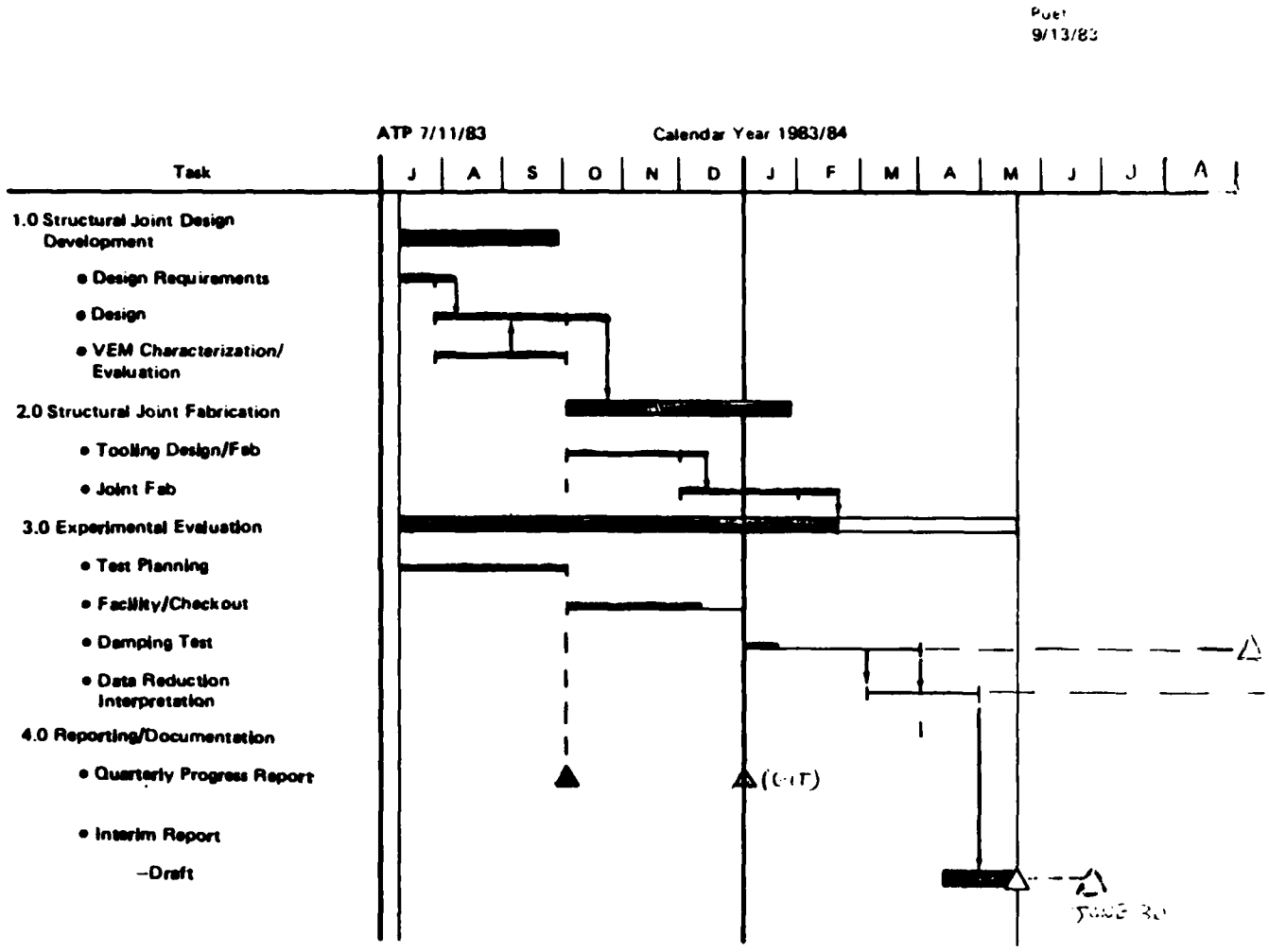

Figure 2-2. Passively Damped Joining Concepts for Advanced Space Structures - Revised Program Schedule - Year 1

completed a unit in March but it did not meet the linearity criterion by a substantial amount. An investigation yielded the fact that a piezoelectric material with good temperature stability had been used without regard to its voltage/displacement characteristics. The vendor is reworking the transducer with a more suitable material at his own expense. A delay of about three months in the joint testing has resulted, with transducer delivery now expected at the end of June. If this date is met, there will be no impact to the program completion date or cost, but the particular task schedules for the second year will be altered as shown in Figure 2-3. The technical work accomplished during the year is contained in the appendices. The following paragraphs summarize this work.

Appendix I contains a summary of the laboratory development work performed to create the first generation of joint test specimens. These specimens are prototypical coupons of truss element damping joints which increase overall truss flexibility by about 10%. The 10% number represents a reasonable compromise between the increase in strain energy resident in the joints for absorption by the damping materials and the decrease in resonant frequencies of the structure. Joint stiffnesses of 50-100,000 lb/in. per inch of width are required to obtain this flexibility increase in a generic space truss (Reference 2). The basis for the design and construction for the first 12 joints (which are all double lap joints with no structural bypass) is given as well as the results of the initial screening tests performed at MDAC. The development of the first three joints containing a structural bypass is described in Annex A of Appendix I.

The hysteresis data from all of the joints tested is contained in Annex B of Appendix I. Based on the initial tests, which were performed only at one frequency and at one temperature, it appears that the basic design goals for each specimen group were met at least approximately. Subsequent testing at Georgia Tech will fully characterize these joints, and a detailed evaluation of both the models and the designs can be accomplished.

The physical properties data from the initial materials survey is contained in Appendix I, Annex C. Some of these materials were discarded from further consideration because of unsuitable properties.

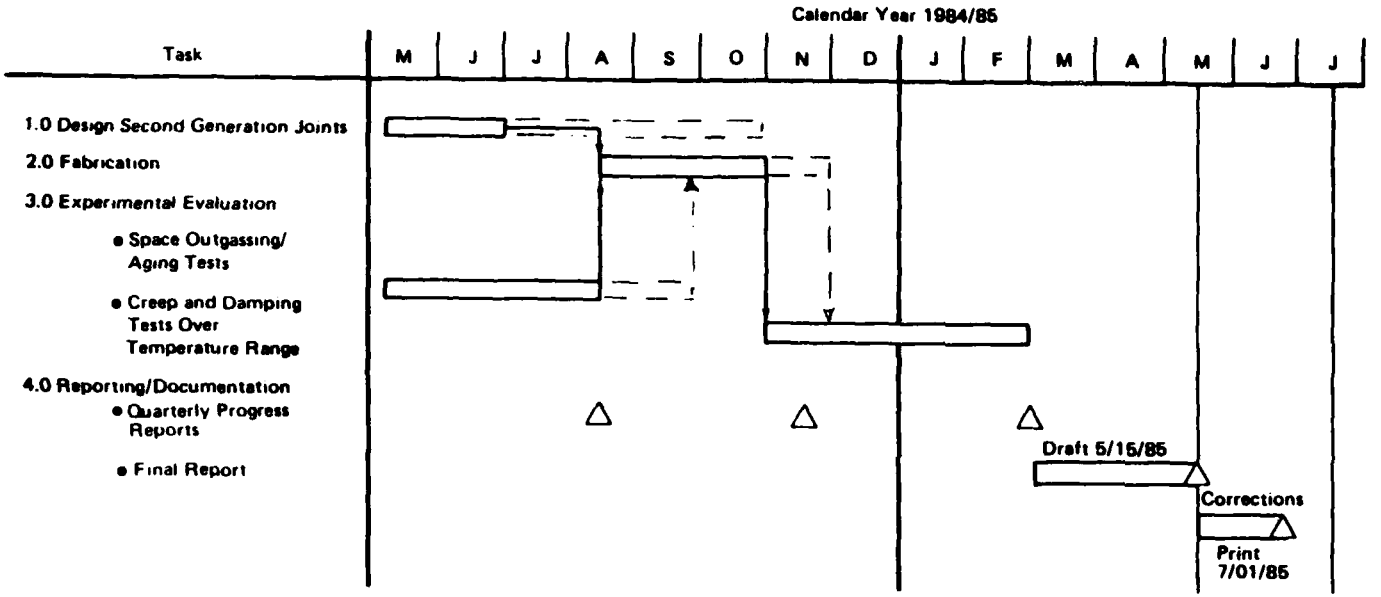

Figure 2-3. Passively Damped Joining Concepts for Advanced Space Structures - Revised Program Schedule - Year 2

Appendix II contains a summary of the development of a lap shear joint model based on the work of L. J. Hart-Smith to permit the prediction of strain energy distributions in joint elements including the effect of structural bypasses. This model is useful for dealing with the cases where the strain in the joint adherends is not trivial compared to the strain in viscoelastic materials. The primary use of this model is to correlate experimental results with predictions where the simplified GA/t shear stiffness model used for joint design might not provide adequate agreement. A FORTRAN computer code of the model was developed and checked out. The source listing is also given in Appendix II.

The Georgia Tech progress for the first year is given in Appendices III and IV in the form of two interim reports. The work in Appendix III deals primarily with the development of a pulse propagation approach to joint characterization. The method uses an energy approach to estimate joint losses. A modified loss factor is defined to allow interpretation of results. Some limited experiments were performed using joint specimens fabricated at Georgia Tech. These specimens have not been characterized in any other way at present, so the results presented are somewhat relative. Correlation between the pulse loss factor and well-established sinusoidal test loss factors will be accomplished when the test facility at GIT is fully operational in July.

Appendix IV gives the technical progress achieved at GIT in the first half of 1984, which includes fixture design and construction, data analysis codes development for both the pulse and steady-state test methods, and the results of an analytic simulation of the pulse approach. The significant aspect of the simulation effort is that the appearance of "noise spikes" observed in the earlier experiments was successfully explained by the simulation (see Section 4) as a real reflection effect. Methods for removing these reflections have been developed and are explained in Section 3.2 of this appendix.

The analytic basis for the steady state test method is summarized in Appendix V. Testing utilizing this method will begin in July of this year. The steady state method will provide a quantitative link between past complex modulus methods of assessing damping loss factor and the energy-based loss factors generated using the newly proposed transient technique in Appendix III and IV.

Section 3
PERSONNEL, PUBLICATIONS, AND INTERACTIONS

3.1 PERSONNEL

The following individuals are active contributors to the research effort:

Name	Title	Function
MDAC		
R. W. Trudell	Principal Engineer Scientist	Principal Investigator
C. E. Blevins	Sr. Engineer - Technology	Materials Engineer
J. H. Peebles	Engineer Scientist Specialist	Structural Dynamics Analyst
B. E. Hom	Engineer Scientist	Structural Statics Analyst
Georgia Tech		
Dr. L. H. Rehfield	Professor of Aerospace Eng'g	Task Leader
Ambur D. Reddy	Sr. Research Engineer	Investigator
Jacky Prucz	Graduate Student	Investigator

The research is also supported by other technical specialists in the laboratories of both MDAC and Georgia Tech.

3.2 PUBLICATIONS AND PATENTS

The principal publication for this past year was MDC paper G9060, Passively Damped Joints for Advanced Space Structures, which was contributed to the AFWAL Damping Workshop proceedings. These proceedings will be published this summer by AFWAL.

There were no patent disclosures or applications filed during the first year of activity.

3.3 INTERACTIONS

The following meetings and conferences were supported during the past year:

- First Forum on Space Structures - September 1983 - MIT. Sponsored by AFOSR - J. H. Peebles of MDAC attended and participated in forum discussions.

- AFWAL Damping Workshop - February 1984 - Long Beach, CA. Paper entitled Passively Damped Joints for Advanced Space Structures was orally presented by R. W. Trudell and L. H. Rehfield.

- 25th Structures, Structural Dynamics and Materials Conference - May 1984 - Palm Springs, CA. Two papers presented at Work-In-Progress sessions:
  - MDAC paper G9059, Designed-in Damping Joints for Advanced Space Structures by R. W. Trudell, MDAC; L. W. Rehfield, GIT
  - MDAC paper G9061, A New Approach to Dynamic Characterization of Structural Joints by J. Prucz, A. D. Reddy, L. W. Rehfield/GIT

- Second Forum on Space Structures - June 1984 - Tyson's Corners, VA. Sponsored by AFOSR - R. W. Trudell of MDAC participated in Passive Control Committee proceedings and GIT participated in the Hardware Issues Committee proceedings. Written inputs were provided to the committee chairmen.

Section 4
SUMMARY AND OUTLOOK

Most of the goals and tasks for the first year have been accomplished, with the single exception of the test activity. The technical difficulty that delayed that task has been resolved and testing should proceed early this summer. Sufficient time and dollar resources remain in the program to complete all of the originally planned tasks prior to the scheduled completion date of 15 May 1985.

Section 5
REFERENCES

1. Trudell, Curley and Rogers. Passive Damping in Large Precision Space Structures. AIAA paper 80-0677-CP, May 1980.

2. McDonnell Douglas funded work in support of NASA Science Applications Space Platform studies.

APPENDIX I

VISCOELASTIC DAMPING JOINT SPECIMEN DESIGN AND DEVELOPMENT

1.0 OBJECTIVE

Many of the intended uses of Large Space Structures (LSS) involve precision optics or radar. There are many sources of vibration which can cause beam jitter, including coolant mass shift, antenna or solar array motion, station-keeping thrusters, etc. It is predicted that most of these vibrations will be in a very low frequency range (0.1-100 Hz). Viscoelastic joint damping is a very promising concept for controlling these low frequency LSS vibrations.

The objective of our test program is to design, fabricate and gather data on prototype LSS damping joints. MDAC-HB awarded Georgia Institute of Technology (GIT) a subcontract to test LSS joints which we will provide them. Design, fabrication and preliminary testing of the joints are being performed by MDAC-HB. At GIT, Dr. Lawrence Rehfield and one graduate student plan to test the joints using the pulse propagation approach. Preliminary GIT testing will take place at room temperature, with advanced testing covering a broad temperature range.

2.0 VISCOELASTIC MATERIAL (VEM) SELECTION

2.1 GOALS

The MDAC-HB joint design was based on a constrained lap joint where the VEM in the lap joint is placed in shear when a vibrational wave passes through it.

Over the operating frequency and temperature ranges, the VEM needs to have good damping to maximize the amount of joint energy dissipated and a relatively flat shear storage modulus to ensure that the desired share of the total strain energy remains in the joints. These principles lead to the following goals for the LSS joint VEM candidates:

1. The VEM loss factor (η) should be over 0.50 over a frequency range of 0.1-100 Hz at 21°C. If the VEM provides damping over a very broad temperature range, a lower loss factor is acceptable.

2. The VEM shear storage modulus (G') should not change by more than an order of magnitude when the temperature changes approximately 20°C.

2.2 ENVIRONMENTAL CONSIDERATIONS

This section will discuss some of the more important environmental considerations for VEM selection. These include the following effects:

1) Temperature and frequency effects.
2) Effects due to imposed loads (creep).
3) Effects due to high vacuum (outgassing).
4) Effects due to UV degradation.

2.2.1 The Effects of Temperature and Frequency Changes on VEM Properties

Satellites go through a temperature cycle as they orbit the earth. Geosynchronous satellites also move in and out of sunlight. Without thermal protection, the temperature may fluctuate from -270 to 200°F[1]. Multilayer thermal insulation and other passive or active means could be used to control this fluctuation to some degree. However, an ideal VEM would perform well over this entire temperature range.

Low frequency vibrations (0.1-100 Hz) are anticipated in Large Space Structures. Again, the VEM candidate should have high damping over this frequency range.

While initial testing of prototype LSS joints will be done at room temperature at 0.1-100 Hz, testing is also planned for a more representative wide temperature range.

The use of VEMs for passive damping is a design challenge because of their sensitivity to temperature and frequency changes. Both the loss factor and shear storage modulus are functions of temperature and frequency, with temperature changes having a larger effect than frequency changes.

The effects of temperature and frequency on G' and η for a typical VEM are shown in Fig. 1. In general, the VEM shear storage modulus (G') will increase as temperature decreases or frequency increases. The loss factor goes through a peak at the VEM glass transition temperature. While peak damping will be achieved over only a small temperature range, acceptably high damping may often be achieved over a fairly wide temperature range (20-50°C).

As will be discussed more in detail in Paragraph 4.3, it is desirable to have η as high as possible over the operating temperature and frequency range, and to have G' remain relatively constant.

VEMs which possess wide temperature damping ranges generally do not have a high loss factor over this range. Silicones and fluorosilicones typically behave in this manner. Rubber/plastic alloys are an exception to this rule.

The effects of thermal strains and thermal cycling may also cause debonds and VEM property degradation.

2.2.2 Creep

Since most VEMs are soft, lossy materials they generally have poor creep, and structural redundancy is needed. The MDAC-HB prototype joints will have redundant elements consisting of thin fiberglass plates connecting the main beams (Fig. 2). As long as the VEM is used in a structurally redundant joint, it does not need to have good creep resistance or low compression set.

If future joints were made without structural redundancy, creep resistance would again be important. There are many sources of disturbance even in zero gravity, such as cryomachinery, stresses due to temperature changes, station-keeping thrusters, and antenna motion. The greatest loads on the joints would probably be experienced at liftoff.

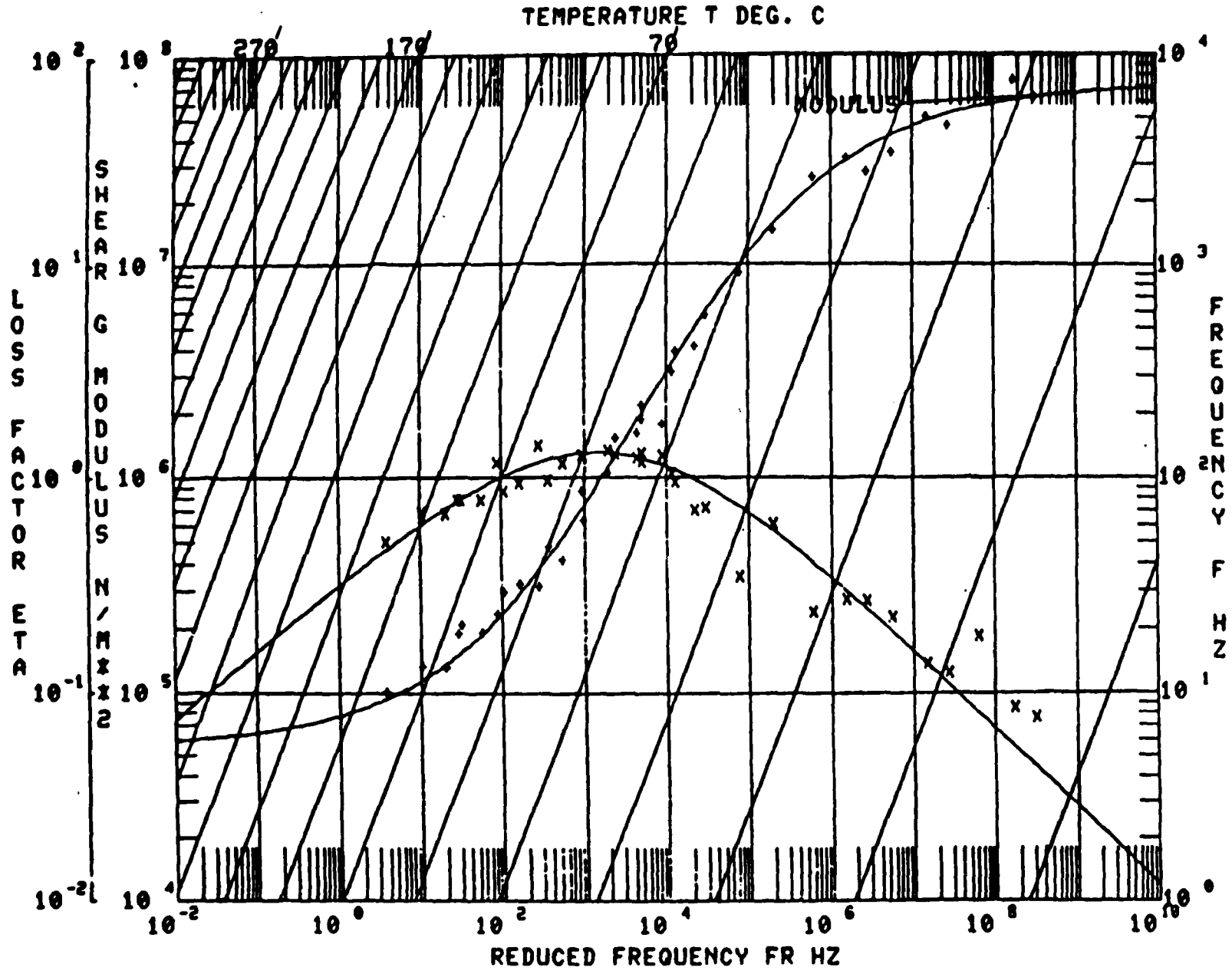

Figure 1. 3M ISD 110

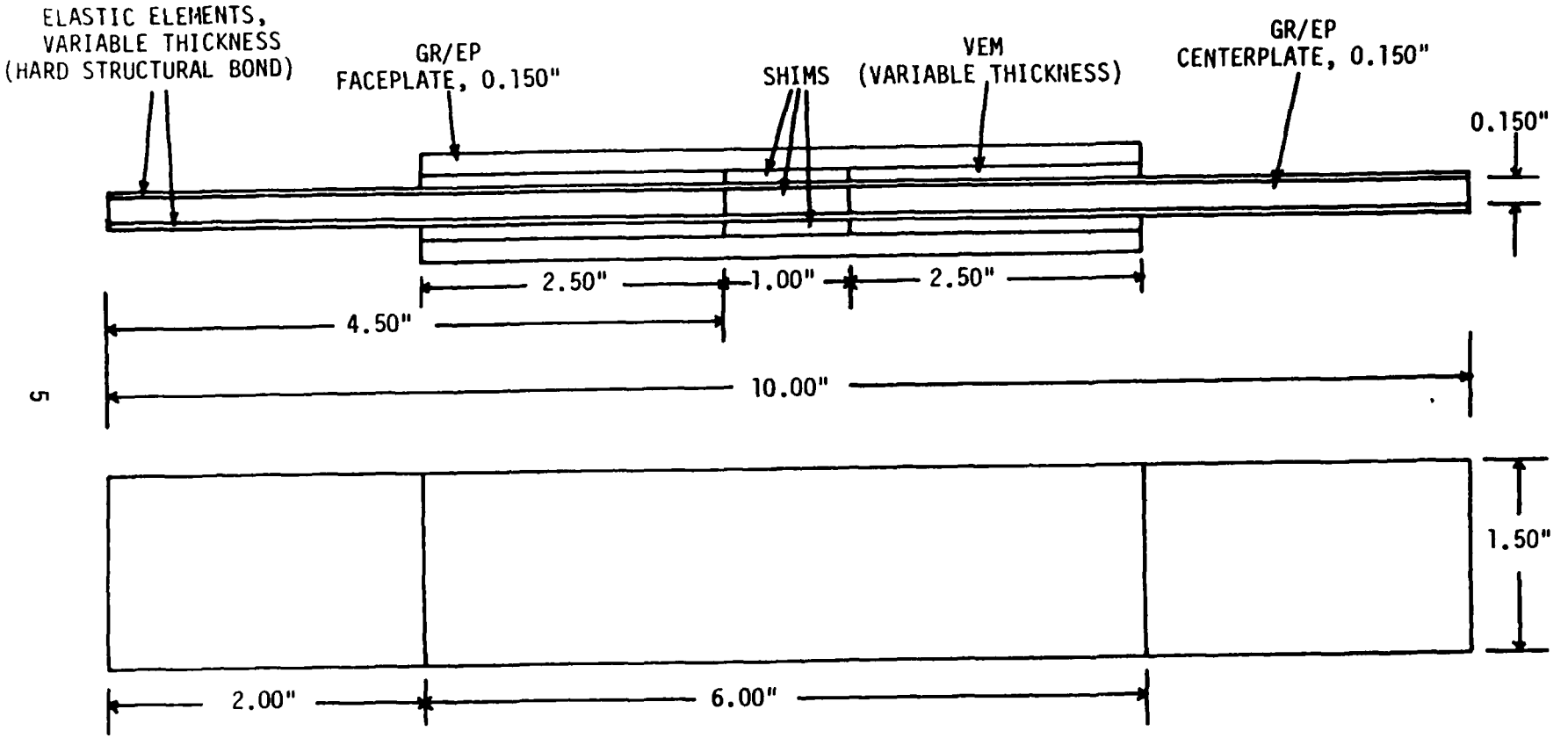

Figure 2. LSS Prototype Joint with Elastic Elements

2.2.3 Outgassing

The high vacuum of space could cause outgassing and loss of low molecular weight components of the VEM, such as plasticizers or absorbed water. High temperatures (200°F) aggravate the outgassing problem and could result from solar heating. The standard outgassing test is ASTM E 595-77.[2] Outgassing is reduced when a VEM sheet has only its edges exposed, as in a constrained layer or lap shear configuration.

Encapsulation of the joint with a low-outgassing sealant can help eliminate outgassing. Baking of the VEM or completed joint will tend to remove low molecular weight components. Volatile materials which do not condense (such as water) pose little threat to optics.

In summary, outgassing should not pose a problem for LSS lap shear or constrained layer VEM joints, since the faceplates will greatly reduce outgassing. If any problem does arise, baking or encapsulation should eliminate it.

2.2.4 UV Degradation

In a lap joint, the faceplates will virtually eliminate UV degradation of the VEM, since only the edges will be exposed. Carbon black or other additives could be mixed with the VEM for added UV resistance. Encapsulation with an opaque low-outgassing sealant could also be used to shield the VEM.

2.3 PROCESSING CONSIDERATIONS

The VEM must be capable of being incorporated into the joint structure. The fabrication techniques will depend on whether the VEM is a gum or a solid rubber at room temperature.

Many commercial VEMs used for damping are gums at room temperature. They are available as thin films with a release paper on either side. If the joint is made up of overlapping plates it can be easily laid up, since the VEMs are gummy and self-bonding. For forming a complex plate-type joint (Fig. 2), a hot air gun or hot press could be used to increase flow. Most VEMs can be bought in bulk form also, for injection molding. Injection molding would probably be needed for cylindrical joints, etc.

Other VEMs are solid rubber at room temperature, with hardnesses ranging from 60-94 Shore A. Cured sheets of these materials can be bonded at room temperature to composites. Experimental techniques have also been developed for vulcanizing uncured stock to composites.

Room-temperature-curing silicones, epoxies, and polyurethanes are sometimes used as VEMs. These materials can be cast or injected into joints and allowed to set up at room temperature. Shims can be used to maintain the desired bondline thickness.

3.0 VEM CANDIDATES AND RATIONALE FOR THEIR SELECTION

The VEM candidates selected for use in MDAC-HB prototype joints and their properties are listed in Tables 1 and 2. A discussion of why each was chosen is given below.

a) 3M's ISD 110

ISD 110 is a gummy acrylic-based damper made by 3M. It is intended for use in constrained layer damping. According to the University of Dayton Research Institute (UDRI),[8] ISD 110 has a loss factor varying from 0.77 to 1.2 from 0.1 to 100° Hz at room temperature, which indicates excellent damping.

While ISD 110 will not provide significant damping over a broad temperature range, it appeared to be an excellent choice for room temperature testing and instrument calibration. If used in LSS joints not subjected to temperature extremes, it would perform well.

ISD 110 requires a minimum 25°C minimum temperature increase to increase the value of G' by one order of magnitude, which is acceptable.

Table 1. LSS VEM CANDIDATE PROPERTIES

Material	Type	0.1 Hz		1 Hz		10 Hz		100 Hz		Maximum G' Slope °C/Decade G'	Estimated Creep Resistance	Meets JSC Outgassing	Estimated UV Resistance	Processing Ease
		η	G', psi	η	G', psi	η	G', psi	η	G', psi					
3M ISD 110	Acrylic	0.77	23	1.2	58	1.2	203	0.95	798	25	Poor	Yes	Good	Good
3M EC 2216	Epoxy	--	--	0.14	21,000	0.14	100,000	--	--	31	Good	Untested	Good	Good
Soundcoat Dyad 606	Polyurethane	0.55	145	0.85	435	1.05	1,590	0.8	8,700	26	Good	Untested	Good	Good
Hysol EA 9326	Polyurethane	(Estimated values: η = 0.1-0.3, G' = 1500 psi)								--	Good	Untested	Good	Good
GE SMRB 100F90	Epoxy-based	0.012*	1200	0.07	1,600	0.39	2,200	1.00*	3,200*	25	Fair	Yes	Good	Good
GE RTV 630	Silicone	(Estimated values: η = 0.1-0.3, G' = 130 psi)								--	Good	Untested	Good	Good
Rubber/Plastic Alloy I	Rubber/Plastic	(Estimated values: η = 0.1-0.7, G' = 5000 psi)								--	Fair-Good	Untested	Good	Good
Alloy II	Rubber/Plastic	(Estimated values: η = 0.1-0.7, G' = 5000 psi)								--	Fair-Good	Untested	Good	Good
Alloy III	Rubber/Plastic	(Estimated values: η = 0.1-0.7, G' = 5000 psi)								--	Fair-Good	Untested	Good	Good

*Extrapolated

Table 2. ADDITIONAL LSS VEM CANDIDATE PROPERTIES

Material	Type	Contains Fillers	Estimated Coefficient of Thermal Expansion (in/in°F x 10^{-5})	Density (gm/cc)
3M ISD 110	Acrylic	No	--	0.965
3M EC 2216	Epoxy	Yes[1]	1.1-2.8	1.29
Soundcoat Dyad 606	Polyurethane	No	5-25	0.965
Hysol EA 9326	Polyurethane	No	5-25	1.08
GE SMRD 100F90	Epoxy-based	Yes[2]	0.6-1.9	0.75-0.82
GE RTV 630	Silicone	Yes[3]	45	1.28
Rubber/Plastic Alloy I	Rubber/Plastic	Yes[4]	5-25	1.0-1.1
Alloy II	Rubber/Plastic	Yes[4]	5-25	1.0-1.1
Alloy III	Rubber/Plastic	Yes[4]	5-25	1.0-1.1

NOTES:

1. Mineral Fillers
2. Microballoons
3. Fumed Silica, etc.
4. Carbon Black

ISD 110 also meets the JSC outgassing requirements.[4] Except for SMRD 100F90, none of the other candidates chosen has been qualified to meet this standard. In a constrained layer joint the VEM is exposed only on the joint edges, so the geometry tends to minimize outgassing; encapsulation with a low-outgassing sealant could be used if outgassing were a problem. However, it is always advantageous if the VEM meets the JSC requirements.

Being a gum, ISD 110 has poor creep resistance. This is of doubtful importance, however, if the joint is structurally redundant.

Like all acrylics, ISD 110 has good UV resistance.

ISD 110 is normally supplied as thin sheets of material with wax paper on both surfaces. A joint can be made most readily by heating the joint plates with a hot air gun and applying layers of the ISD 110 until the desired thickness is attained. The ISD 110 must be rolled during application to break any air bubbles formed by entrapment. After the joint is assembled, soaking at 150°F for one hour has been found to improve the bond strength[9].

b) 3M EC 2216

EC 2216 is a flexible two-part, room-temperature-curing epoxy made by 3M for structural bonding purposes where high peel strength is required. Anatrol, Inc. has found that it will provide significant damping over an unusually broad temperature range.

The peak loss factor of EC 2216 at 1Hz has been found to be 0.14 at 66°F. Therefore, EC 2216 will not provide the extremely high damping of ISD 110, etc. However, a loss factor of 0.05-0.14 is seen from -10°F to 255°F at 10 Hz. It is unusual for a VEM to provide damping over such a broad temperature range. For this reason, EC 2216 was included as a VEM candidate.

EC 2216 requires a 31°C minimum temperature change to change the value of G' by one order of magnitude, which is excellent performance.

EC 2216 is an epoxy and is therefore more crosslinked and rigid upon cure than elastomeric or gummy VEMs. This tends to give the EC 2216 good creep resistance compared to other VEMs.

EC 2216 can be predicted to have poor outgassing properties. This is because it contains volatile flexibilizing agents.

The UV resistance of EC 2216 should be good, since it is a highly filled epoxy. The fillers have a shielding effect on the epoxy.

The processing characteristics of EC 2216 are very good. It is a two-part, room-temperature-curing epoxy paste. It can be readily injected into a joint and allowed to cure at room temperature.

c) DYAD 606

Soundcoat's Dyad 606 is a polyurethane-based VEM, intended for use in constrained-layer damping. It is supplied in the form of tough, cured sheets.

According to UDRI, Dyad 606 has a loss factor varying from 0.55 to 1.05 from 0.1 to 100 Hz at room temperature, which indicates excellent damping.

Dyad 606 is not a broad temperature range damper but appears to be a good choice for room temperature testing and instrument calibration. If used in LSS joints not subjected to temperature extremes, it would perform well.

Dyad 606 requires a 26°C minimum temperature change to change G' by one order of magnitude, which is acceptable.

Dyad 606 has not been tested for outgassing. As mentioned earlier, the exposed VEM edges could be encapsulated if Dyad 606 failed the outgassing test.

Dyad 606 has not been tested for creep, although creep is not an important consideration in a redundant joint. It is a strong, well-crosslinked elastomer, so it should have good creep resistance.

Polyurethanes, like Dyad 606, have good UV resistance. Fillers could be added if necessary or the joint could be encapsulated with an opaque sealant.

Processing Dyad 606 is not difficult. It is supplied in the form of cured sheets from the manufacturer. These cured sheets can be bonded in joints using an epoxy adhesive.

d) Hysol EA 9326

Hysol's EA 9326 is a two-part, room-temperature-curing polyurethane intended for use as a cryogenic adhesive. No data are available on its damping characteristics. However, previous experience with EA 9326 indicated that it showed a negligible increase in stiffness when it was taken from room temperature to -40°F.[5] This meant that EA 9326 had some promise as a broad temperature range damping material. Polyurethanes were known to have good damping, in general.

Upon cure, EA 9326 forms a very tough elastomer. It has not been tested for creep, but polyurethanes as hard as EA 9326 usually have good creep resistance.

EA 9326 has not been tested for outgassing. Outgassing should pose no great obstacles even if EA 9326 were to fail the JSC test requirements.

UV resistance of polyurethanes is good. Fillers could be added or the joint could be encapsulated if it were necessary to improve the UV resistance.

The processing ease of EA 9326 is very good. It is a two-part, room-temperature-curing polyurethane which can be readily injected into a joint. A primer, such as PRC 420, can be applied to the bonding surfaces to get increased joint strength.

e) G.E. SMRD 100F90

SMRD 100F90 is a commercial aerospace VEM supplied as cured sheet stock by G.E. It is epoxy-based and contains microballoons to lower the coefficient of thermal expansion. It is flexible, however, not rigid. According to Anatrol, Inc., it has a loss factor varying from 0.07 to 1.0 from 0.1-100 Hz, which indicates excellent damping.

SMRD 100F90 shows promise as a broad temperature range damper. The loss factor is at least 0.1 from -3°F to 110°F at 10 Hz.

SMRD 100F90 requires a 25°C temperature change to change the value of G' by one order of magnitude, which indicates good performance.

SMRD 100F90 has not been tested for creep resistance or UV resistance. It does pass the JSC outgassing requirements.

Joints are readily fabricated with SMRD 100F90. It is supplied as cured sheet stock which can be readily bonded into a joint.

f) G.E. RTV 630

RTV 630 is a two-part, room-temperature-curing silicone elastomer intended for use as an adhesive. No data are available on its damping characteristics. Previous experience with RTV silicones indicated that they showed a negligible increase in hardness or stiffness when taken from room temperature to -40°F.[s] The flexibility of silicone at low temperatures has been documented by other research.[e] This meant that RTV 630 had some promise as a broad temperature range damping material.

Upon cure, RTV 630 forms a tough elastomer. It should have good creep resistance, although it has not been tested.

RTV 630 has not been tested for outgassing.

RTV 630, like other silicone elastomers, should have good UV resistance.

RTV 630 processes readily. It is a two-part, room-temperature-curing silicone which can be easily injected into a joint. The catalyst is easily poisoned, so reactive or toxic materials including masking tape must be kept away from the joint during cure.

g) Rubber/Plastic Alloy I

By making an alloy of immiscible rubbers and plastics having differing glass transition points, a broad-temperature-range VEM can be made. Data by F. S. Owens[7] indicates that, with such alloys, a loss factor varying from 0.1 to 0.7 from -50 to 200°F at 100 Hz is possible (See Fig. 3). A loss factor peak is seen at each T_G.

MDAC-HB proposes to use an alloy composed of the following materials:

Material	T_G, °F
Butyl rubber (Enjay 268)	-50
Acrylonitrile rubber (Paracril-D)	60
Polyvinyl butyral plastic	130

These polymers are mixed on a heated rubber mill and certain additives are mixed in. Uncured rubber results. It can either (1) be vulcanized into the joint, or (2) a cured rubber sheet can be formed which is then bonded into the joint. MDAC-HB has all the equipment to do this and has successfully made rubber/plastic alloys before.

MDAC-HB predicts that the formulation above should give a loss factor varying from 0.1-0.7 from -75 to +150°F at 10 Hz. The shear storage modulus is estimated to be around 5000 psi at room temperature and 10 Hz.

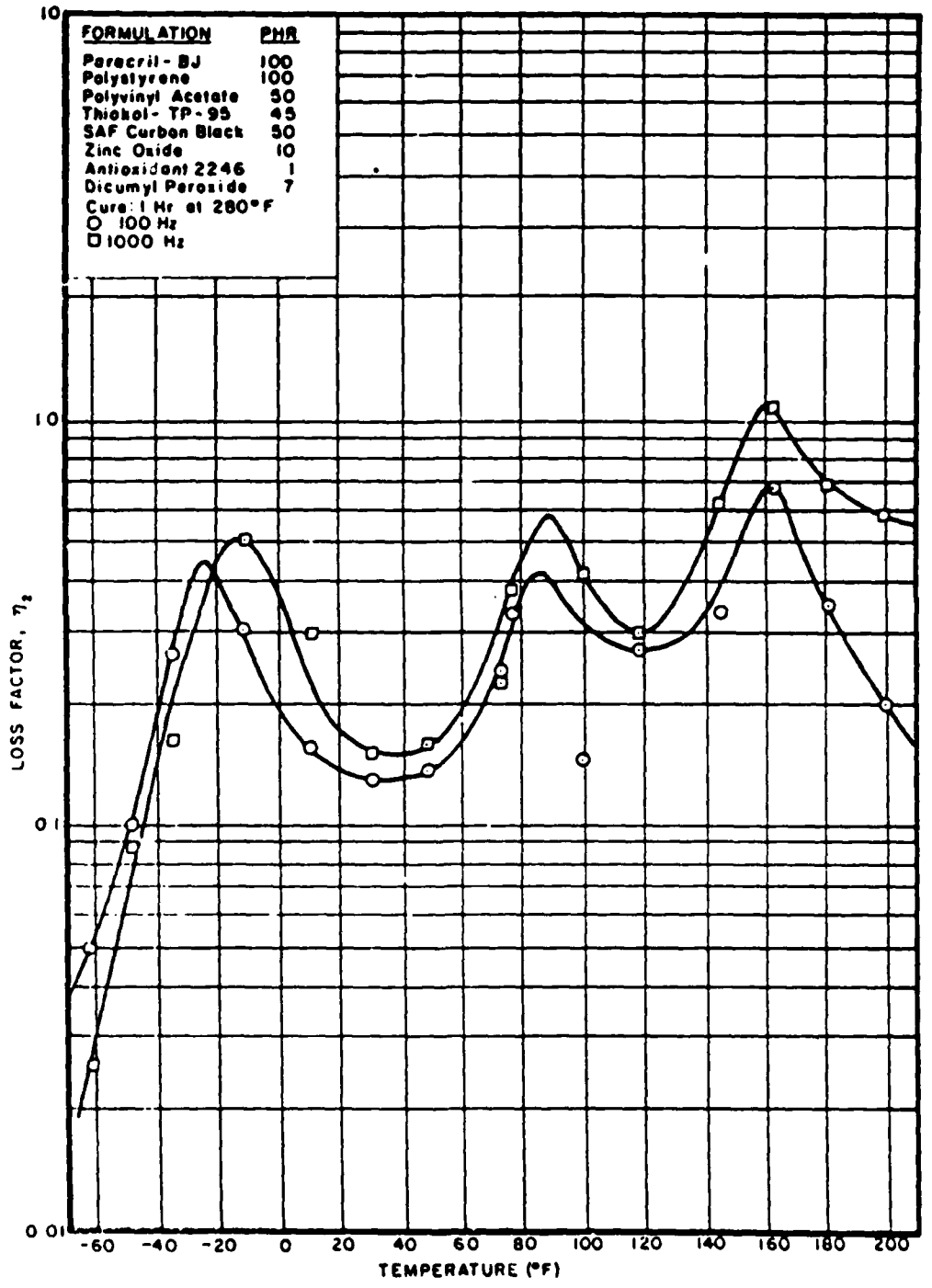

Figure 3. Loss Factor vs. Temperature of a Potential Low Temperature Damping Material

Rubber plastic alloys have not been tested for creep. They are strong, rigid materials, however, so they should have fair-good creep resistance.

Rubber/plastic alloys have not been tested for outgassing or UV resistance. Carbon black will be present in the formulation, which will give good UV resistance.

Processing of the rubber plastic alloys is not difficult. As mentioned above, the alloys can be bonded or vulcanized in place. Mixing on a heated mill is not difficult.

h,i) Rubber/Plastic Alloys II, III

These will be variations of the formulation for alloy I. Their compositions will be decided later.

4.0 JOINT DESIGN

The joint designs selected for testing are shown in Figures 2 and 4. They are of a double lap shear configuration. In this design, the VEM is placed in shear as the center plates move axially. In Figure 2, elastic elements have been added to prevent creep and add strength to the joint. To obtain a given spring rate, the shear area, VEM thickness and elastic element stiffness can be varied. Each of these topics will be discussed below.

4.1 JOINT PLATE SELECTION AND PROPERTIES

The materials and design selected for the LSS joint plates were based on earlier MDAC-HB work. MDAC-HB has done a great deal of work developing a graphite/epoxy truss structure for possible use on large space structures, such as SASP. A half scale truss was built, and its longerons were 0.065" thick. The laminate layup consisted of 10 plies of unidirectional graphite tape prepreg with a layer of graphite cloth prepreg on each face. In making the LSS joint plates, the number of unidirectional plies was increased to 22, so that the overall thickness would be about 0.125 inch. The actual thickness obtained was 0.150 inch. Table 3 gives information on the laminate layup and mechanical properties.

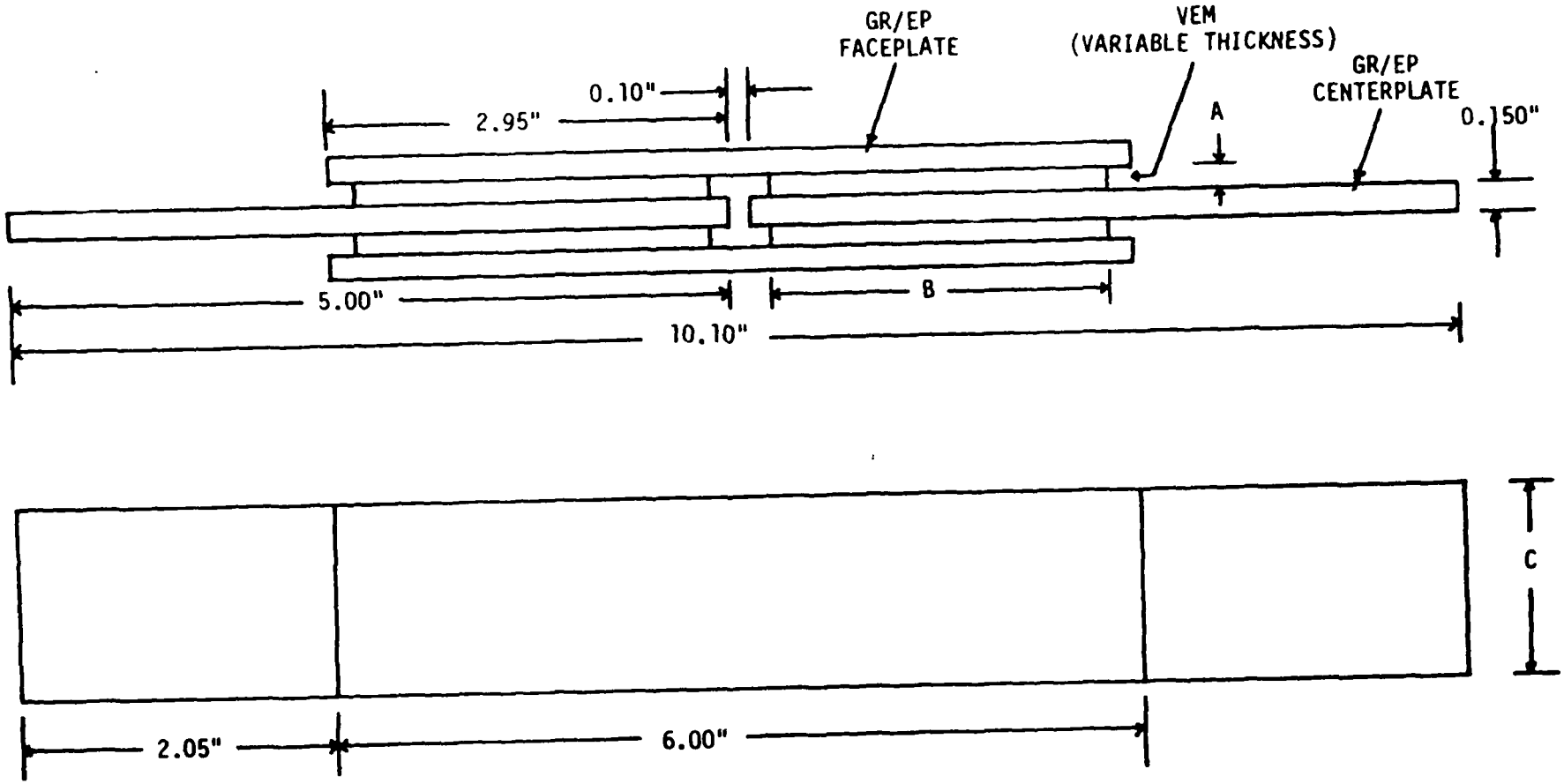

Figure 4. LSS Prototype Joint Without Elastic Elements

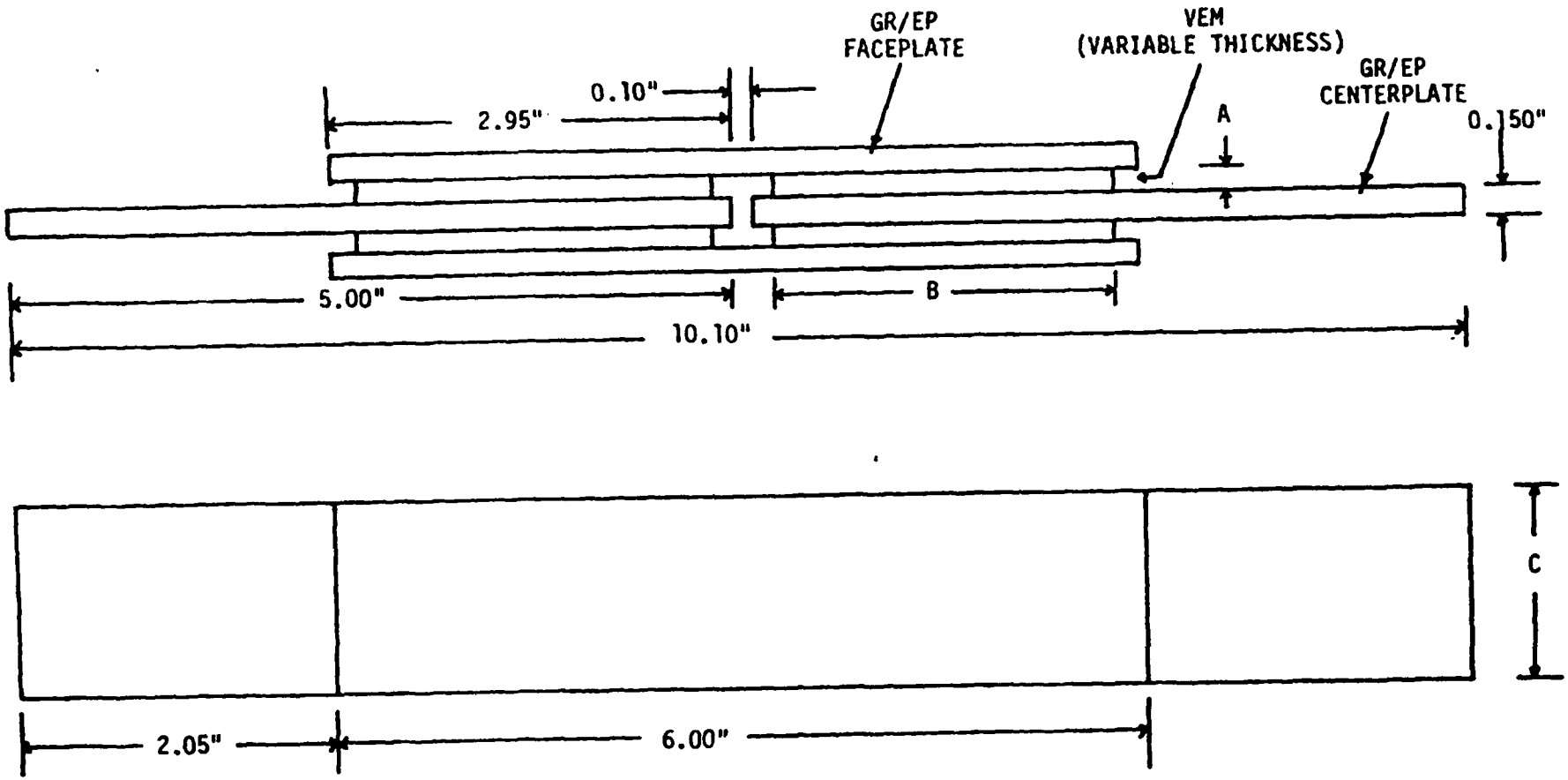

Figure 4. LSS Prototype Joint Without Elastic Elements

Table 3. GRAPHITE/EPOXY PROPERTIES

Average Thickness: 0.150"

Layup: $\pm 45_{1F}$, 0_{22}, $\pm 45_{1F}$ (Total of 24 plies)

Fabric: AS-1/3501-6

Unidirectional Tape: AS-4/3501-6

$E_L = 15.6 \times 10^6$ PSI

Ult. Tensile Strength = 135,000 psi

G = 600,000 psi

Density = 1.511 gm/cc

Graphite/epoxy was selected for the SASP truss and the LSS joints for several reasons:

1) The strength/weight and stiffness/weight ratios of graphite/epoxy are very high. This permits larger structures to be made from a given payload weight.

2) Graphite/epoxy composites have a coefficient of thermal expansion approaching zero. This helps the LSS remain dimensionally stable when sunlight heats some parts of it and not others.

3) The composites chosen pass JSC outgassing requirements.

4.2 JOINT CONFIGURATION

A double lap shear configuration was chosen (see Figure 4). To prevent creep and add strength, elastic elements (such as thin fiberglass sheets) could be added as in Figure 2. All of the joints shipped to GIT so far do not have elastic elements since testing should normally progress from the simple to the more complex. Joints with elastic elements are currently being made, however. Shims are included to prevent buckling of the thin elastic elements under compression.

The width of the joint was set at 1.50 inches, since this was equal to the width of the flat sections of the SASP longeron. The overall specimen length was limited to about 10 inches by the GIT test apparatus. GIT also requested a 1-2" grip length at each end.

Preliminary calculations indicated that the desired spring rate could be obtained using the configurations shown in Figures 2 and 4.

4.3 OPTIMIZING JOINT DESIGN

To optimize the conversion of mechanical energy to thermal energy in the LSS joints, it is necessary to maximize both the VEM strain energy and the VEM loss factor.

The highest VEM strain energy will be obtained if no elastic element is present and the VEM spring rate, K_{VEM}, approaches zero.

If an elastic element is present, the VEM strain energy can be maximized if the elastic element spring rate (K_{EL}) equals K_{VEM} and both approach zero.

In the MDAC-HB LSS joint design, there were two objectives:

1) The ultimate tensile strength of the joint was equal to 1/10 that of the longerons.

2) The VEM strain energy was to be optimized ($K_{VEM} = K_{EL}$). Since K_{EL} does not vary significantly with temperature changes, this meant K_{VEM}, and therefore the magnitude of the VEM shear modulus, had to remain as constant as possible when the temperature changed.

Preliminary calculations made it clear that elastic elements would generally be required to accomplish the first objective. Elastic elements would also eliminate creep.

The ultimate strength of a 0.125 x 1.50 inch longeron would be about 26,200 lbs. The elastic element should therefore have a strength of 2620 lbs. Two plies of unidirectional glass/epoxy (DMS 2191) which were 1.5 inches wide and each 0.0055 inch thick would provide 3280 lbs tensile strength. If the elastic elements were 1.00 inch long, K_{EL} would be 118,800 lb/in. K_{VEM} had to equal this if the VEM strain energy was to be maximized.

For K_{VEM} for the joint to equal 118,800 lb/in., the K_{VEM} for each joint end had to be twice that amount (237,600 lb/in.) since the joint ends act as springs in series.

K_{VEM} for a given joint end can be readily calculated.

$$K_{VEM} = \frac{G_M A}{t}$$

where

G_M = magnitude of VEM shear modulus = $[(G')^2 + (G'')^2]^{0.5}$

where G' = shear storage modulus, psi
G" = shear loss modulus, psi.

A = Shear area, in^2, of joint end

t = VEM thickness, in.

The preliminary calculations were performed using the shear storage modulus, G', to approximate G_M. An overlap distance of 3 inches at each joint end would provide 9 in^2 of shear area there. ISD 110 is reported to have a G' value of 250 psi (R.T., 1 Hz)[3]. The VEM thickness required to provide K_{VEM} = 237,600 lb/in. is readily calculated:

$$t = \frac{GA}{K} = \frac{250(9)}{237600} = 0.0094 \text{ in.}$$

The results for these calculations are shown in Table 4 for all of the LSS VEM candidates.

5.0 LSS VEM JOINT FABRICATION

The joints were fabricated without elastic elements using the processing methods described in paragraph 3.0. Two specimens each were made of all VEM specimens except the rubber/plastic alloys. Joints with elastic elements and the rubber/plastic alloy joints will be made in the second contract year. Removable shims had to be used in some specimens to obtain the desired VEM thickness. This resulted in shear areas less than 9 in^2 per end for certain specimens.

In the preparation of all joints, the bonding surfaces of the graphite/epoxy were lightly scuff-sanded with 400 grit paper and lightly solvent wiped with MEK. Primers were used as necessary.

The Dyad 606 and SMRD 100F90 specimens were made by bonding sheet stock to the plates with epoxy adhesives. A 4 mil glass scrim cloth was used for bondline control in these cases. This prevented all of the epoxy from being squeezed out of the bond line when weights or clamps were applied to the specimens during the bonding process. This scrim cloth should have no effect on the joint behavior.

The ISD 110 specimens were made by building up plies of ISD 110 to the desired thickness using a hot air gun. Air bubbles were rolled out. The specimens were then soaked 16 hours at 150°F with 10 pounds of weight on them.

Injection was used to make the EC 2216, EA 9326 and RTV 630 specimens. The plates were clamped together with shims and then the degassed VEM was injected

Table 4. DESIGN PARAMETERS USED FOR VEM JOINT SIZING
(Target Stiffness = 118,800 lb/in)

Material	G', psi	Thickness, in.	Overlap Area, in^2	Overlap Distance, in.	Comments
ISD 110	250	0.008	7.60	2.53	Available in 2 mil film only, which may be plied up.
ISD 110	250	0.010	9.50	3.17	
EC2216	3200	0.120	8.91	2.97	
DYAD 606	2000	0.020	2.38	0.792	Available only in 20 and 50 mil thicknesses.
DYAD 606	2000	0.050	5.94	1.98	
EA 9326	1500	0.055	8 71	2.90	
SMRD 100F90	1600	0.060	8.91	2.97	
RTV 630	131	0.004	7.25	2.42	
RTV 630	131	0.005	9.07	3.02	
Rubber/Plastic Alloy I	5000	0.189	9.00	3.00	

using a Semco gun. The EA 9326 plates were primed with PRC 420 and the RTV 630 plates were primed with DC 1200. No primer was used for the EC 2216 specimens.

After bonding, a 0.100" gap was carefully drilled out between the two center plates so they could move longitudinally with no interference (See Fig. 4).

6.0 TESTING AND RESULTS

The ISD 110 and EC 2216 joints were tested in a slightly different way from the other joints, so their results will be reported separately.

6.1 TESTING AND RESULTS FOR ISD 110 AND EC 2216

The specimens were tested in an Instron tensile test machine set for cyclic loading before being sent to GIT for in-depth testing. All specimens were tested at room temperature (75°F). Two joints each were made of ISD 110 and EC 2216. The VEM layer dimensions are listed in Table 5. A, B and C refer to the VEM layer thickness, length and width, respectively (see Fig. 4). The width, in all cases, is close to 1.5 inches.

The joints were deflected 5 mils in tension and then returned to zero deflection (see Fig. 5a).

This cyclic loading was repeated about 5 times (see Figs. 6-7). The target test frequency was 0.1 Hz, but machine elasticity dropped this to 0.0354-0.0666 Hz. The cycling was linear, not sinusoidal.

The joints were sized to give overall spring rates of 118,800 lb/in. at 1 Hz and 70°F. Anatrol data were used for this sizing(*).

In testing, the extensiometer was attached as shown in Fig. 8a. The deflection measured was the sum of the VEM and faceplate strains. The sideplate strain was calculated and considered negligible (0.00022 in. for the EC 2216 specimens). The calculated center plate elongation was not considered negligible (0.000438 in. for EC 2216 specimens).

Table 5. JOINT VEM LAYER DIMENSIONS

Material	No.	Average VEM Layer Dimensions, in.			Total VEM Area, in^2
		Thickness, A	Length, B	Width, C	
3M ISD 110 Acrylic	1	0.0062	2.94	1.520	17.85
3M ISD 110 Acrylic	2	0.0051	2.96	1.520	17.97
3M EC 2216 Epoxy	3	0.1260	2.80	1.510	16.93
3M EC 2216 Epoxy	4	0.1270	2.83	1.500	16.99
DYAD 606 Polyurethane	5	0.0515	1.97	1.491	11.75
DYAD 606 Polyurethane	6	0.0515	1.96	1.501	11.77
EA 9326 Polyurethane	7	0.0480	2.67	1.514	16.17
EA 9326 Polyurethane	8	0.0505	2.72	1.508	16.38
SMRD 100F90 Epoxy	9	0.0580	2.74	1.388	15.21
SMRD 100F90 Epoxy	10	0.0580	2.76	1.400	15.45
RTV 630 Silicone	11	0.0073	2.64	1.506	15.90
RTV 630 Silicone	12	0.0063	2.62	1.506	15.78

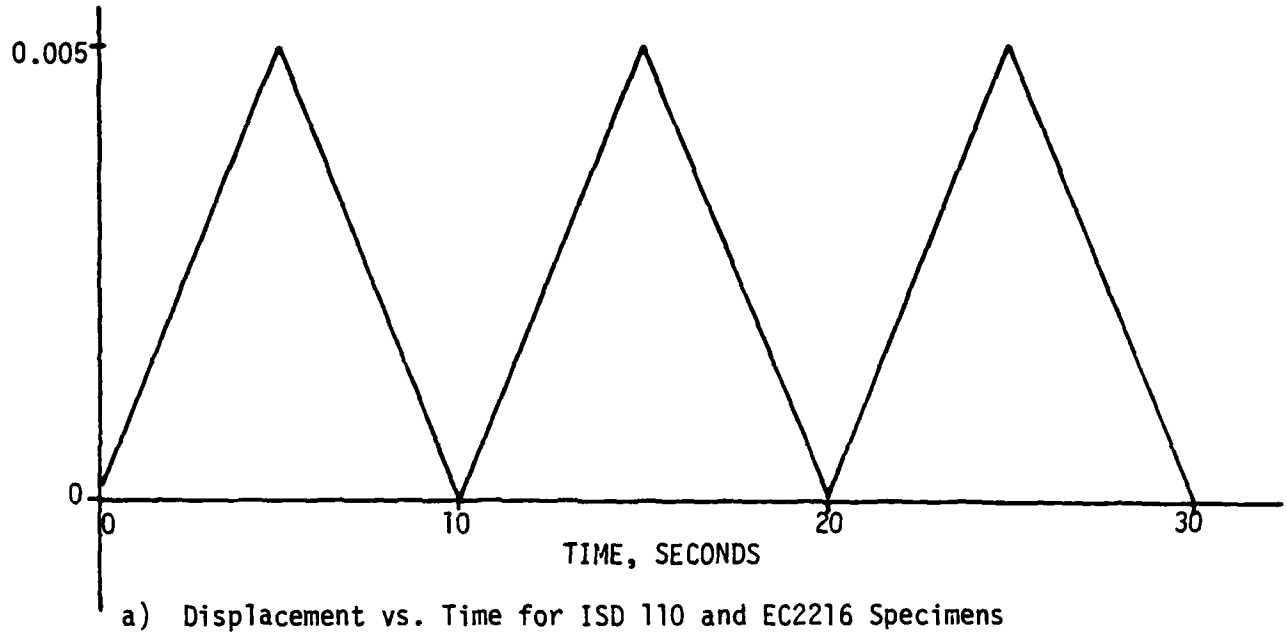

a) Displacement vs. Time for ISD 110 and EC2216 Specimens

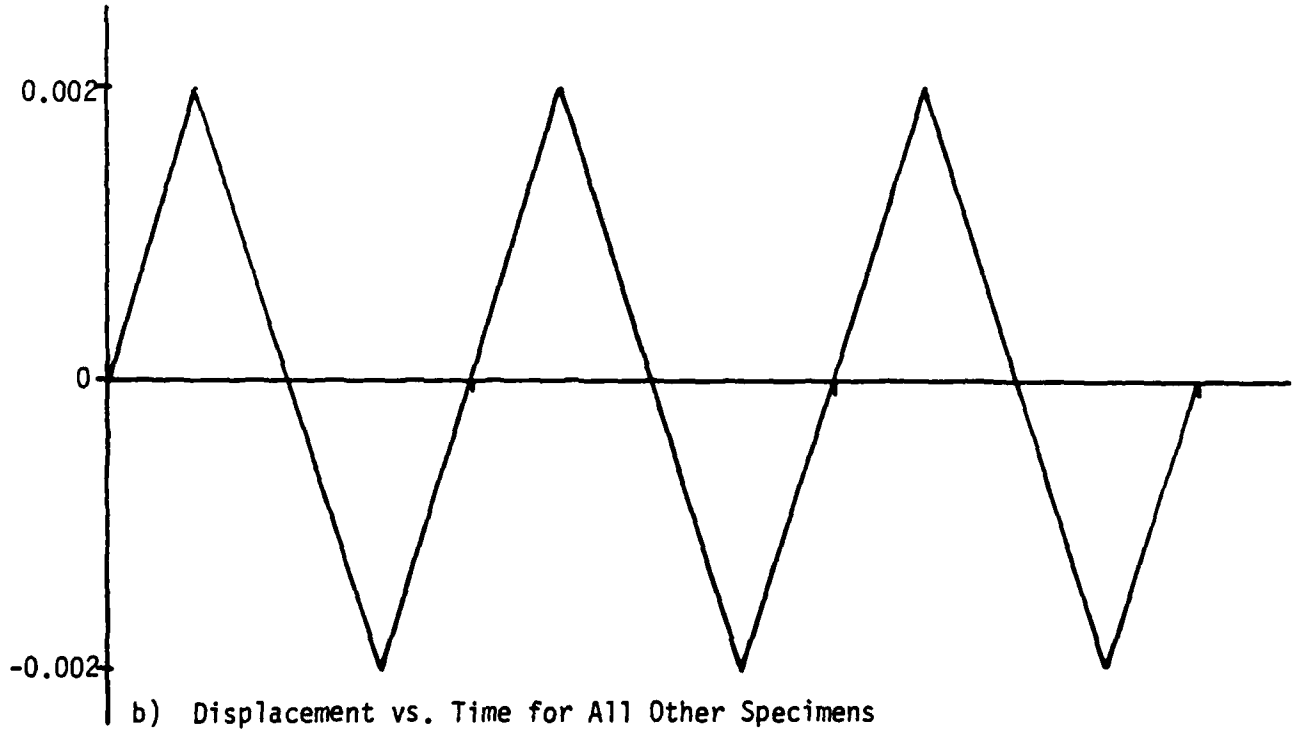

b) Displacement vs. Time for All Other Specimens

Figure 5. Displacement vs. Time

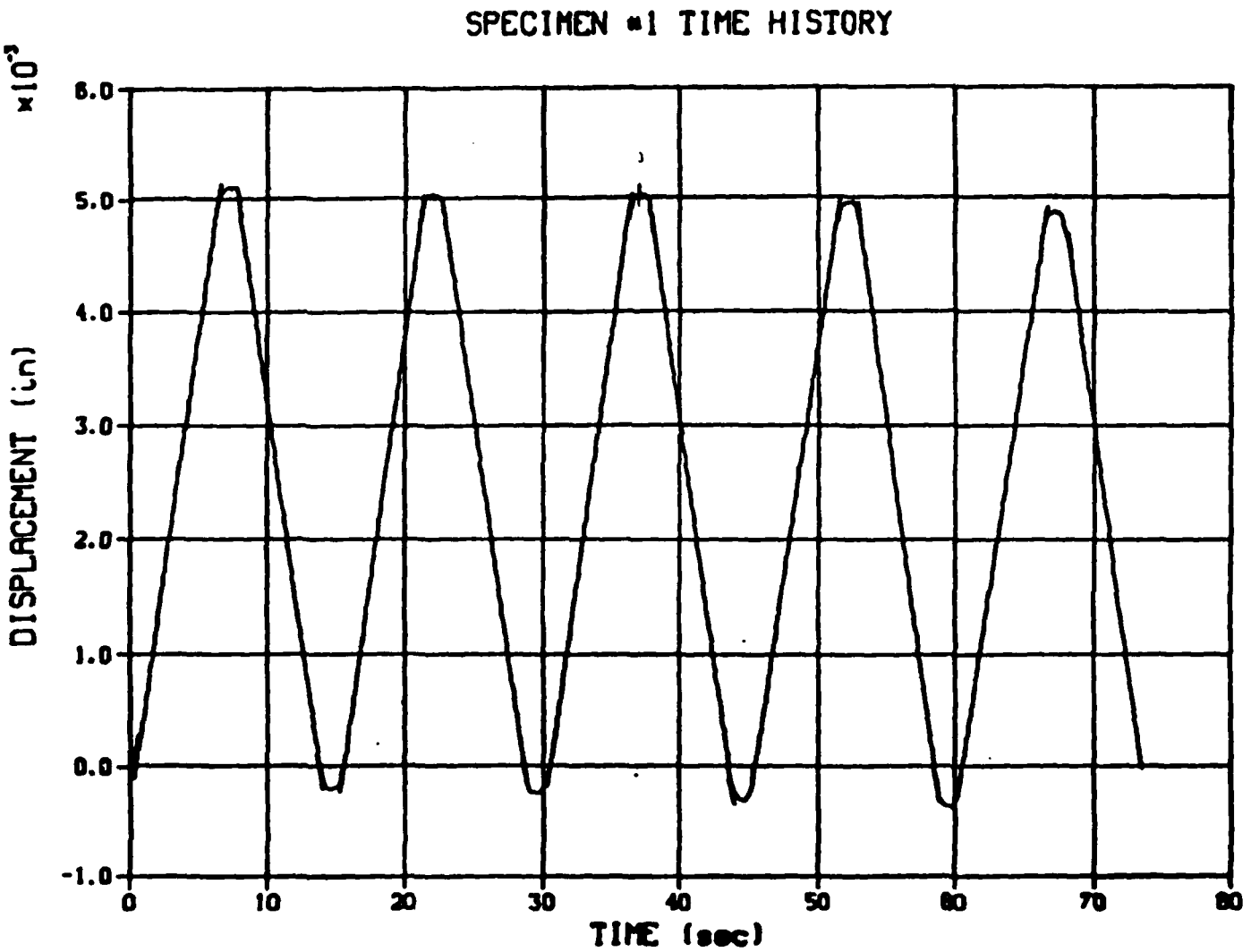

FIGURE 6. DISPLACEMENT VS. TIME (ISD 110 JOINT, SPECIMEN 'A)

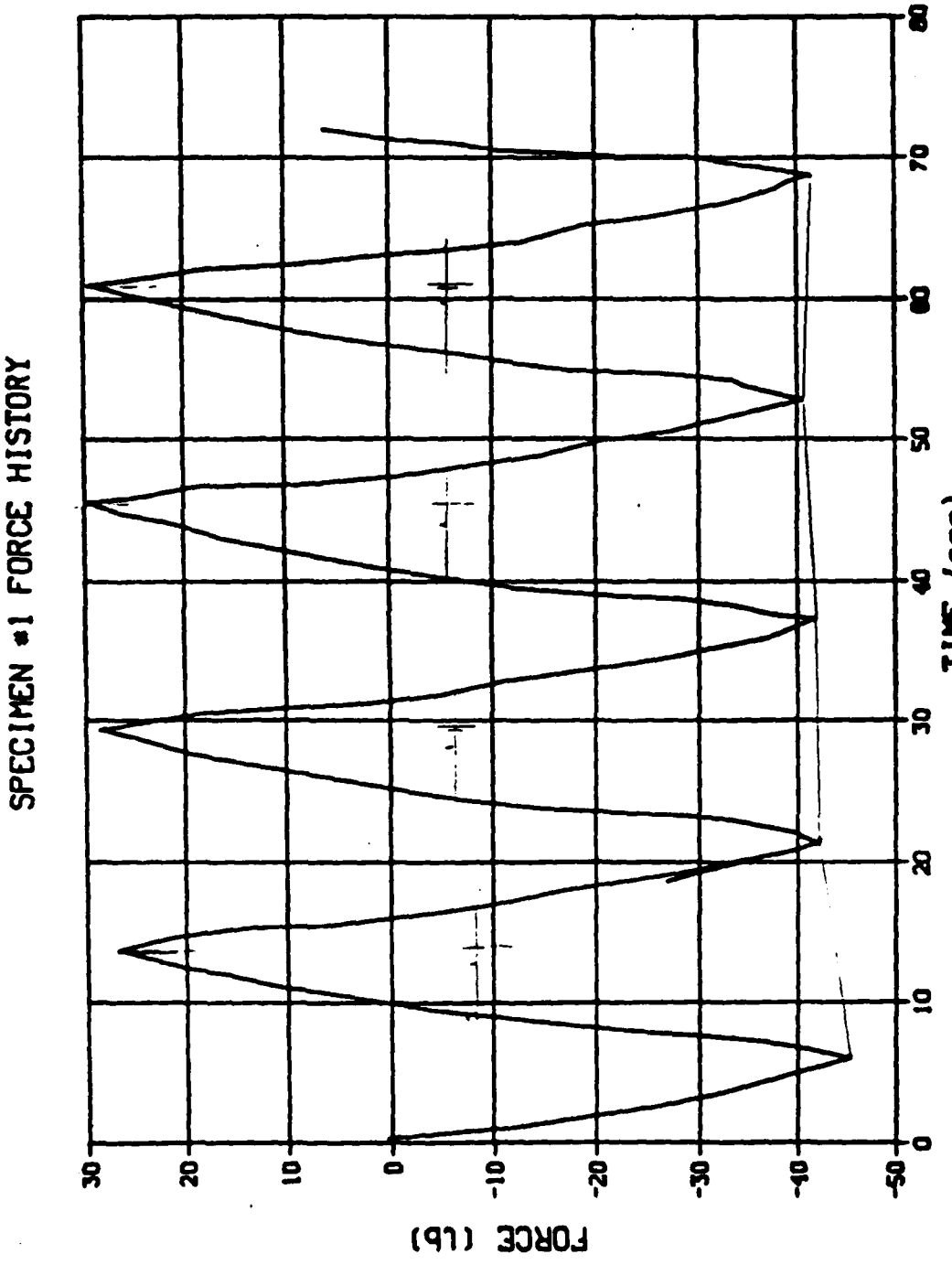

FIGURE 7. FORCE VS. TIME (ISD 110 JOINT, SPECIMEN A)

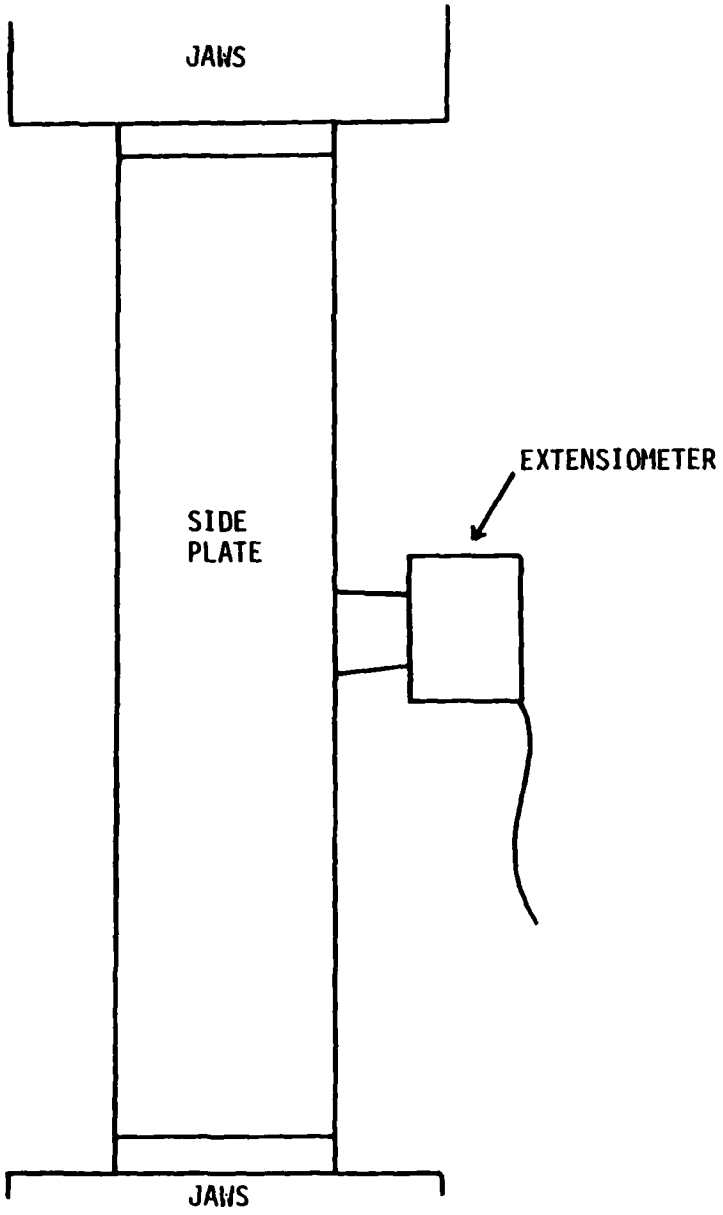

a) Extensiometer Setup for ISD 110, EX2216

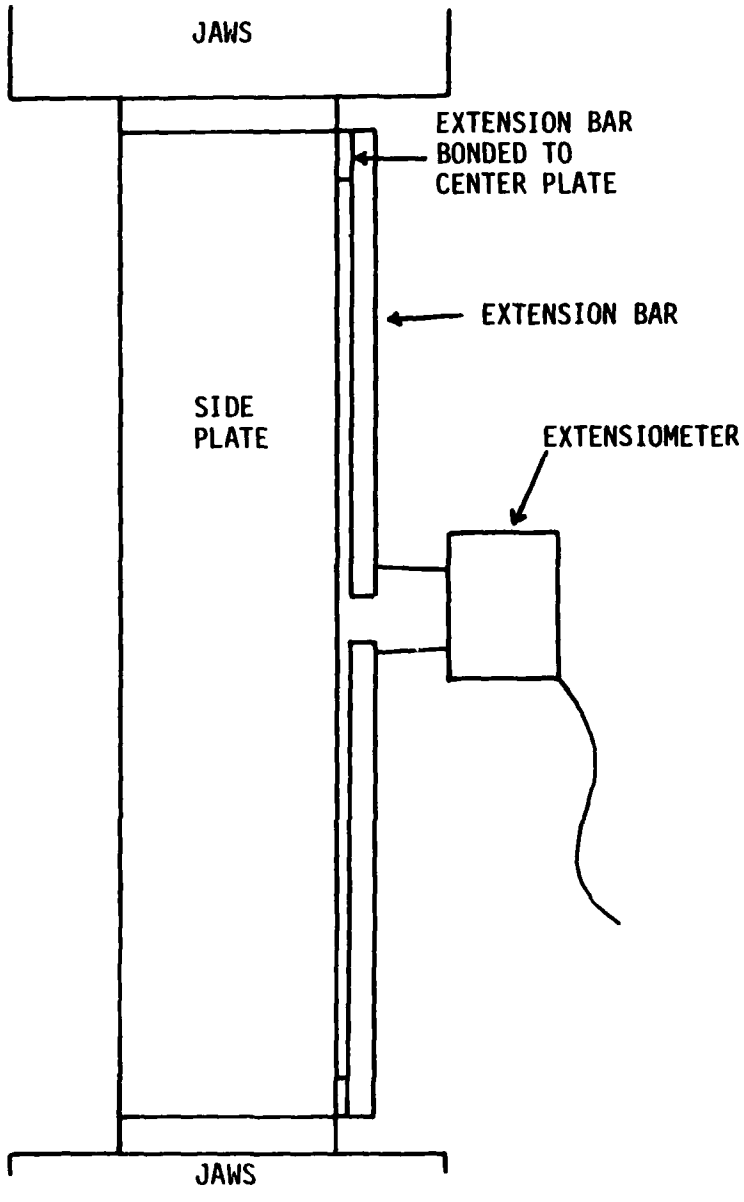

b) Extensiometer Setup for All Other Specimens

Figure 8. Extensiometer Setups

The overall joint spring rates measured for the specimens are listed in Table 6. The overall joint spring rate, corrected to add the center plate strain, is also listed. This latter spring rate is what would have been obtained if the extensiometer had measured the clamp separation distance.

The theoretical spring rates for our specimens are also presented in Table 6. Our results for EC 2216 agree well with those predicted using Anatrol data. The spring rates for ISD 110 were found to be about half those predicted using UDRI data. The UDRI data, however, had to be extrapolated a great deal to obtain values for 0.06 Hz, so they are not judged very reliable. There were undoubtedly some small air bubbles in the ISD 110 specimens, which could also have lowered the spring rate perhaps 10%.

The spring rates are less than 118,800 lb/in., because they were tested at a much lower frequency than 1 Hz.

The loss factors, η, were calculated using the equation

$$\eta = \tan \theta,$$

where θ is the number of degrees strain lagged force.

G_M was calculated using

$$G_M = \frac{Kt}{A}$$

Once G_M and η were known, G' and G" were readily calculated using the relations below:

$$\eta = G"/G'$$

$$G_M = [(G')^2 + (G")^2]^{0.5}$$

These results are shown in Table 7. The loss factors for EC 2216 and ISD 110 agreed well with those determined by UDRI and Anatrol, Inc. G' and G" for EC 2216 agreed well with Anatrol's data. G' and G" for ISD 110 were found to be about half those predicted using UDRI data. The UDRI data, however, had to

Table 6. ACTUAL & THEORETICAL SPRING RATES FOR MDAC-W TEST JOINTS
(ISD 110, EC 2216)

Material	No.	Frequency Hz	Force Lbs.	Deflection, Total, In.	Joint Spring Rate, lb/in. w/o K_{cp}** MDAC (Measured)	w/o K_{cp}** UDRI	w/o K_{cp}** Anatrol	w/ K_{cp}** MDAC (Calc.)	w/ K_{cp}** UDRI	w/ K_{cp}** Anatrol
ISD 110	1	0.0666	40	0.005	8,000	14,970*	--	7,874	14,537*	--
ISD 110	2	0.0645	45	0.005	9,000	18,322*	--	8,841	17,676*	--
EC 2216	3	0.0354	440	0.005	88,000	--	103,595*	74,862	--	85,857*
EC 2216	4	0.0410	415	0.005	83,000	--	113,278*	71,212	--	92,403*

*Extrapolated Values of G' and G" Used in Calculation.

**K_{cp} = Graphite/Epoxy Centerplate Spring Rate Contribution

Table 7. ACTUAL & THEORETICAL DAMPING PROPERTIES OF MDAC-W TEST JOINTS (ISD 110, EC2216)

Material	No.	Frequency Hz	G'			G"			G_M			η		
			MDAC	UDRI	ANATROL	MDAC	UDRI	ANATROL	MDAC	UDRI	ANATROL	MDAC	UDRI	ANATROL
ISD 110	1	0.0666	8.99	17.4*	--	6.52	11.3*	--	11.11	20.8	--	0.725	0.65*	--
ISD 110	2	0.0645	8.02	17.4*	--	6.31	11.3*	--	10.21	20.8	--	0.787	0.65*	--
EC 2216	3	0.0354	2518	--	3050*	720	--	458*	2619	--	3084	0.286	--	0.15*
EC 2216	4	0.0410	2413	--	3350*	574	--	503*	2481	--	3387	0.238	--	0.15*

*Extrapolated

be extrapolated a great deal to obtain values for 0.06 Hz, so they are probably not very reliable. Again, air bubbles in the ISD 110 specimens could have lowered the moduli perhaps 10%.

6.2 TESTING AND RESULTS FOR OTHER SPECIMENS

This section covers testing and results of joints other than ISD 110 and EC 2216. Two joints of each material were tested at room temperature (75°F). The preliminary, target VEM pad areas and thicknesses are listed in Table 4, and the actual sizes used are summarized in Table 8.

The joints were deflected 2 mils in tension, passed through zero, and then were deflected 2 mils in compression (see Fig. 5b). The cycling was linear, not sinusoidal. This cyclic loading was repeated about 10 times. The target test frequency was 0.1 Hz, but machine elasticity decreased this to as low as 0.069 Hz. Hysteresis loops were also obtained (see Annex B).

The joints were sized to give overall spring rates of 118,800 lb/in. at 1 Hz and 70°F Anatrol and UDRI data were used for this sizing.

In testing, the extensiometer was attached as shown in Fig. 8b. The deflection measured was the sum of the VEM, sideplate and centerplate strains. Again, the sideplate strains were negligible compared to the centerplate strains.

The overall joint spring rates measured for the specimens are listed in Table 8. The overall joint spring rate, corrected to subtract the center plate strain, is also listed. This latter spring rate is what would have been measured if the center plates had been inflexible.

The actual and theoretical values for G_M are presented in Table 9. The theoretical G_M values were calculated using Anatrol and G.E. data for the Dyad 606 and SMRD 100F90, respectively. The actual G_M values were about 2 to 4 times as stiff as predicted. This is not surprising, since the Anatrol and G.E. data had to be extrapolated a great deal to obtain values for 0.07-0.11 Hz.

The loss factors are presented in Table 9. They were calculated using the equation below:

Table 8. ACTUAL AND THEORETICAL SPRING RATES FOR MDAC-HB TEST JOINTS
(DYAD 606, EA 9326, SMRD 100F90, RTV630)

Material	Specimen	Frequency, Hz	Max. Load, lbs	Deflection, ± in.	Area, End, in^2	VEM Thickness in.	Spring Rate, lb/in.			
							Overall	Overall*	End	End*
DYAD 606	5	0.0795	72	0.00210	5.87	0.0515	34300	36800	68600	73600
DYAD 606	6	0.0740	78.9	0.00208	5.89	0.0515	38000	41000	75900	82100
EA 9326	7	0.0698	356	0.00205	8.09	0.0480	174000	265000	347000	530000
EA 9326	8	0.1107	326	0.00212	8.19	0.0505	154000	222000	308000	444000
SMRD 100F90	9	0.0878	127	0.00208	7.61	0.0580	61000	67000	122000	134000
SMRD 100F90	10	0.0768	164	0.00204	7.73	0.0580	80500	96000	161000	192000
RTV 630	11	0.103	84.5	0.00206	7.95	0.0073	41000	44700	82000	89300
RTV 630	12	0.109	78.5	0.00199	7.89	0.0063	39500	42800	78900	85600

*Corrected for GR/EP Plate Spring Rate

Table 9. ACTUAL AND THEORETICAL DAMPING PROPERTIES OF MDAC-HB TEST JOINTS
(DYAD 606, EA 9326, SMRD 100F90, RTV 630)

Material	Specimen	Frequency, Hz	Loss Factor*			G', psi			G", psi			Actual G_M, psi	Actual G_M,** psi	G_M, psi	
			Actual	UDRI	GE	Actual**	UDRI	GE	Actual**	UDRI	GE			UDRI	GE
DYAD 606	5	0.0795	0.249	0.53	--	627	143	--	156	76.1	--	602	646	165	--
DYAD 606	6	0.0740	0.249	0.51	--	697	138	--	173	70.3	--	664	718	155	--
EA 9326	7	0.0698	0.0229	--	--	3150	--	--	72	--	--	2060	3150	--	--
EA 9326	8	0.1107	0.0223	--	--	2740	--	--	61	--	--	1900	2740	--	--
SMRD 100F90	9	0.0878	0.109	--	0.57	1010	--	399	110	--	227	930	1020	--	459
SMRD 100F90	10	0.0768	0.0961	--	0.57	1430	--	399	138	--	227	1210	1440	--	459
RTV 630	11	0.103	0.0375	--	--	81.9	--	--	3.1	--	--	75.3	82.0	--	--
RTV 630	12	0.109	0.0422	--	--	68.3	--	--	2.9	--	--	63.0	68.4	--	--

*Calculated using $\eta = \frac{\text{work}}{2\pi(\text{stiffness})\left(\frac{\text{total deflection}}{2}\right)^2}$, where stiffness = max. load/max. deflection

and work = hysteresis loop area, in-lbs

**Corrected for GR/EP spring rate

$$\eta = \frac{\text{Work}}{2\pi(\text{Stiffness})(\text{Total Deflection}/2)^2}$$

where work = hysteresis loop area, in-lb

stiffness = maximum load/maximum deflection

G' and G" were calculated as in Paragraph 6.1.

The results are shown in Table 9. The loss factors are 1/4 to 1/2 those predicted from Anatrol and G.E. data. G' and G" were 2 to 4 times as stiff as predicted. Again, this is not surprising, since the Anatrol and G.E. data had to be extrapolated so far to obtain values for 0.07-0.11 Hz.

7.0 CONTROL SPECIMENS

Two graphite/epoxy control specimens (specimens 13, 14) were made and sent to GIT. No testing was done on them at MDAC-HB.

Specimen 13 consisted of a simple, solid bar of graphite/epoxy, cut from the same laminate the joint plates were cut from. Its dimensions are given in Table 10.

Specimen 14 was a standard double lap shear specimen (see Fig. 4), but it was bonded together with a thin layer of highly rigid epoxy (EA 956). Its dimensions are also given in Table 10. Standard 0.150 inch graphite/epoxy plate stock was used to construct it.

Table 10. CONTROL SPECIMEN DIMENSIONS

Specimen Number	Specimen Type	Adhesive			Overall Specimen Dimensions, in.
		Thickness, in.	Overlap, in.	Total Area in^2	
13	GR/EP Bar, Solid	--	--	--	0.148 x 1.503 x 9.988
14	Double Lap Shear, Bonded with EA956 Epoxy	0.022	2.925	17.43	0.150 x 1.490 x ≈10.1

REFERENCES

1. R. W. Trudell, R. C. Curley, L. C. Rogers, "Passive Damping in Large Precision Space Structures," Paper No. AIAA-80-0677-CP. Presented at the AIAA/ASME/ASCE/AHS 21st Structures, Structural Dynamics & Materials Conference, Seattle, WA, May 12-14, 1980.

2. ASTM E 595-77, "Total Mass Loss and Collected Volatile Condensible Materials from Outgassing in a Vacuum Environment," American Society for Testing and Materials, 1977.

3. M. L. Drake and G. E. Terborg, "Polymeric Material Testing Procedures to Determine Damping Properties and the Results of Selected Commercial Materials," Air Force Materials Laboratory Report AFWAL-TR-80-4093, July 1980.

4. Anon, "Compilation of VCM Data of Nonmetallic Materials," NASA-JSC Report JSC 08962, Rev. U and Addendums 1-9, May 1979-Aug. 1982.

5. C. E. Blevins, "Test Report - MMS Compliant Elevation Gear Elastomer Development," MDAC-W MDC H1006, Dec. 1983.

6. C. T. Coote, "Measurement of the Damping Properties of Silicone-Based Elastomers over Wide Temperature Ranges," Journal of Sound and Vibration, Vol. 21, Part 2, pp. 133-147, 1972.

7. F. S. Owens, "Wide Temperature-Range Free-Layer Damping Materials," Air Force Materials Laboratory Report AFML-TR-70-242, Dec. 1970.

8. A. D. Nashif, "Control of Noise and Vibration with Damping Materials," Sound and Vibration Magazine, Vol 17, Number 7, pp 28-36, 1983.

APPENDIX I

ANNEX A

SPECIMEN 15-17 DEVELOPMENT

1.0 OBJECTIVE

Since most VEMs are soft materials they generally have poor creep resistance, and structural redundancy is needed. MDAC-HB has designed, built and tested three prototype joints so far (15, 16, 17) which have redundant, elastic elements. These joints were recently sent to GIT for testing. Joints 1-14 did not contain elastic elements.

The following topics will be discussed in this appendix:

a) Elastic Element Joint Design (2.0)
b) Elastic Element Joint Fabrication (3.0)
c) MDAC-HB Testing and Results (4.0)

2.0 ELASTIC ELEMENT JOINT DESIGN

MDAC-HB decided to implement the elastic restoring elements in the form of two fiberglass strips running the length of each specimen (see Figure 2, Appendix I).

The fiberglass strips were made using epoxy/fiberglass (DPM 4700, STM0043-03, American Cyanamid). The properties of this material are listed in Table 1. The fiberglass strips used in the joints were 0.0235 inch thick, 1.5 inches wide, and ran the length of each specimen. The fiberglass was rigidly bonded to the graphite/epoxy centerplates except for a 1-inch section in the center. This 1-inch section acted as the elastic element.

Nonadhering shims were placed on both sides of the elastic elements to prevent buckling of the elements under compression.

The combined spring rate for the two pieces of fiberglass is readily calculated:

$$K_{EL} = \frac{EA}{\ell} = \frac{(3 \times 10^{-6})(2)(1.5)(0.0235)}{1} = 211{,}500 \text{ lb/in.}$$

To optimize the strain energy, K_{VEM} (overall) must equal K_{EL}. K_{VEM} at each end of the joint must be 2(211,500) = 423,000 lb/in. A stiff VEM such as

EC 2216 (G_M = 2,600 lb/in. at 0.1 Hz, 22°C) must be used. Assume that each VEM layer measures 2.5 inches long and 1.5 inches wide. The required VEM thickness to obtain K_{VEM} = 423,000 lb/in. can be readily calculated:

$$t = \frac{G_M A}{K} = \frac{2600\ (1.5)(2.5)(2)}{423{,}000} = 0.0460 \text{ inch}$$

3.0 ELASTIC ELEMENT JOINT FABRICATION

All bonding surfaces of the graphite/epoxy plates and elastic elements were lightly scuff sanded with 400 grit paper and lightly solvent wiped with MEK. No primers were used.

The two centerplates were first bonded to the elastic element strips with EA 956 epoxy. A 4 mil glass scrim cloth was used for bondline control. A nonadhering shim was inserted between the elastic elements in the 1 inch elastic center section before bonding. Two specimens (15 and 16) were made with silicone rubber shims. One specimen (17) was made with graphite/epoxy and aluminum shims, to offer even more support against buckling. A small elastic pad was placed at the end of each rigid shim so that axial movement (±0.007") would be possible. The adhesive was allowed to cure before proceeding to the next step.

The sideplates were then clamped to the bonded assembly with shims. The degassed EC 2216 was injected using a Semco gun. Again, nonadhering shims were inserted in the 1-inch center section before bonding.

The VEM layer dimensions actually achieved were close to the target dimensions. A VEM thickness of 0.0573-0.0615 inch was achieved with a 2.29-2.32-inch overlap (Table 2).

4.0 MDAC-HB TESTING AND RESULTS

A cyclic load/deflection test was performed at 75°F on each joint in an Instron test machine. The joints were deflected ±2 mils. This cyclic loading was repeated about 10 times with a target test frequency of 0.1 Hz. The actual test frequency range from 0.116-0.144 Hz. Hysteresis loops were also generated.

In testing, the extensiometer was attached to the centerplates near where the grip area started, 2 inches from the end. The deflection masured was, therefore, the sum of the centerplate and elastic element strains.

The overall joint spring rates measured for our specimens are listed in Table 2. The overall joint K_{VEM} is also listed. K_{VEM} is obtained by subtracting the centerplate and elastic element spring rate contribution from the overall spring rate.

G_M was calculated for each specimen once K_{VEM} was known; η was obtained from hysteresis loop areas using:

$$\eta = \frac{\text{Work}}{2\pi(\text{Stiffness})\left(\frac{\text{Total Deflection}}{2}\right)^2}$$

where stiffness = max. load/max. deflection
work = hysteresis loop area, in/lbs.

The hysteresis loops are shown in Figures 1-3.

G_M and η are listed in Table 3. Once G_M and η were known, G' and G" were calculated using the following equations:

$$\eta = G''/G'$$

$$G_M = [(G')^2 + (G'')^2]^{0.5}$$

G' and G" are also listed in Table 3, along with extrapolated values for G_M, G', G" and η from some Anatrol data. The test values for G_M, G' and η agree well with the Anatrol data. G" for specimens 16 and 17 is low.

The apparent variation in specimen properties may be caused by slight variations in fabrication or testing. A slight misalignment of the elastic element could change its apparent spring rate, for instance. Shim type did not have any apparent effect on damping or moduli.

TABLE 1

FIBERGLASS ELASTIC ELEMENT PROPERTIES

Glass Fabric:	MIL-C-9084, TY VIII B (#181 Cloth)
Epoxy Resin:	MIL-R-9300
Ult. Tensile Strength	50,000 psi
Tensile Modulus	3.0×10^6 psi
Ult. Flexural Strength	55,000 psi
Flexural Modulus	3.2×10^6 psi
Ult. Compressive Strength, Edgewise	50,000 psi
Interlaminar Shear Strength	3,000 psi
Density	1.72 GM/CC

TABLE 2

LSS PROTOTYPE JOINTS WITH ELASTIC ELEMENT: TEST MEASUREMENTS

SPECIMEN	VEM	SHIM TYPE	VEM LAYER DIMENSIONS, IN			AREA, END, IN^2	FREQUENCY, HZ	AVERAGE		SPRING RATE	
			THICKNESS	LENGTH	WIDTH			LOAD, LB.	DEFLECTION, IN.	OVERALL LB./IN.	K_{VEM}* LB./IN.
15	EC 2216	Silicone Rubber	0.0573	2.32	1.497	6.95	0.116	925	±0.00179	516,759	354,227
16	EC 2216	Silicone Rubber	0.0582	2.30	1.490	6.86	0.141	780	±0.00199	391,959	229,427
17	EC 2216	GR/EP, Aluminum	0.0615	2.29	1.502	6.88	0.144	750	±0.00195	384,615	222,083

*$K_{VEM} = K_{OVERALL} - \frac{K_{CP} K_{EL}}{K_{CP} + K_{EL}}$, Where K_{CP} = GR/EP Centerplate Spring Rate = 702,000 lb/in; K_{EL} = 211,500 lb./in;

$K_{VEM} = K_{OVERALL}$ - 162,532 lb./in.

TABLE 3

LSS PROTOTYPE JOINTS WITH ELASTIC ELEMENT: CALCULATED DAMPING RESULTS

SPECIMEN	VEM	G_M*, PSI	G'*, PSI	G"*, PSI	η	ANATROL RESULTS** G_M PSI	G' PSI	G" PSI	η
15	EC 2216	5840	5762	950	0.165	5090	5000	950	0.140
16	EC 2216	3893	3863	483	0.125	-	-	-	-
17	EC 2216	3970	3942	473	0.120	-	-	-	-

* USING K_{VEM}

**FOR 0.1 Hz, 75 F (Extrapolated).

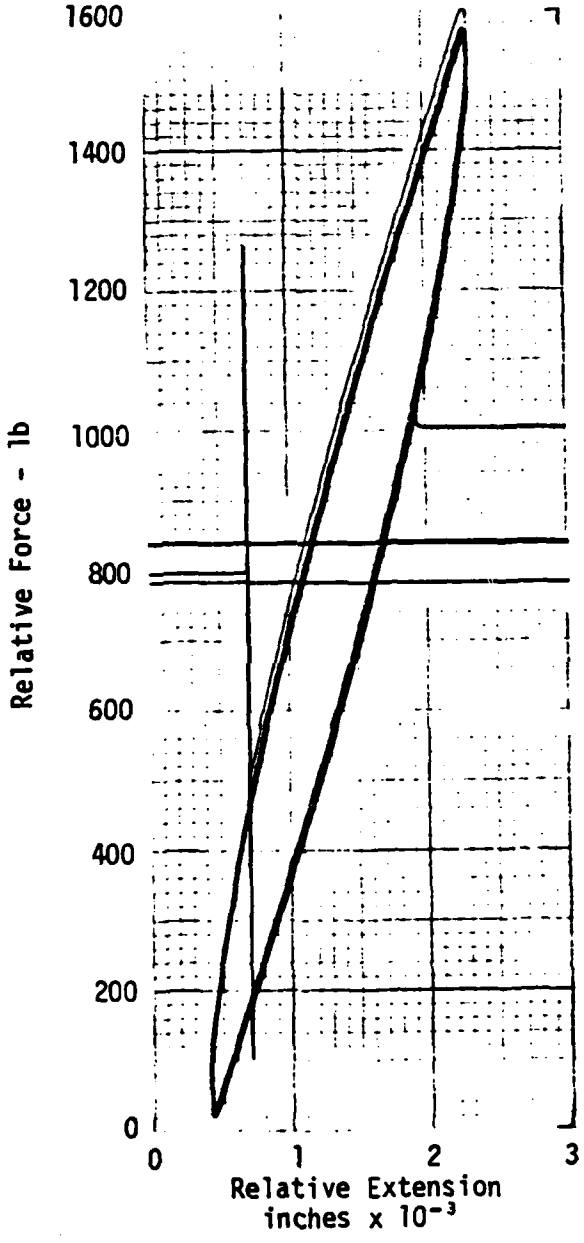

Figure 2. Hysteresis Characteristics of Test Specimen 16 Containing EC 2216

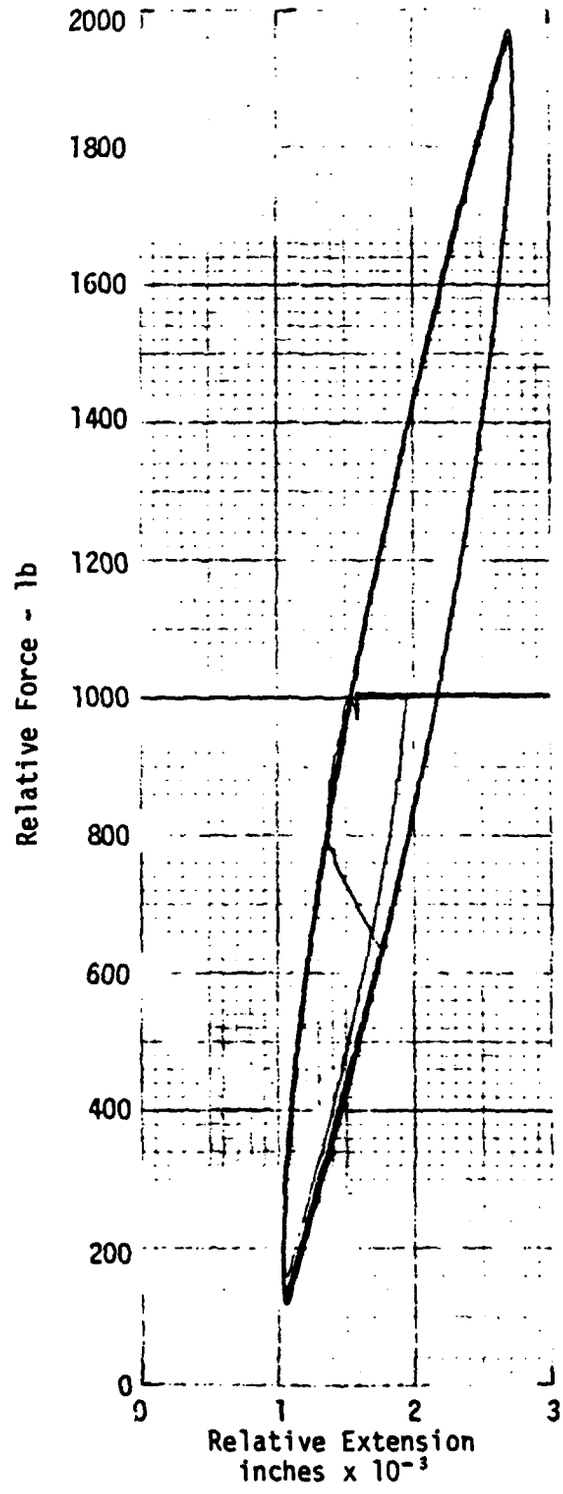

Figure 1. Hysteresis Characteristics of Test Specimen 15 Containing EC 2216

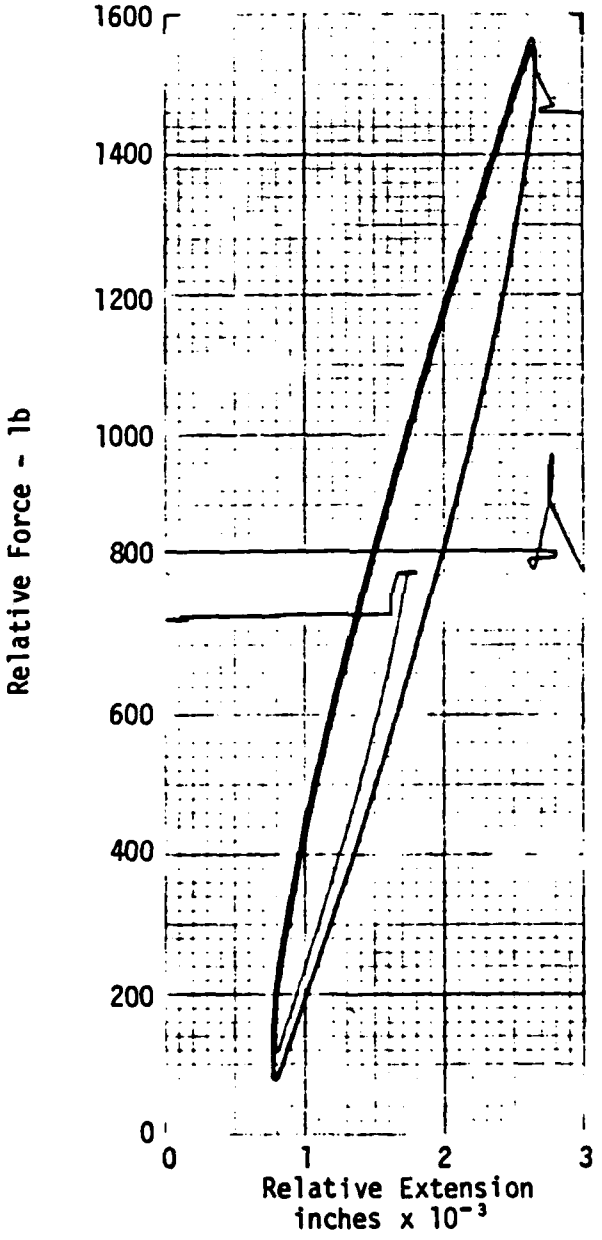

Figure 3. Hysteresis Characteristics of Test Specimen 17 Containing EC 2216

APPENDIX I

ANNEX B

JOINT HYSTERESIS DATA

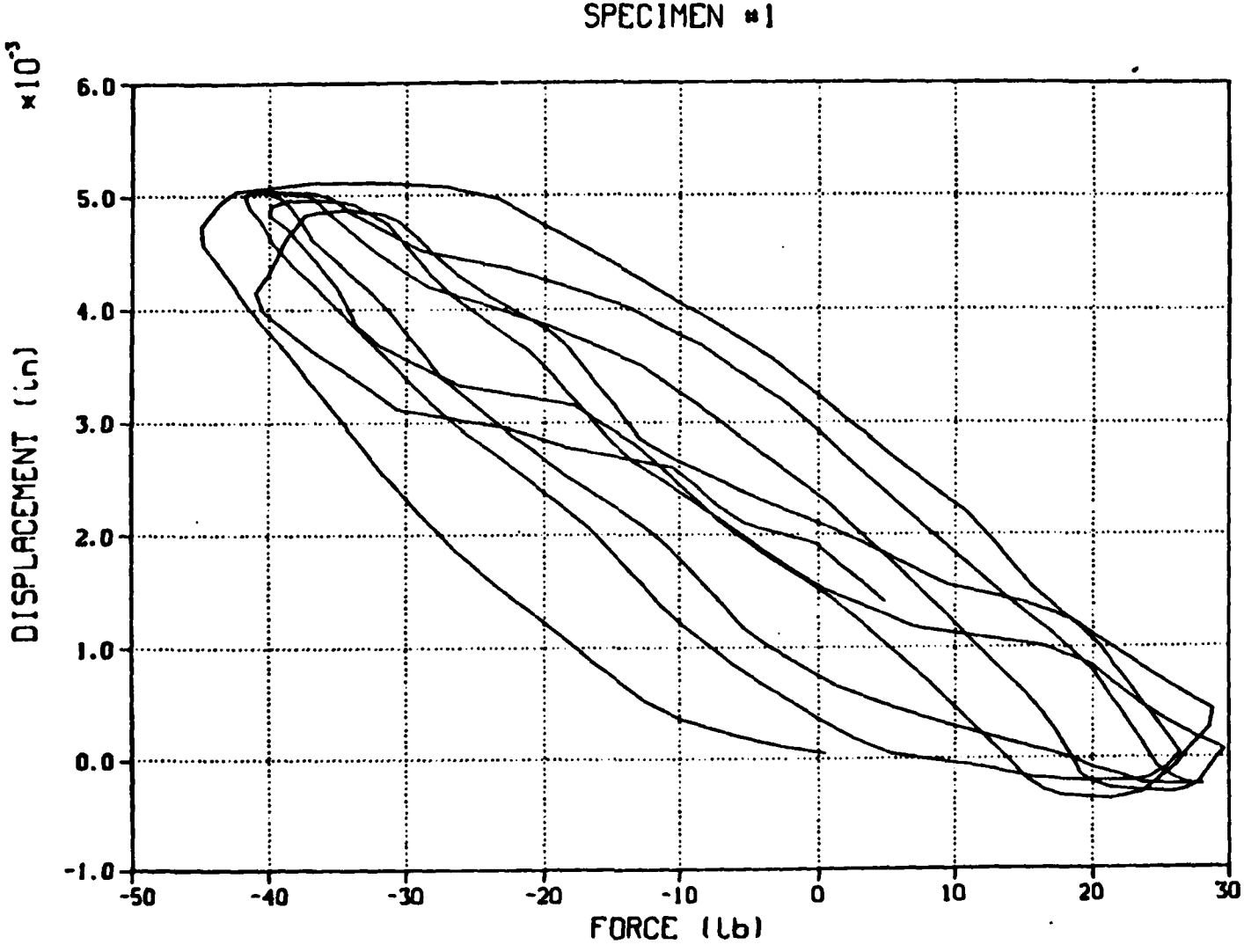

Figure 1. Hysteresis Characteristics of Test Specimen 1 Containing ISD 110

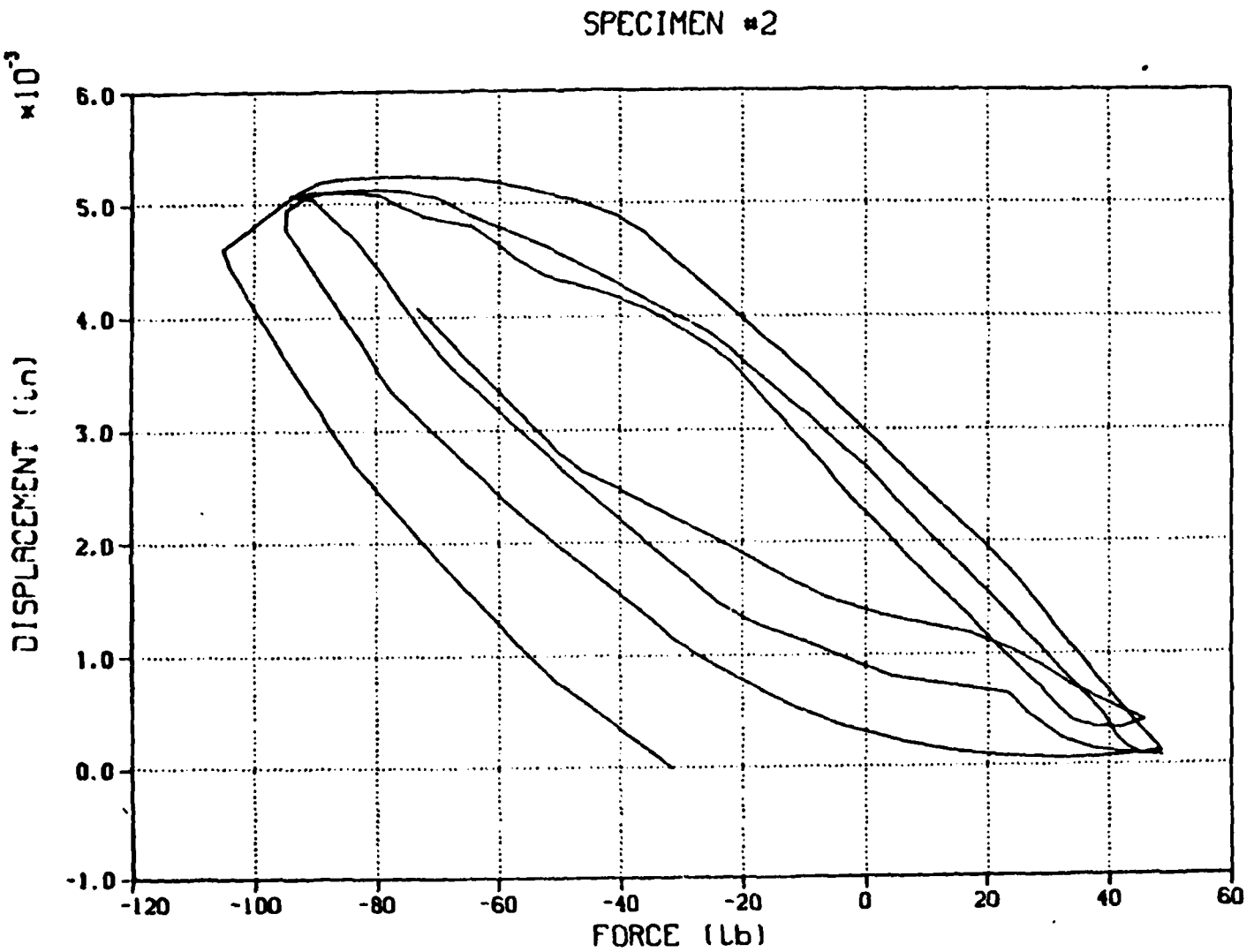

Figure 2. Hysteresis Characteristics of Test Specimen 2 Containing ISD 110

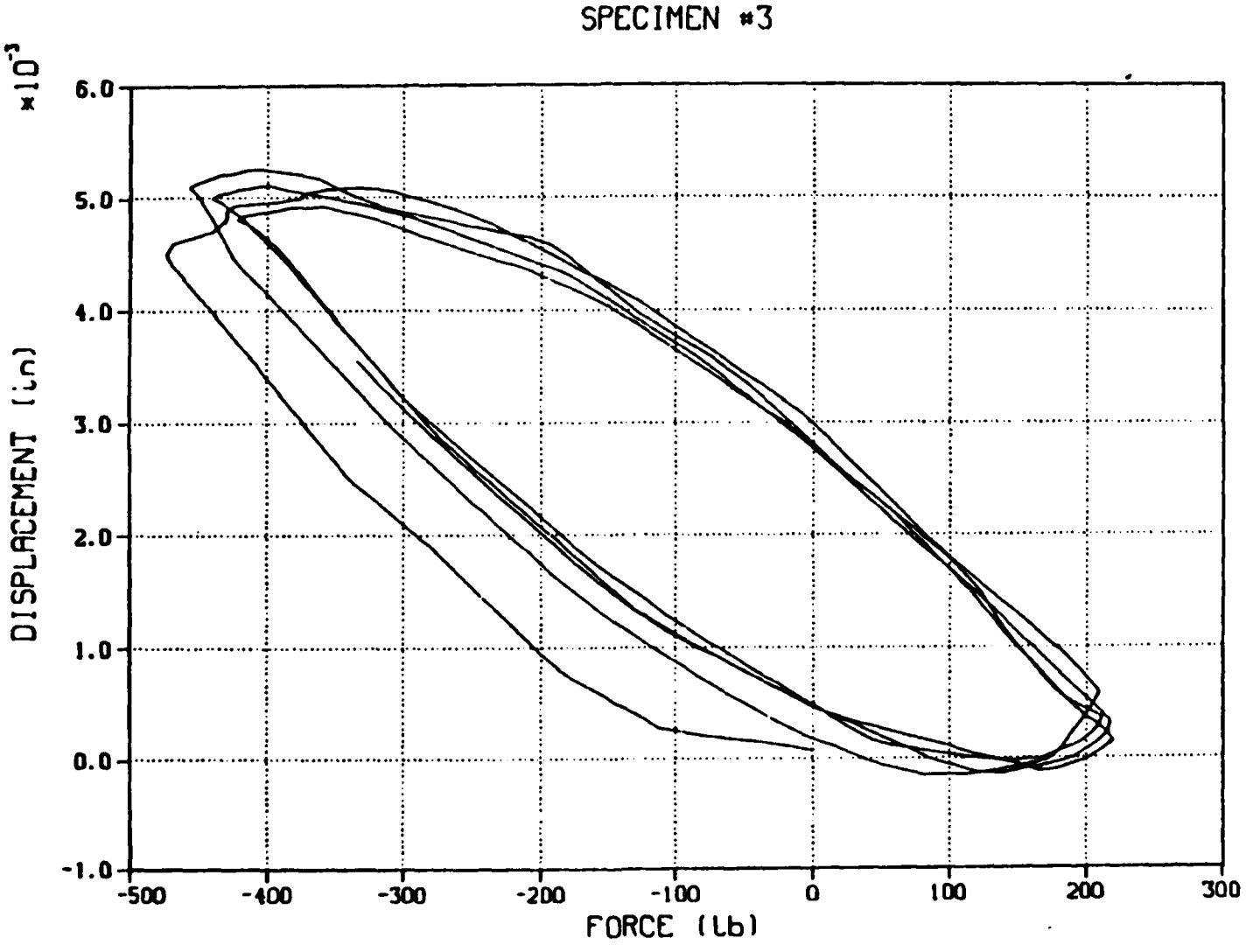

Figure 3. Hysteresis Characteristics of Test Specimen 3 Containing EC2216

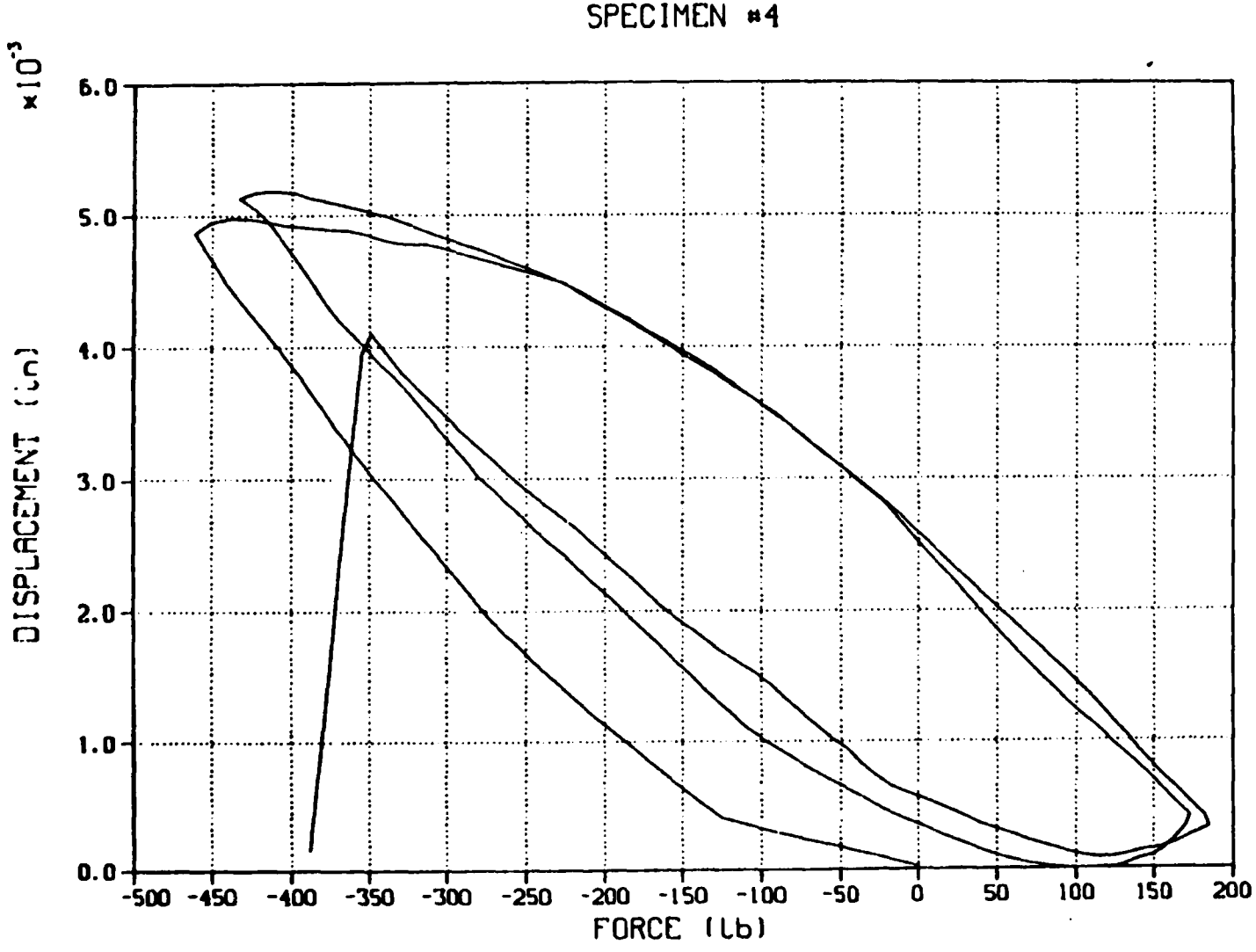

Fiugre 4. Hysteresis Characteristics of Test Specimen 4 Containing EC2216

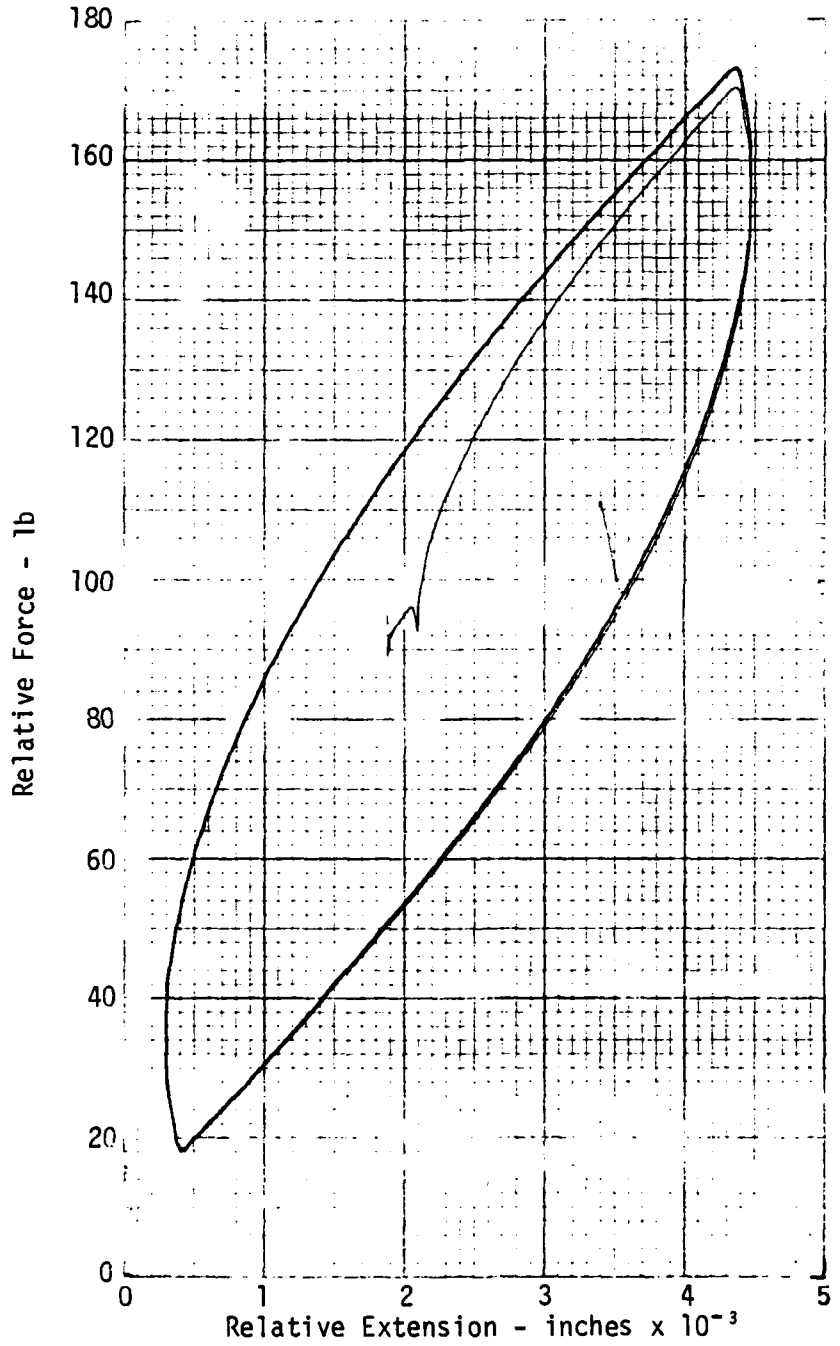

Figure 5. Hysteresis Characteristics of Test Specimen 5 Containing DYAD 606A

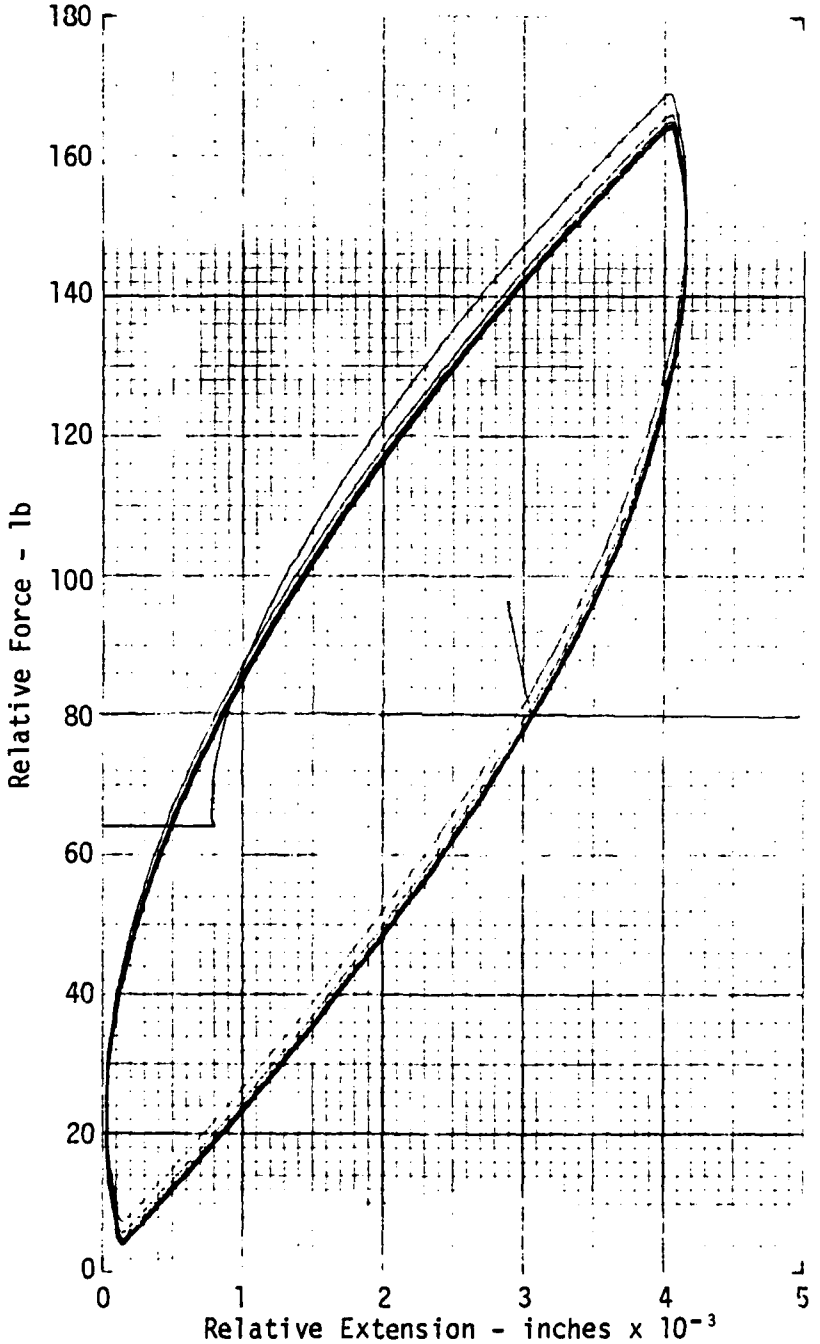

Figure 6. Hysteresis Characteristics of Test Specimen 6 Containing DYAD 606/B

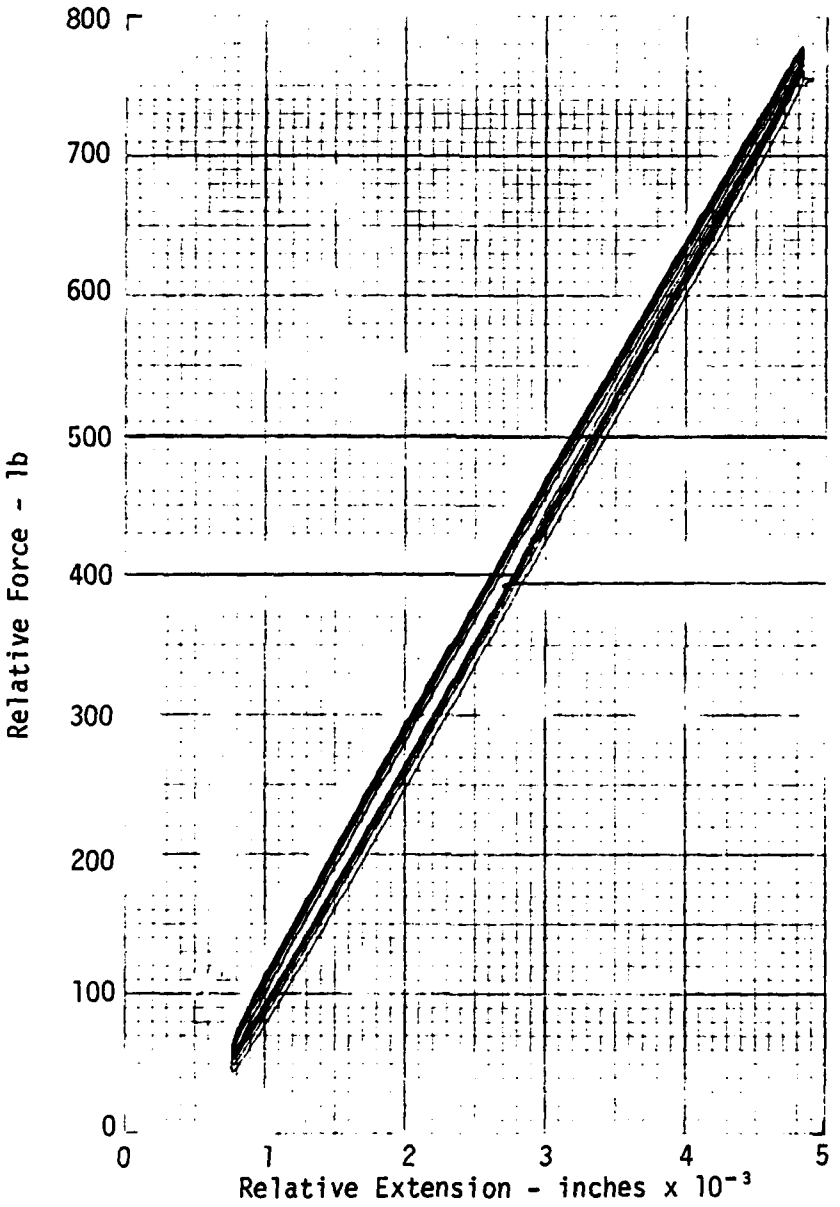

Figure 7. Hysteresis Characteristics of Test Specimen 7 Containing EA9326A

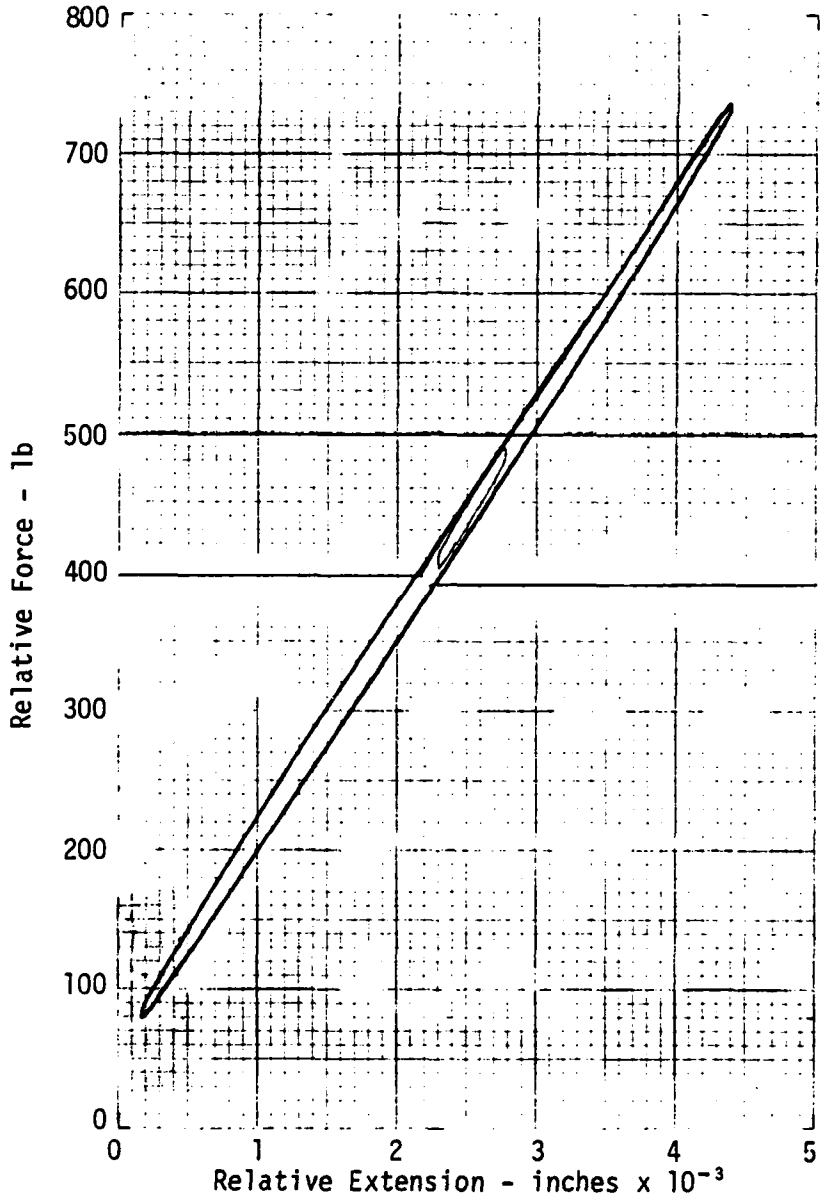

Figure 8. Hysteresis Characteristics of Test Specimen 8 Containing EA9326B

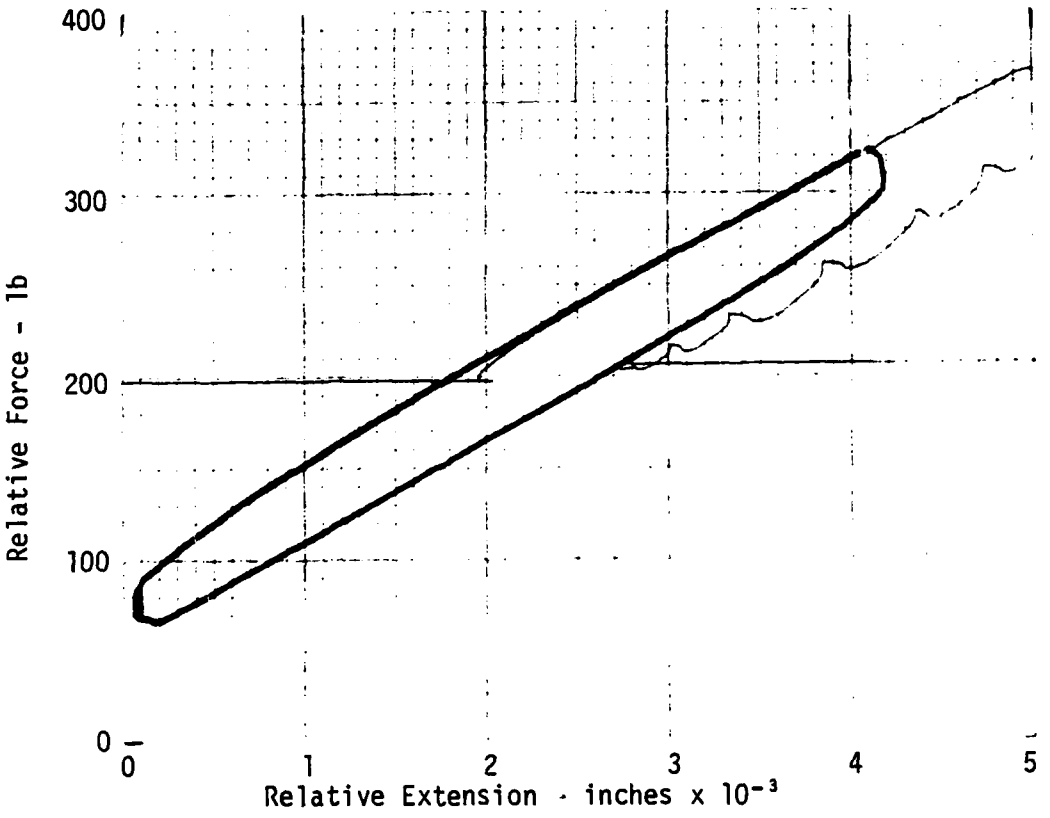

Figure 9. Hysteresis Characteristics of Test Specimen 9 Containing SMRD-A

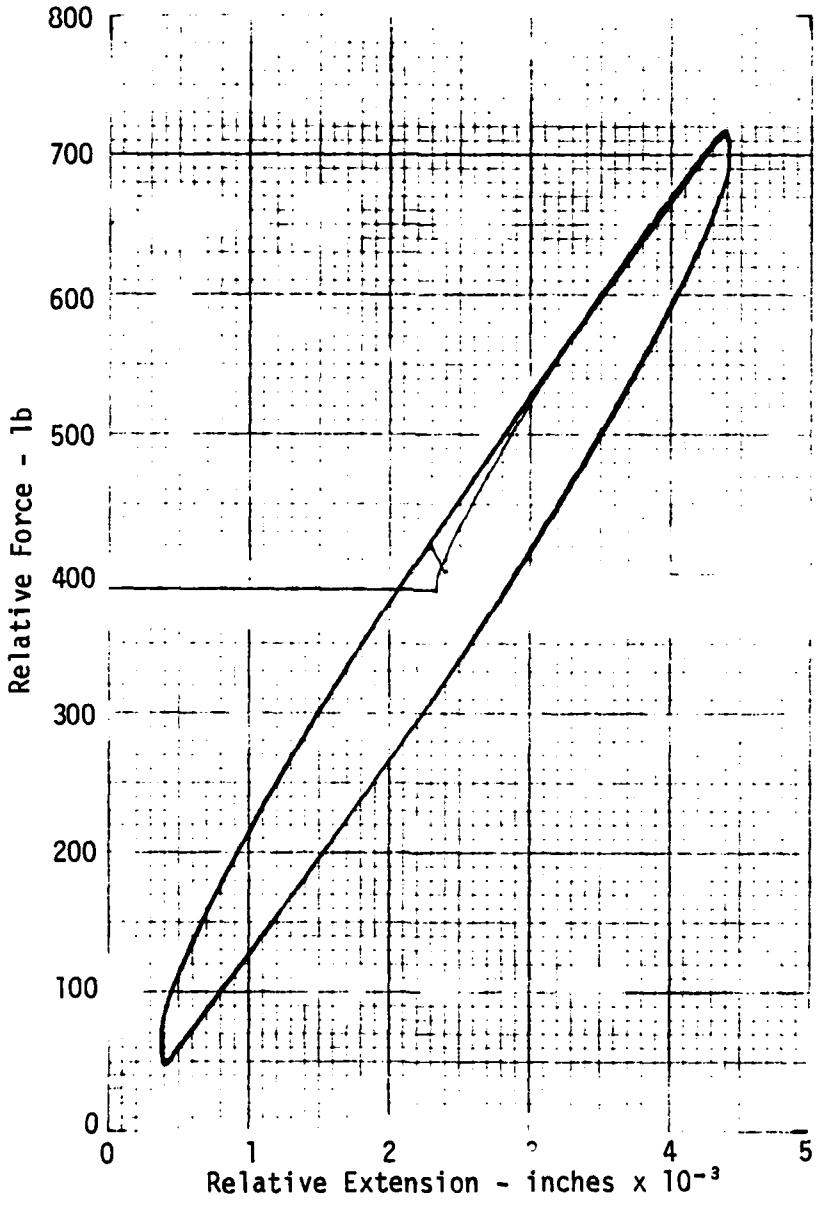

Figure 10. Hysteresis Characteristics of Test Specimen 10 Containing SMRD/B

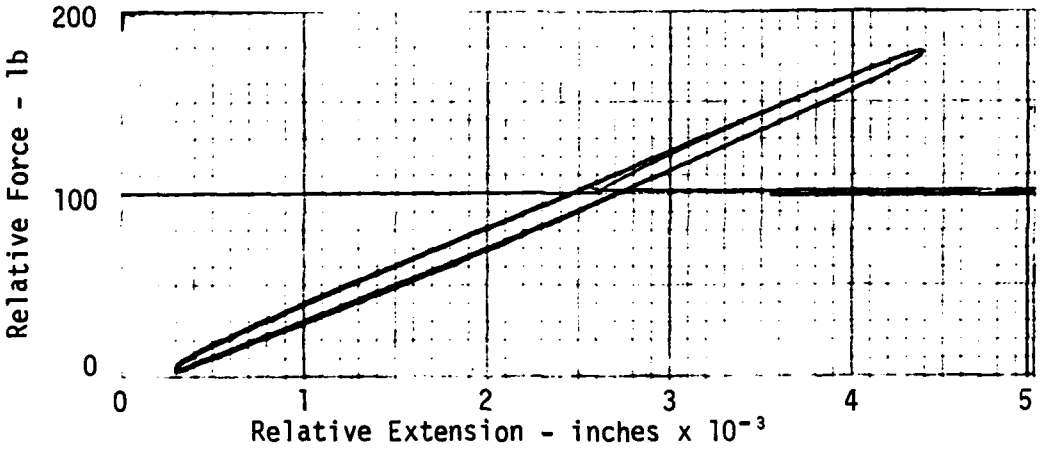

Figure 11. Hysteresis Characteristics of Test Specimen 11 Containing RTV 630A

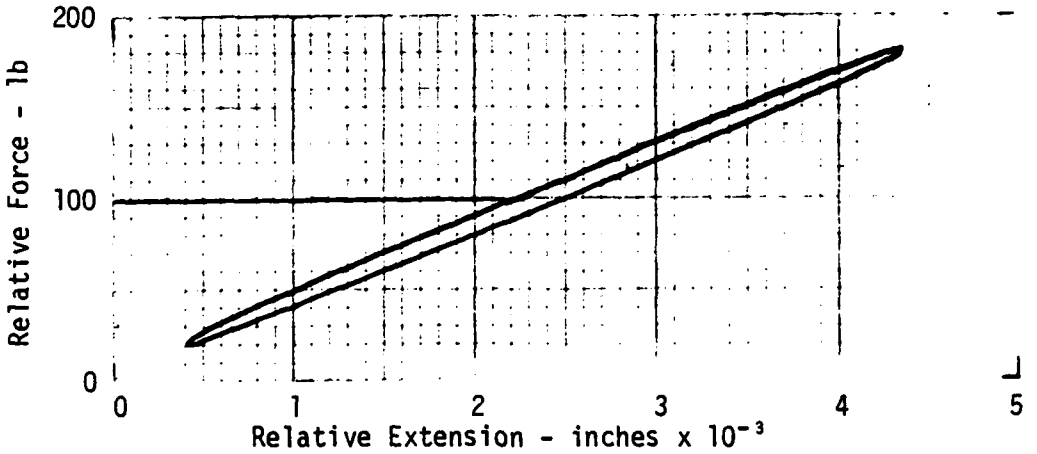

Figure 12. Hysteresis Characteristics of Test Specimen 12 Containing RTV 630B

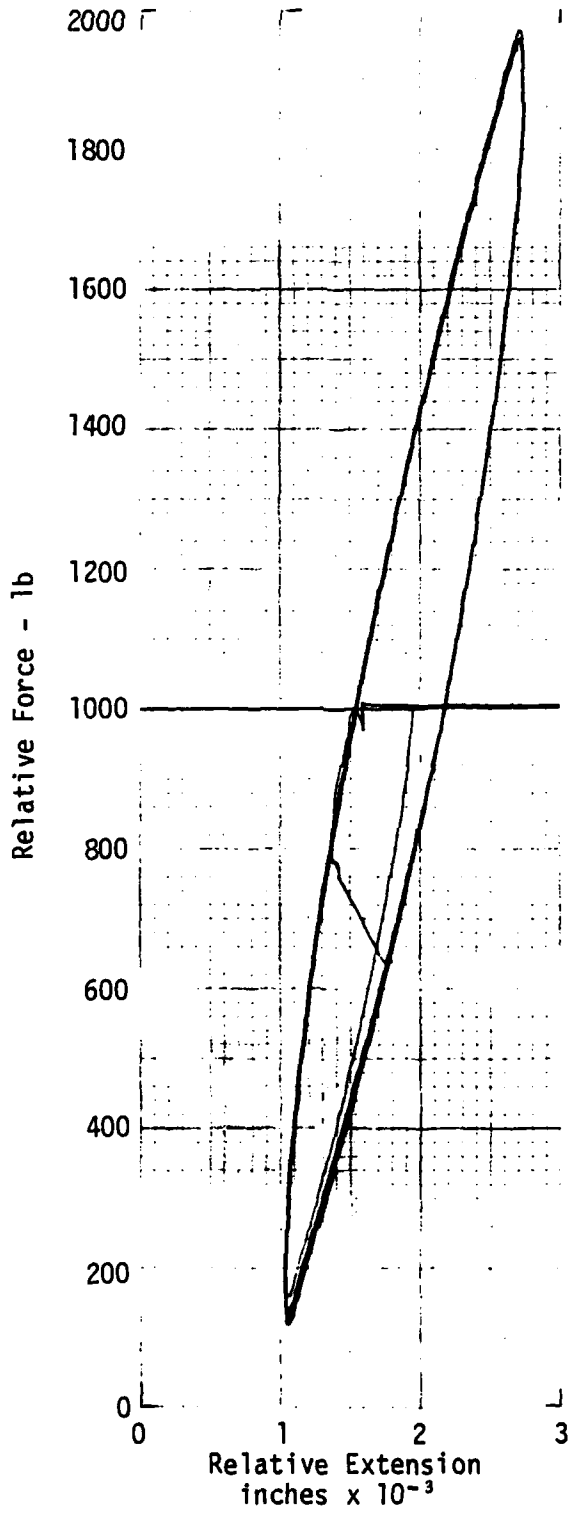

Figure 13. Hysteresis Characteristics of Test Specimen 15 Containing EC 2216

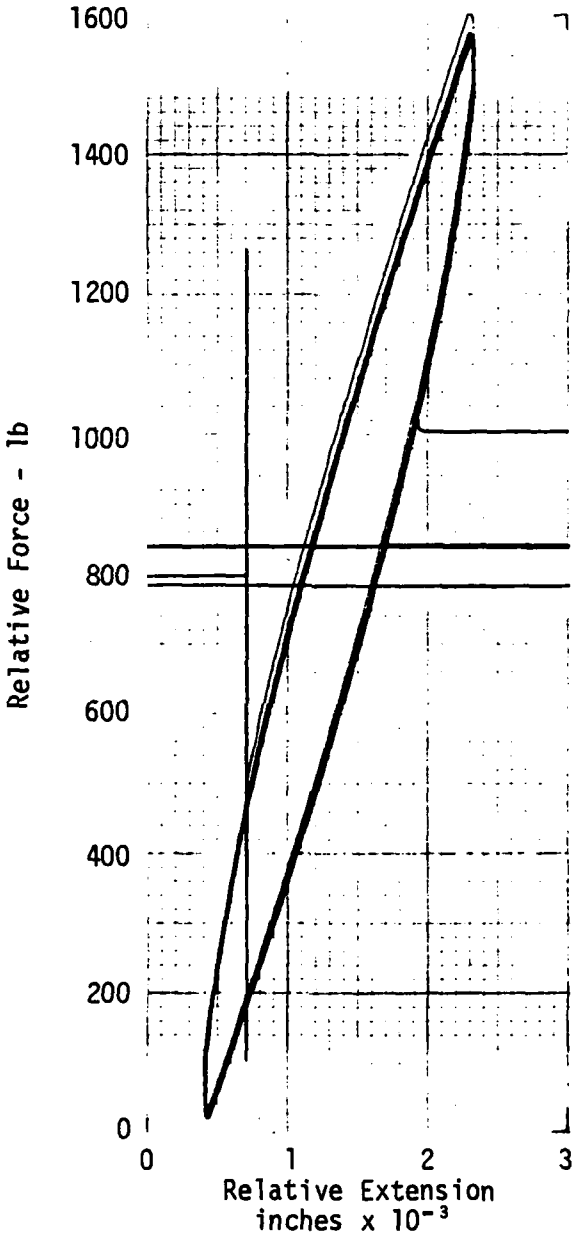

Figure 14. Hysteresis Characteristics of Test Specimen 16 Containing EC 2216

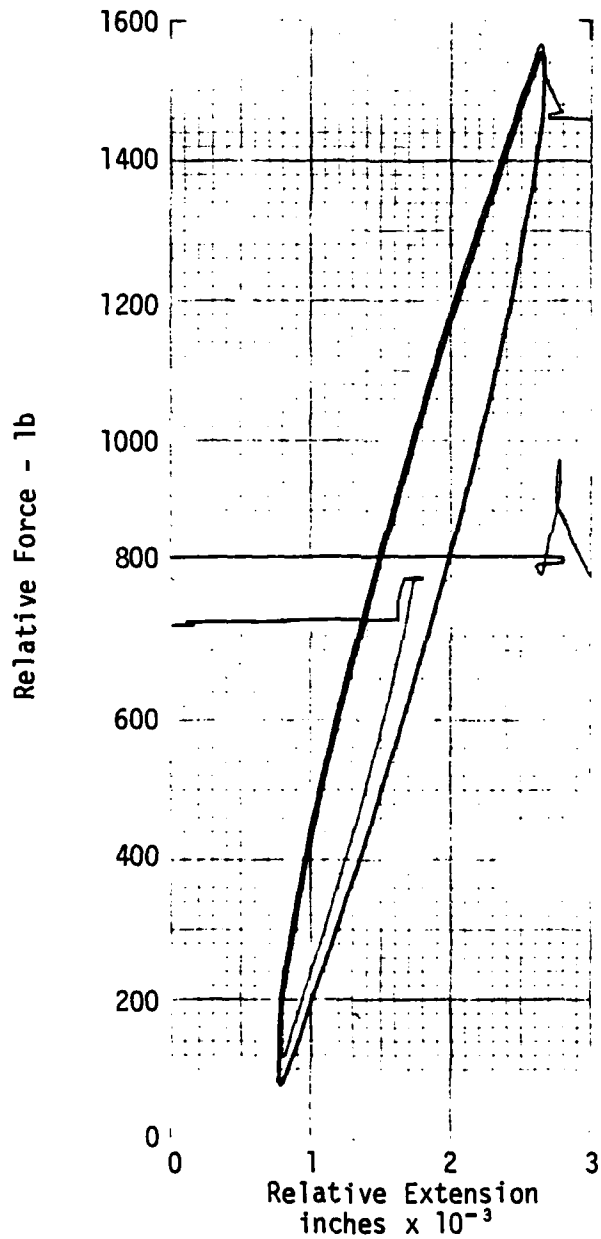

Figure 15. Hysteresis Characteristics of Test Specimen 17 Containing EC 2216

APPENDIX I

ANNEX C

INITIAL SURVEY OF VEM DAMPING PROPERTIES

INITIAL SURVEY OF VEM DAMPING PROPERTIES

1.0 INTRODUCTION

This report consists of a survey of the damping properties of VEM candidates for use in prototype large space structure (LSS) damping joint testing. Initial testing would be done at low frequencies (0.1-100 Hz) and ambient temperature (21°C).

The design of the MDAC-HB prototype joints will be based on a lap joint approach, when the VEM in the joint is placed in shear when a vibrational wave passes through it (Figure 1).

To optimize damping, the following goals were set up for VEM selection:

1. The loss factor (η) must be over 0.50 over a frequency range of 0.1-100 Hz at 21°C.

2. The shear storage modulus (G') should not change by more than an order of magnitude when the temperature changes approximately 20°C.

2.0 DESIGN DATA FOR VEM CANDIDATES (21°C, 0.1-100 Hz)

This section will present and discuss design considerations and VEM data for possible LSS joint elastomer candidates from 0.1-100 Hz at 21°C. The topics considered include: sources of damping data, VEM damping properties, outgassing, creep and fabrication. Outgassing and creep should generally be minimized. The VEM damping properties should meet the goals presented in paragraph 1.0.

2.1 Sources of Damping Data

The vendor damping data were generally scanty and of vague origin. They were therefore used only as a reference for the other standard physical properties such as tensile strength, etc. All of the damping information in this report was gathered from Air Force Materials Laboratory reports[1,2] which used University of Dayton Research Institute (UDRI) data.

STRUCTURAL DAMPING JOINT

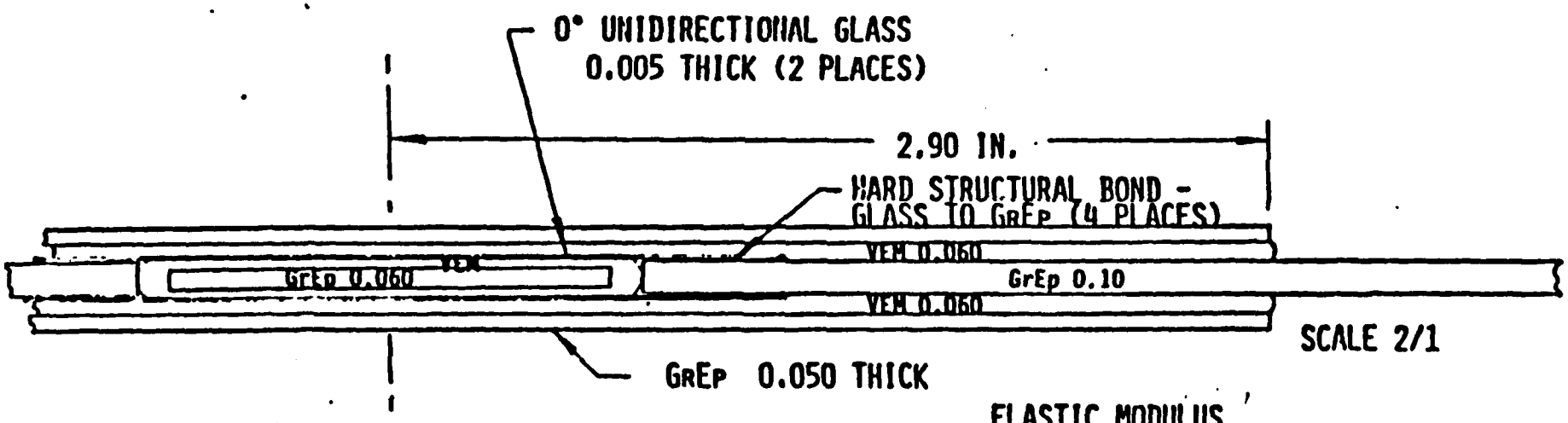

MATERIAL	ELASTIC MODULUS (10^6 PSI) LONG	TRANS
GLASS (S-2)	7.0	1.2
GrEp (AS OR T300)	12.9	2.1
ALTERNATE GrEp (P75)	26.0	2.5

VEM MODULUS = 250 PSI

Figure 1. Structural Damping Joint

UDRI damping data are generally the most reliable. This is because their damping data were generated using ASTM E756-8 ("Standard Method for Measuring Vibration - Damping Properties of Materials"), which UDRI played a major role in writing and getting adopted.

2.2 VEM Low Frequency Damping Properties

Some low-frequency data for most of the commercially available damping VEM's are presented in Table 1.

The temperature range (°C) for which η is greater than 0.5 is presented for 1 and 100 Hz. If the VEM had a loss factor of at least 0.5 at 21°C for 0.1 and 100 Hz, it was also examined at 0.1 Hz. The 0.1 Hz data is extrapolated. Four VEMs provided loss factors at 21°C of at least 0.5 at 0.1, 1 and 100 Hz; four others came close to meeting this goal.

The various VEM's studied have damping peaks at a wide variety of temperatures. Soundfoil LT-12 will provide peak damping at 1 Hz at -101°C. 3M 467 will provide peak damping at 100 Hz at 98°C.

The loss factor is highest at the VEM's glass transition temperature, T_G. The T_G is presented for all of the VEMs at 5 Hz. The shear storage modulus at T_G is also presented. This listing of G' at T_G gives the reader an idea of the relative stiffnesses of the VEMs.

In the last column, the temperature change required to change G' by an order of magnitude is given. This allows the reader to compare the temperature sensitivity of the various VEMs. Almost all of the VEMs in Table 1 require a 14-26°C temperature change to alter G' one decade. Soundcoat D is less sensitive, with a 46°C temperature change required to alter G' one decade. Sylgard 188, a silicone, is the least sensitive at 76°C/decade. However, Sylgard 188 does not have a high loss factor (0.3).

In Table 2, more detailed information on the eight 21°C, 0.1-100 Hz candidates is presented. The best candidates are EAR C2003, Soundcoat Dyad 606, 3M ISD 110 and 3M 467. These materials have a great range in stiffness for a given temperature and frequency. EAR C2003 is by far the stiffest. The G' of EAR C2003 at its T_G is 9,140 psi. EAR C2003 has a hardness of 93-94 Shore A at

AD-A162 257 PASSIVELY DAMPED JOINTS FOR ADVANCED SPACE STRUCTURES 2/2
(U) MCDONNELL DOUGLAS ASTRONAUTICS CO-HB HUNTINGTON
BEACH CA R W TRUDELL ET AL. 30 JUN 84 MDC-H1178
UNCLASSIFIED AFOSR-TR-85-1078 F49620-83-C-0117 F/G 13/5 NL

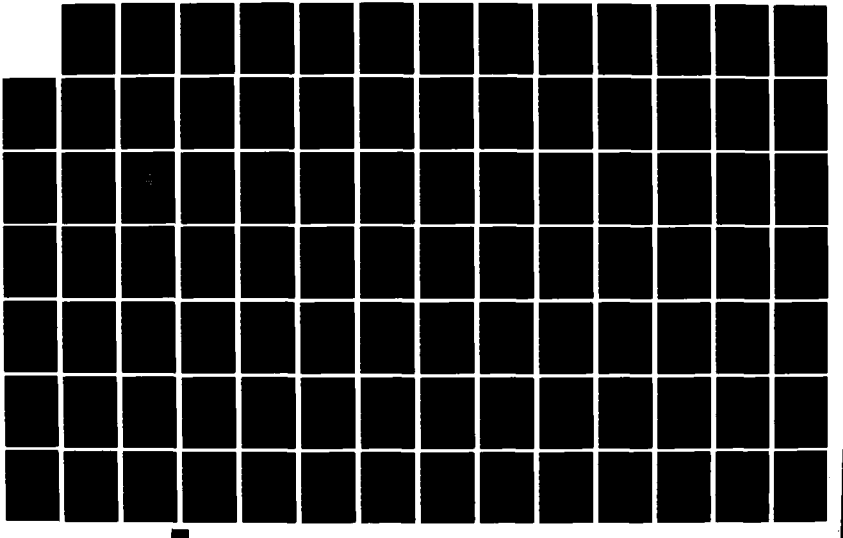

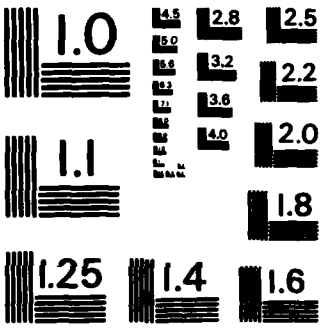

Table 1. VEM LOW FREQUENCY DAMPING PROPERTIES

Material	Temperature Range for $\eta > 0.5$, °C			T_G at 5 Hz °C	G' at T_G N/m^2, (psi)	Maximum G' Slope °C/Decade G'
	0.1 Hz	1 Hz	100 Hz			
EAR C2003	-2 to 38	4 to 50	21 to 75	30	6.3×10^7 (9,140)[1]	20
EAR C1002	-	-16 to 14	-4 to 31	4	4.0×10^7 (5,800)[1]	14
MACBOND IB1120	-	-43 to 5	-16 to 48	-10	2.8×10^6 (406)	20
" IB1160	-	-50 to -2	-20 to 42	-16	8.5×10^5 (123)	14
" IB1200	-	-56 to -16	-30 to 25	-26	6.0×10^6 (870)	14
" IB1220	-	-40 to 0	-10 to 42	- 8	1.7×10^6 (246)	14
" IB1248	-	-62 to -26	-35 to 14	-40	5.0×10^6 (725)	15
" IB1320	-	-43 to 7	-15 to 51	- 9	4.5×10^6 (653)	16
" IB1400	-	-51 to -13	-21 to 27	-21	4.0×10^6 (580)	17
" IB1401	-	-61 to -15	-31 to 29	-28	4.5×10^6 (653)	17
" IB1622	-	-62 to -31	-34 to 7	-37	5.0×10^6 (725)	15
" IB2101	-	-57 to 8	-31 to 56	-29	1.3×10^7 (1,890)	21
" IB2107	-54 to 3	-43 to 21	-17 to 67	-13	6.0×10^6 (870)	24
" IB2130	-	-58 to -2	-32 to 42	-31	7.5×10^6 (1,090)	19
SOUNDCOAT D	-12 to 53	0 to 75	31 to 134	52	7.5×10^5 (109)	46
SOUNDCOAT M	-	-78 to -27	-47 to 25	-26	4.3×10^6 (624)	18
SOUNDCOAT N	-	-43 to 14	-24 to 49	- 8	4.0×10^6 (580)	20
SOUNDCOAT R	-	-67 to -16	-40 to 30	-35	3.0×10^6 (435)	15
" DYAD 601	-	-43 to 4	-15 to 46	-12	7.0×10^6 (1,020)	19
" DYAD 606	-24 to24	-14 to 40	11 to 83	17	1.2×10^7 (1,740)	26
" DYAD 609	-19 to 7	-7 to 23	23 to 60	18	1.5×10^7 (2,180)	26
SOUNDFOIL LT-12	-	-101 to -63	-70 to -18	-74	1.0×10^7 (1,450)	19

Table 1. VEM LOW FREQUENCY DAMPING PROPERTIES (Cont'd)

Material	Temperature Range for $\eta > 0.5$, °C 0.1 Hz	1 Hz	100 Hz	T_G at 5 Hz °C	G' at T_G N/M^2, (psi)	Maximum G' Slope °C/Decade G'
3M ISD 110	-32 to 34	-21 to 55	6 to 105	21	1.0×10^6 (145)	25
" 112	-	-49 to 10	-23 to 55	-14	1.6×10^6 (232)	25
" 113	-	-72 to -17	-43 to 29	-36	2.0×10^6 (290)	16
" 113M	-	-71 to -25	-42 to 19	-44	3.0×10^6 (435)	19
" 830	-	-97 to -60	-67 to -19	-74	9.0×10^6 (1,300)	16
ENJAY BUTYL 268	-	-78 to -28	-52 to 15	-45	1.6×10^7 (2,320)	18
3M 467	-53 to 21	-45 to 43	-23 to 98	-2	1.2×10^6 (174)[1]	22
SYLGARD 188	-	-38 to 33[2]	-27 to 74[2]	-6	2.8×10^6 (406)[1]	76
LD 400	-16 to 16	- 4 to 31	18 to 71	17	1.3×10^8 (18,900)[1]	16
PARACRIL BJ NITRILE	-	-28 to 9	-19 to 13	-18	8.3×10^7 (12,000)[1]	7
3M 428	-	-107[3] to -23	-77[3] to 18	-59	1.2×10^7 (1,740)[1]	17

NOTES:

1. Estimated from E' using G' = 1/3 E'
2. $\eta > 0.3$
3. Extrapolated

Table 2. DETAILED VEM CANDIDATE DAMPING PROPERTIES (0.1-100 Hz)

Material	0.1 Hz		1 Hz		10 Hz		100 Hz	
	η	G', N/m² (psi)	η	G', N/m² (psi)	η	G', N/m² (psi)	η	G', N/m² (psi)
PRIMARY CANDIDATES								
EAR C2003	0.85	3.3×10^7 (4,790)	0.95	8.7×10^7 (12,600)	0.75	2.7×10^8 (39,200)	0.5	6.7×10^8 (97,200)
SOUNDCOAT DYAD 606	0.55	1.0×10^6 (145)	0.85	3.0×10^6 (435)	1.05	1.1×10^7 (1,590)	0.8	6.0×10^7 (8,700)
3M ISD 110	0.77	1.6×10^5 (23)	1.2	4.0×10^5 (58)	1.2	1.4×10^6 (203)	0.95	5.5×10^6 (798)
3M 467	0.50	4.1×10^4 (5.95)	0.8	1.1×10^5 (16.0)	1.2	3.7×10^5 (53.7)	1.40	1.15×10^6 (167)
SECONDARY CANDIDATES								
MACBOND IB2107	0.35	1.9×10^5 (27.5)	0.50	3.0×10^5 (43.5)	0.75	6.5×10^5 (94.3)	1.01	2.0×10^6 (290)
SOUNDCOAT D	0.95	7.5×10^5 (109)	0.80	1.4×10^6 (203)	0.60	3.0×10^6 (435)	0.40	6.0×10^6 (870)
SOUNDCOAT DYAD 609	0.31	2.3×10^6 (334)	0.50	5.0×10^6 (725)	0.60	1.7×10^7 (2,470)	0.47	7.0×10^7 (10,200)
LD 400	0.40	1.5×10^7 (2,180)	0.70	3.3×10^7 (4,790)	1.2	1.7×10^8 (24,700)	0.50	1.4×10^9 (203,000)

room temperature. The others provide G's up to three orders of magnitude more flexible. This allows the joint designer a good variety of VEM choices to achieve a particular joint stiffness.

The UDRI reduced temperature and frequency plots for the four candidates are shown in Figures 2-5. To use these charts, one must first select a frequency from the right hand side of the chart and find its intersection with a temperature selected from the diagonal temperature lines. The intersection forms a point. A line projected vertically through the point will intersect the proper η and G' values.

Four secondary VEM candidates are also listed. These materials come close to meeting the design requirements. The loss factor, however, falls below 0.5 at one of the frequencies between 0.1-100 Hz at 21°C. These materials may still be of interest to the design engineer because of certain redeeming properties. The G' for Soundcoat D, for instance, is less sensitive to temperature changes than that of any of the seven other candidates.

2.3 Outgassing

Outgassing results for VEM damping candidates and related materials are shown in Table 3. These data were obtained from NASA-JSC[3] and are rather scanty. Most of the eight damping candidates have not been tested by NASA, but inferences can be made from results for related materials. To meet the outgassing requirements of JSC specification SP-R-0022A[4], par. 4, TWL-RML should be less than 1% and VCM should be less than 0.1%.

Outgassing data could be found for only two of the four primary candidates. Bare ISD 110 is acceptable. 3M 467 does not pass unless postcured to remove volatiles and is still marginal. No data could be found for EAR C2003 or Soundcoat Dyad 606. Among the four secondary candidates, outgassing data were found only for LD 400, which had high outgassing. While Scotchdamp Y370 is not a candidate material, postcuring it reduces its outgassing to acceptable levels.

Many VEMs are acrylic based. By looking at the outgassing of aluminum-foil-covered acrylic tapes, one can see how a constraining faceplate would improve outgassing. Mystic 6468, 7452, 7453 and the other aluminum foil/acrylic tapes

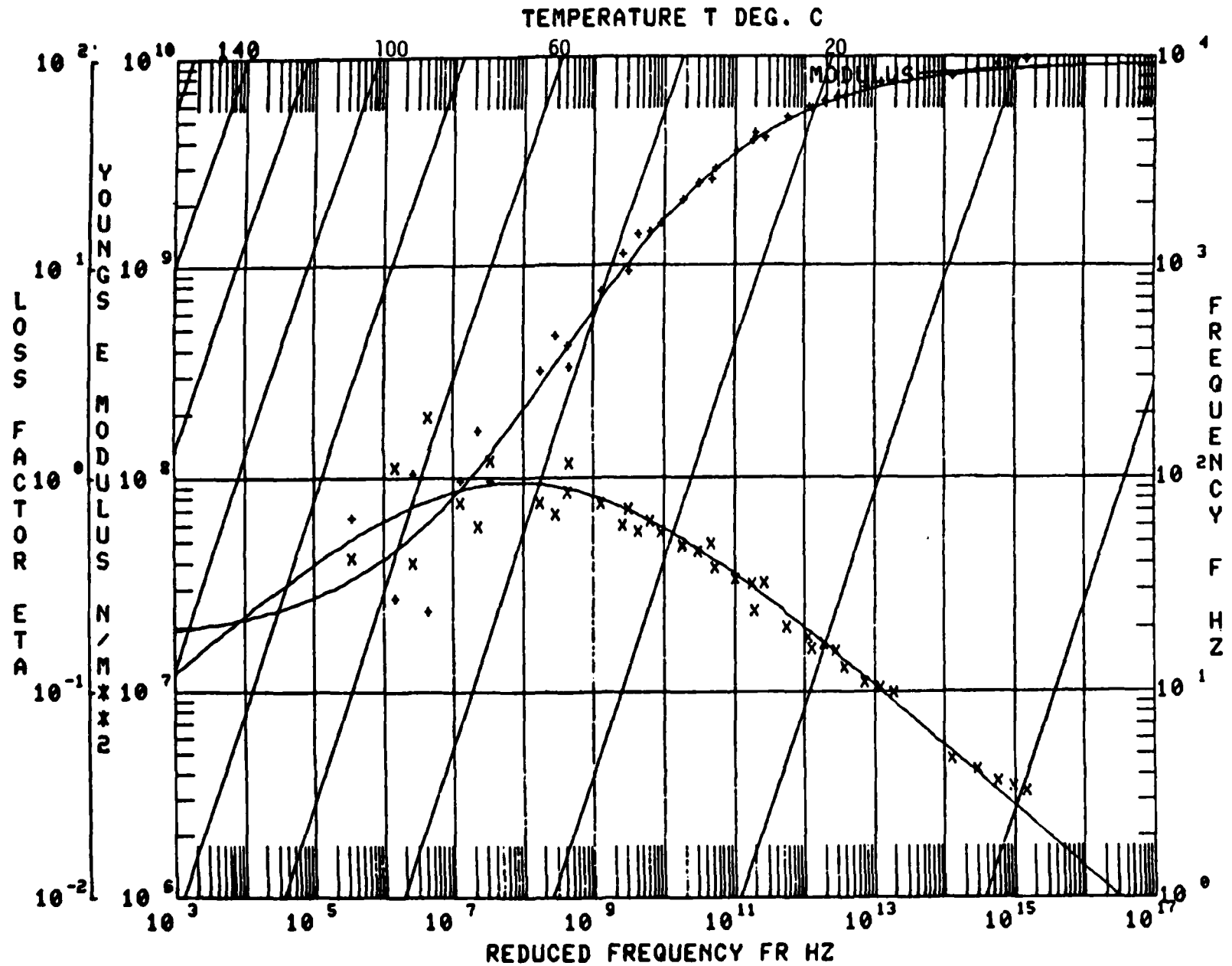

Figure 2. EXODAMP C-2003

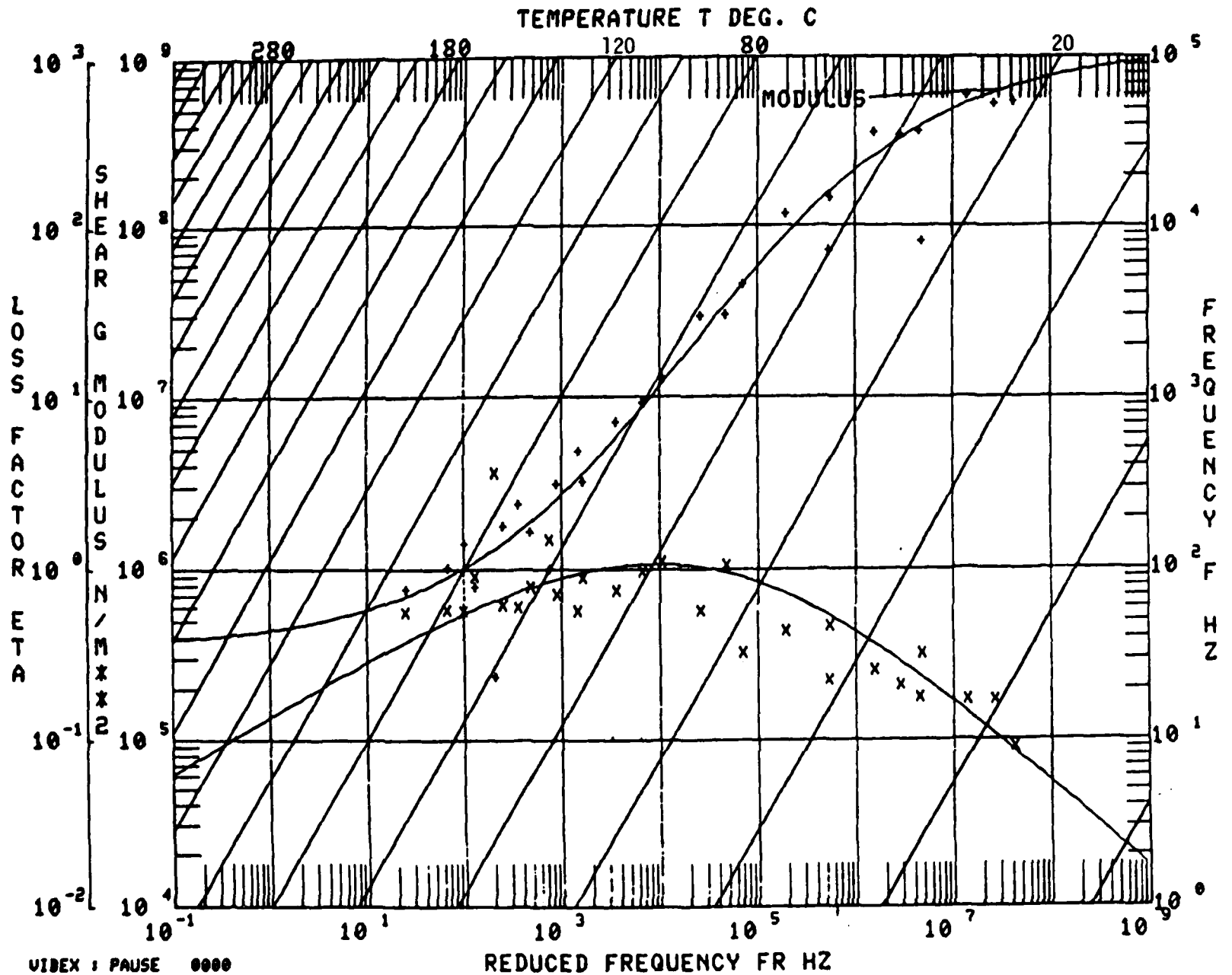

Figure 3. SOUNDCOAT DYAD 606

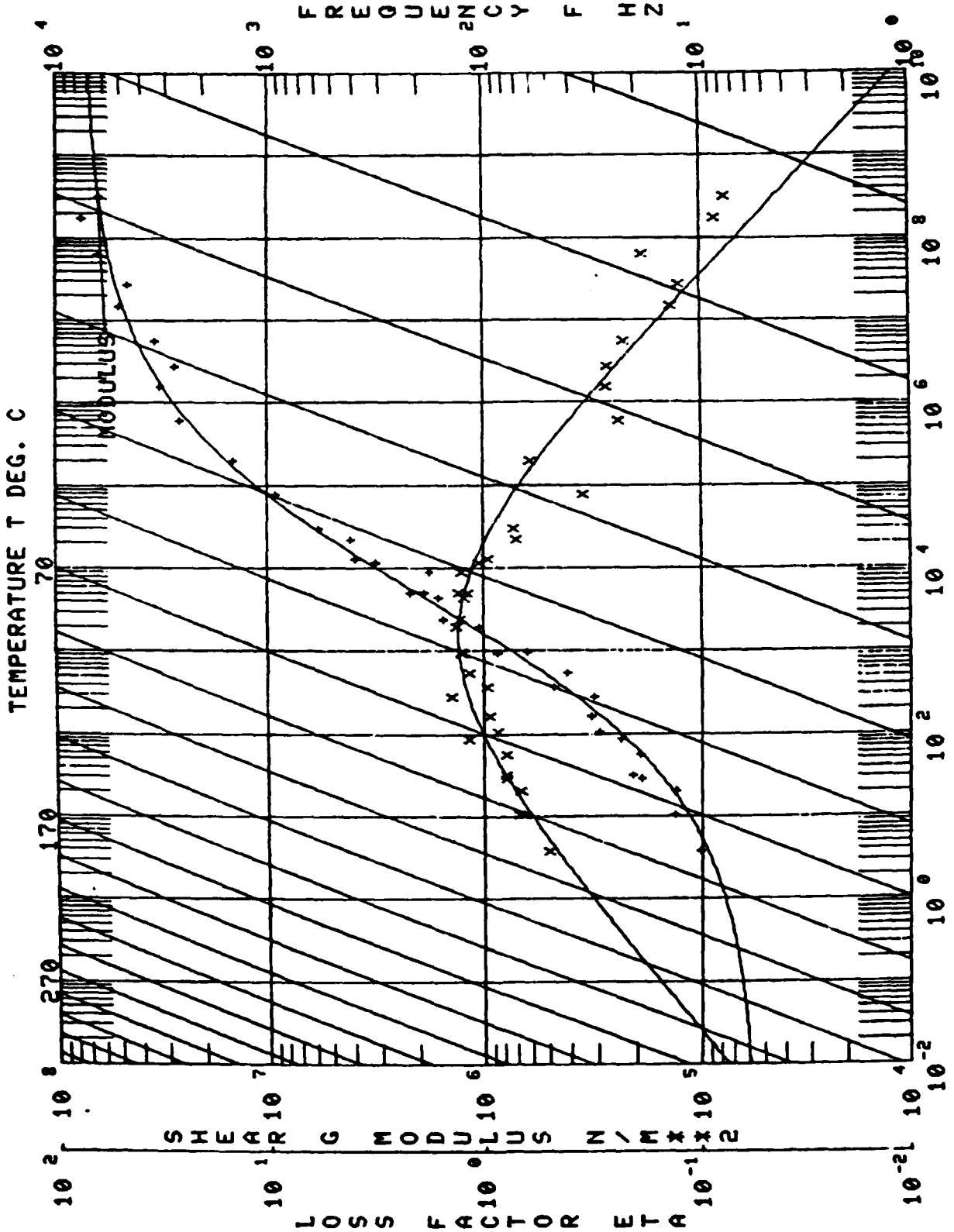

Figure 4. 3M ISD 110

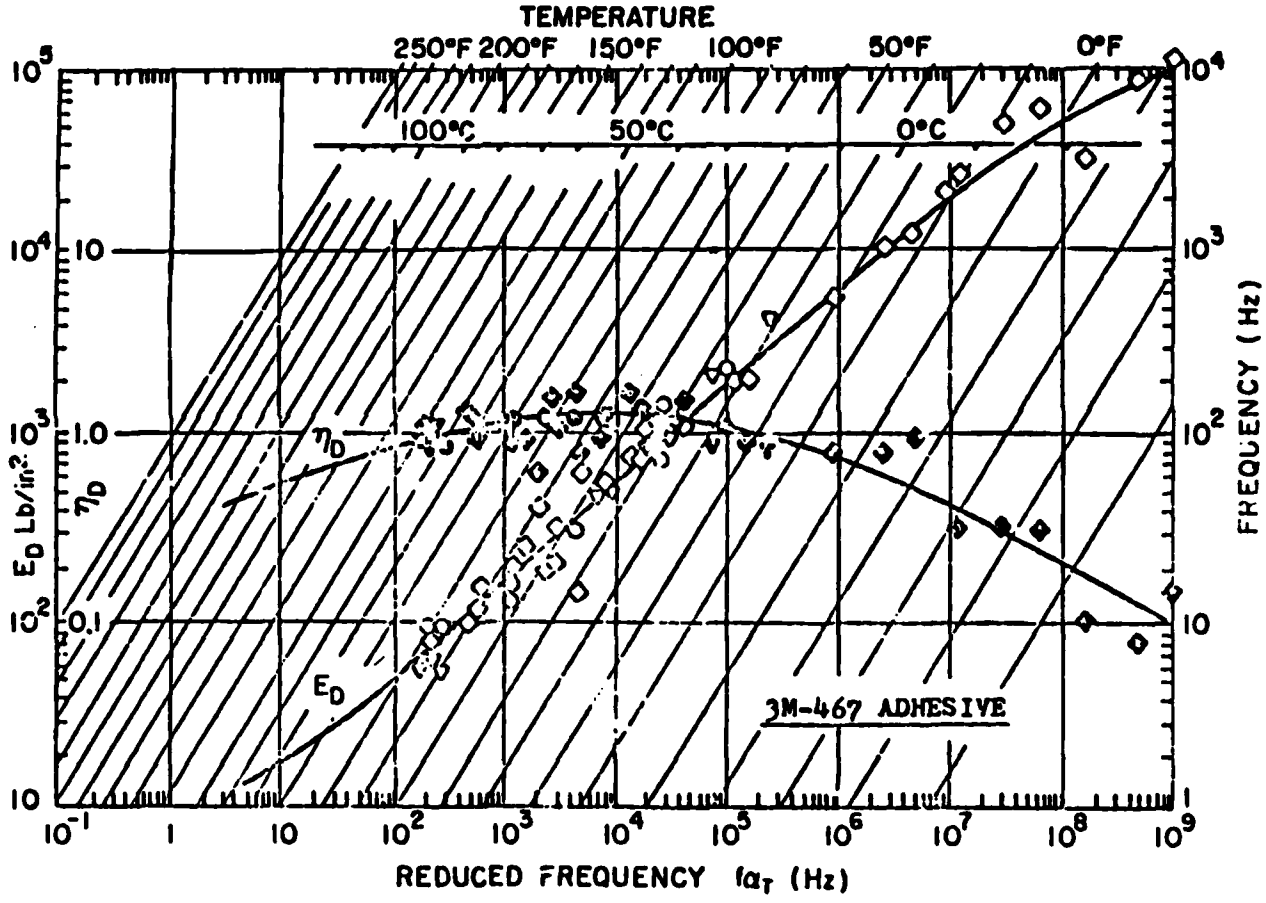

Figure 5. Reduced Temperature Curves for 3M-467 Adhesive

Table 3. OUTGASSING RESULTS FOR DAMPING CANDIDATES AND RELATED MATERIALS

Material	TWL (Total Weight Loss, %)	RML (Recovered Mass Loss, %)	VCM (Volatile Condensible Materials, %)	Notes
SCOTCHDAMP ISD 110	1.51	0.84	0.03	GOOD
3M 467	4.24	0.43	0.02	HIGH
"	0.83	-	0.04	GOOD (POSTCURED 4 HRS AT 38%C)
"	1.32	-	0.08	"
"	1.20	-	0.06	"
"	1.46	-	0.06	"
"	0.98	-	0.15	"
LD 400	12.82	-	6.35	HIGH
MACBOND 18 1200	1.56	-	0.05	FAIR
3M Y966 TRANSFER TAPE (ACRYLIC)	1.60	1.46	0.00	FAIR-GOOD
"	1.00	-	0.00	"
"	1.02	-	0.01	"
MYSTIK 6468 ACRYLIC TRANSFER TAPE	1.52	-	0.01	FAIR
MYSTIC 7452 AL FOIL/ACRYLIC	0.25	-	0.03	GOOD (SHOWS SHIELDING EFFECT OF FOIL)
" 7453 " "	0.64	-	0.04	" "
PERMACEL P11 AL FOIL/ACRYLIC	0.36	-	0.01	" "
3M 425 AL FOIL/ACRYLIC	0.14	-	0.07	" "
3M Y427 " "	0.12	0.03	0.02	" "
3M 428 " "	0.29	-	0.05	" "
3M SCOTCHDAMP Y370	5.66	5.10	0.30	HIGH
" "	6.39	6.21	0.31	HIGH (POSTCURED 24 HR AT 50°C)
" "	1.03	0.85	0.11	GOOD (POSTCURED 24 HR AT 125°C)

all have extremely low outgassing. Outgassing would therefore probably not be a problem for a constrained-layer or lap joint.

In summary, ISD 110 is the only current candidate which meets the JSC outgassing requirements. The data indicate that the other candidates would probably pass if confined between faceplates. Further research should be done to see if this is the case. If outgassing is still a problem, postcuring or encapsulation could be examined to decrease outgassing. A low outgassing material, such as G.E.'s RTV 566 silicone, could be used for joint encapsulation.

2.4 Creep

Creep or compression set data are listed on Table 4. This type of data is not available for most VEMs. Compression set data were available for EAR C2003 and C1002, two of the stiffest VEMs available.

The compression sets of C1002 and C2003 are shown for a constant load (400 psi) or deflection (25%) for about 24 hours at room temperature. The values range from 4.6 to 17.7%, although the values for C2003 decreased after prolonged recovery.

EAR C2003, C1002, Dyad 609 and Dyad 606 are strong, cured rubbers of 59-94 Shore A hardness (Table 5) at room temperature. All have G's of about 8,000 psi or more at 21°C and 100 Hz. Although no compression set data are available for Dyad 606 or 609, their compression sets should be similar to those of C1002 or C2003.

Materials such as ISD 110, 3M 467, IB 2107 and Soundcoat D are soft gums which would probably show extremely high creep and compression set under a sustained high load, with resultant joint failure. A structurally redundant joint is needed for such soft materials. Tests should be performed to characterize these materials. The tests should simulate the joint geometry, loads, VEM thickness and expected temperatures. Temperature is an important consideration. Elevated temperatures will tend to increase creep while low temperatures should slow it.

Table 4. VEM COMPRESSION SET

Material	Hardness Shore A	Test Method	Compression Set, %
EAR C-2003	93-94	Constant load (ASTM D395-69, Method A) 400 psi for 24 hrs at 72°F	6.9 (< 1.0% set after prolonged recovery)
" "	"	Constant deflection (ASTM D395-69, Method B) 25% deflection for 24 hrs at 73°F	17.7 (< 5% set after prolonged recovery)
EAR C-1002	59-64	Constant load (ASTM D395-67, Method A) 400 psi for 22 hrs at 72°F	6.3
" "	"	Constant deflection (ASTM D395-67, Method B) 25% deflection for 22 hrs at 72°F	4.6

Table 5. PHYSICAL PROPERTIES OF VEM CANDIDATES

Material	Density GM/CC	Hardness, Shore A	Brittle Point, °F	Tensile Strength, psi	Ultimate Elongation, %	Tear Resistance, PLI
SOUNDCOAT DYAD 606	1.105	67	-20	2400	425	-
" " 609	1.106	94	-22	4800	250	-
EAR C-2003	1.71	93-94	-	1323	123	191
EAR C-1002	1.27	59-64	-	1350	414	199
3M ISD 110	0.98	-	-	-	-	-
MACBOND IB2107	1.05	-	-	-	-	-

2.5 Fabrication

Some VEMs are gums at room temperature, while others are hard, solid rubbers. VEMs which are hard, solid rubbers could be incorporated in the joint in several ways. Cured sheets of these materials could be bonded at room temperature to composites. Scuff sanding and the application of an epoxy primer such as BR 127 to the composite may be necessary. Some experimental work has been done on vulcanizing uncured rubber stocks to composites, with mixed success. Again, careful surface preparation and some experimentation will be required. If metal plates only are used in the joint, the rubber can be easily vulcanized in place or adhesively bonded at room temperature. Selection of the adhesive should be carefully made. The adhesive should be at least as strong as the rubber and should be close to it in flexibility.

The softer VEMs (ISD 110, 3M467, IB2107, Soundcoat D) are self-adhering. A hot press could be used to increase flow for a complex joint. Soaking a laid-up joint at 52-66°C for 1 hour has been found to improve the bonding of ISD 110[1].

If outgassing is expected to be a problem, the joint could be encapsulated with a low outgassing material like G.E. RTV 566 silicone.

3.0 CONCLUSIONS

1. EAR C2003, Dyad 606, ISD 110 and 3M 467 meet all of the minimum design goals. Selection among them will depend on what G' the engineer needs for his particular joint design.

2. Soundcoat D comes close to meeting the design goals and has the advantage of being less temperature sensitive than the other candidates. It should therefore be given some consideration if its G' is acceptable.

3. In a constrained layer or lap joint, only the VEM edges will be exposed. This should decrease outgassing. Further testing should be done in this area. Postcuring or encapsulation should be examined to reduce outgassing if necessary.

4. Creep could be a problem for the softer VEMs and a redundant joint structure is needed. At elevated temperatures, the harder VEMs may also have

excessive creep. They have good compression set at room temperature. Testing should be performed to characterize the creep of the candidate VEMs using dead weights on simple double lap shear specimens. The creep could be measured as a function of temperature, time, load/area and VEM layer thickness.

5. Fabrication would be easiest if a soft, self-bonding VEM were selected. If a harder (millable) VEM is selected, fabrication will be facilitated if metal joint plates are used. With some effort and experimentation a joint using a hard VEM and composite plates could be made.

4.0 REFERENCES

1. M. L. Drake and G. E. Terborg, "Polymeric Material Testing Procedures to Determine Damping Properties and the Results of Selected Commercial Materials", Air Force Materials Laboratory Report AFWAL-TR-80-4093, July 1980.

2. D.I.G. Jones, "Introduction to Damping Materials and Systems for Vibration Control in Structures", Report No. AFFDL-TM-78-78-FBA. Presented at the Conference on Aerospace Polymeric Viscoelastic Damping Technology for the 1980's, Dayton, Ohio, Feb. 7-8, 1978.

3. Anon, "Compilation of VCM Data of Nonmetallic Materials", NASA-JSC Report JSC 08962, Rev. U and Addendums 1-9, May 1979-Aug 1982.

4. Anon, "General Specification - Vacuum Stability Requirements for Polymeric Materials for Spacecraft Applications", JSC Specification SP-R-0022A, Sept. 1974.

APPENDIX II

DAMPING JOINT LAP SHEAR MODEL

To determine effects of the design parameters in the proposed joint (Figure 1), a one-dimensional analysis of a double-lap joint was modified to include the effect of a restoring spring acting on the inner adherend. The original analysis of the double lap joint performed by L. J. Hart-Smith is a fully elastic one-dimensional problem. The differential equation governing the adhesive shear stress distribution is

$$\frac{d^2\tau}{dx^2} - \lambda^2\tau = 0 \qquad (1)$$

where

$$\lambda^2 = \frac{G}{\eta}\left(\frac{1}{E_o t_o} + \frac{2}{E_i t_i}\right)$$

G = shear modulus of adhesive
η = adhesive layer thickness
E_o = outer adherend Young's modulus
E_i = inner adherend Young's modulus
t_o = outer adherend thickness
t_i = inner adherend thickness
T_o = force in outer adherend
T_i = force in inner adherend
ℓ_g = gap length
$k = EA_{spring}/\ell_g$

The general solution of this differential equation is

$$\tau(x) = A \sinh(\lambda x) + B \cosh(\lambda x)$$

Boundary conditions on $d\tau/dx$ will yield the constants A and B.

$$\frac{d\tau}{dx} = A\lambda \cosh(\lambda x) + B\lambda \sinh(\lambda h) = \frac{G}{\eta}\left(\frac{T_i}{E_i t_i} - \frac{T_o}{E_o t_o}\right)$$

Evaluating the boundary condition at $x = \ell/2$;

$$A\lambda \cosh\left(\frac{\lambda\ell}{2}\right) + B\lambda \sinh\left(\frac{\lambda\ell}{2}\right) = \frac{G}{\eta}\left[\frac{T_i(\ell/2)}{E_i t_i} - 0\right] \qquad (2)$$

Also, for $x = -\ell/2$;

$$A\lambda \cosh\left(-\frac{\lambda\ell}{2}\right) + B\lambda \sinh\left(-\frac{\lambda\ell}{2}\right) = \frac{G}{\eta}\left[\frac{T_1(-\ell/2)}{E_1 t_1} - \frac{T_o(-\ell/2)}{E_o t_o}\right] \qquad (3)$$

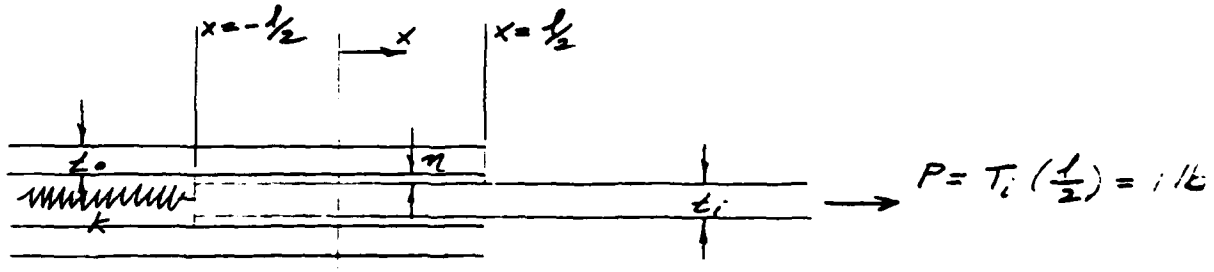

Figure 1

Solving equations (2) and (3) for the constants A and B,

$$A = \frac{G}{2\eta\lambda}\left[\frac{T_1(\ell/2) + T_1(-\ell/2)}{E_1 t_1} - \frac{T_o(-\ell/2)}{E_o t_o}\right] \frac{1}{\cosh(\lambda\ell/2)}$$

$$B = \frac{G}{2\eta\lambda}\left[\frac{T_1(\ell/2) - T_1(-\ell/2)}{E_1 t_1} + \frac{T_o(-\ell/2)}{E_o t_o}\right] \frac{1}{\sinh(\lambda\ell/2)}$$

Equation I

$$\tau(-\ell/2) = A \sinh\left(-\frac{\lambda\ell}{2}\right) + B \cosh\left(-\frac{\lambda\ell}{2}\right)$$

$$\frac{T_o(-\ell/2)\,\ell_g}{E_o t_o(1)} = \delta_o(-\ell/2) = \delta_1(-\ell/2) - \frac{\eta t(-\ell/2)}{G}$$

Equation II

$$\delta_1(-\ell/2) = \frac{T_o(-\ell/2)\,\ell_g}{E_o t_o} + \tau(-\ell/2)\,\frac{\eta}{G}$$

Equation III Overall Equilibrium

$$\delta_1(-\ell/2) = \frac{P}{k} - \frac{2}{k} T_o(-\ell/2)$$

Equation IV Spring Equation

$$T_1(-\ell/2) = k\,\delta_1(-\ell/2)$$

Solve equations I-IV for $T_0(-\ell/2)$, $\tau(-\ell/2)$, $\delta_1(-\ell/2)$, $T_1(-\ell/2)$. Evaluation of these unknowns will yield values for A, B and the shear stress distribution $\tau(x)$.

To determine the strain energy in an adhesive layer,

$$U = \frac{1}{2}\int_v \tau\,\gamma\,dv$$

$$\tau = G\gamma$$

$$U = \frac{1}{2G}\int_v \tau^2\,dv$$

Hence a closed form solution for strain energy U is obtained.

To determine the deflection at $x = \ell/2$ in the inner adherends:

$\delta_1(-\ell/2)$ is known from solution of Equations I-IV.

Strain in outer adherend, $\varepsilon(x)$

$$\varepsilon(x) = \frac{1}{E_0 t_0}\int_{x_1}^{x_2} \tau(x)\,dx$$

$$\delta_1(\ell/2) = \delta_1(-\ell/2) + \int_{-\ell/2}^{\ell/2} \varepsilon(x)$$

$$\delta_1(\ell/2) = \delta_1(-\ell/2) + \frac{1}{E_0 t_0}\int_{-\ell/2}^{\ell/2}\int_{-\ell/2}^{x} \tau(x)\,dx$$

Again, a closed form solution can be obtained by direct integration of $\tau(x)$. $\delta_1(\ell/2)$ provides a measure of relative stiffness in each joint.

Studies were completed by varying three of the more interesting parameters: overlap length of adherends, adhesive thickness, and adhesive shear modulus. Both a stiff and soft restoring spring were used to observe the relative effects upon the adhesive layer strain energy and overall joint deflection. The following baseline model was used:

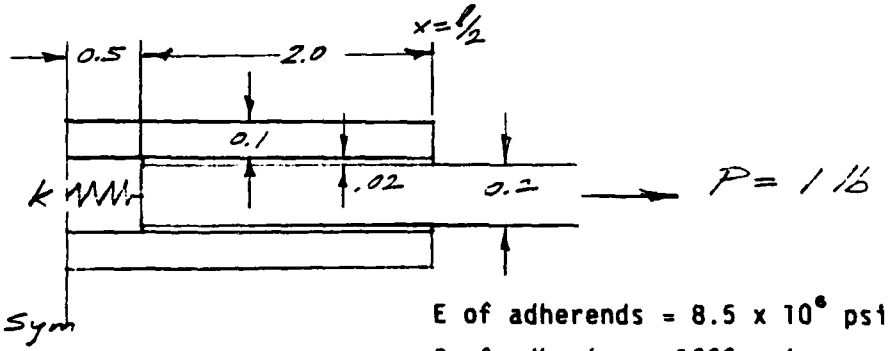

E of adherends = 8.5×10^6 psi

G of adhesive = 1000 psi

stiff spring $K = \frac{EA}{\ell} = \frac{10{,}000 \text{ lb}}{.5 \text{ in.}} = 20{,}000$ lb/in.

soft spring $k = \frac{10}{.5} = 20$ lb/in.

As a check case, the shear modulus of the adhesive is allowed to approach zero. The deflection of the joint at $x = \ell/2$ proceeds to approach .00005 in. (1 lb/ 20,000 lb/in.), the correct displacement for the spring alone (assuming adherends are rigid).

Figure 2 shows the strain energy in an adhesive layer as a function of the overlap length for both a stiff and soft restoring spring. As expected, the softer spring allows more strain energy in the adhesive for a given overlap length. The deflection also decreases at the end of the joint as the overlap length increases. Both deflection and strain energy become asymptotic to zero as the overlap length (and the joint total stiffness) become large.

Figure 3 is a similar plot vs. adhesive thickness. Again the trends are as one would expect, i.e. greater deflection with increased adhesive layer thickness and even more so for the less stiff spring. For the stiff spring, adhesive strain energy becomes asymptotic with increased adhesive thickness (and, hence, increased joint flexibility) since the strain energy in the spring becomes the dominant term.

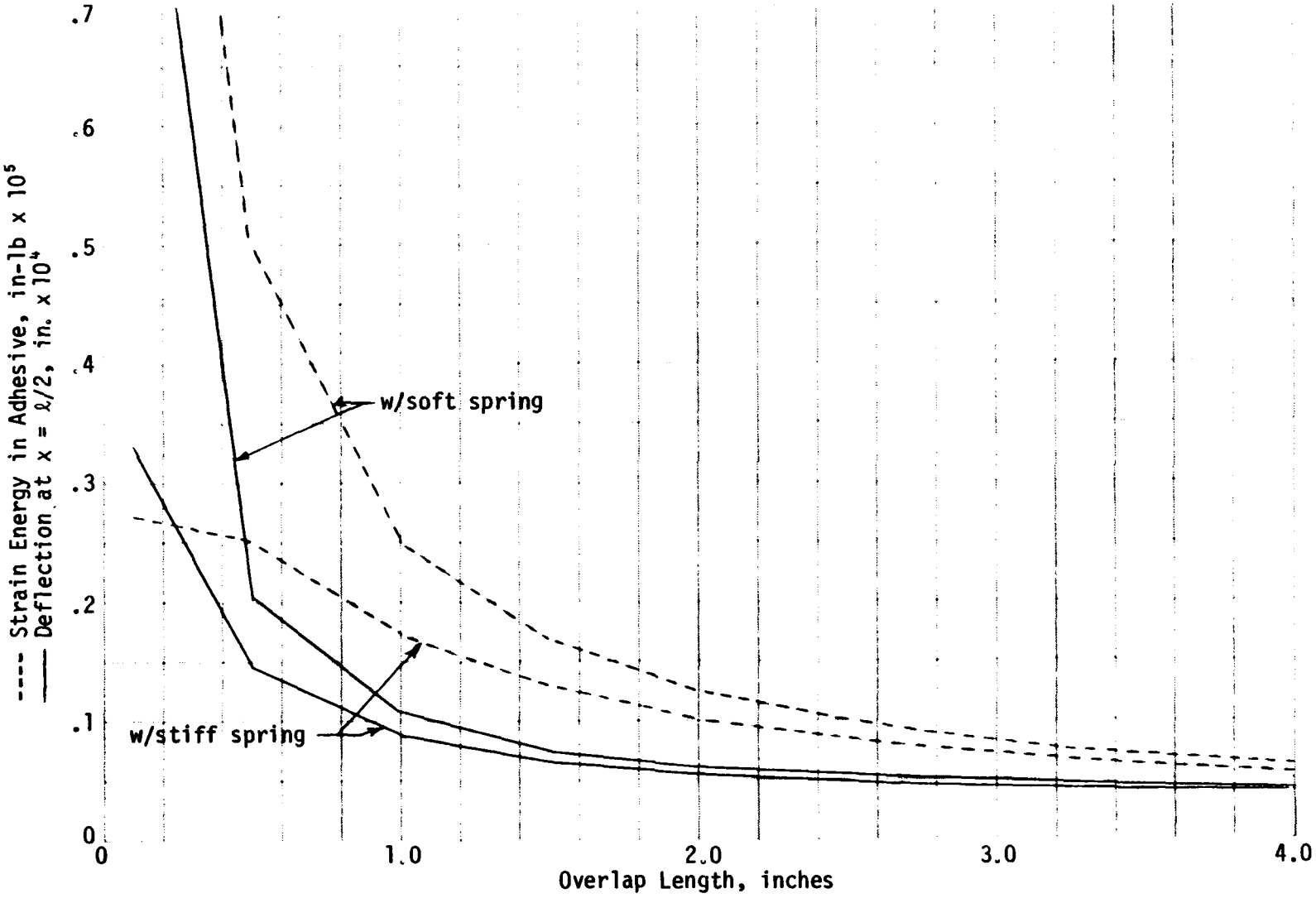

Figure 2. Strain Energy in One Adhesive Layer and Deflection vs. Overlap Length

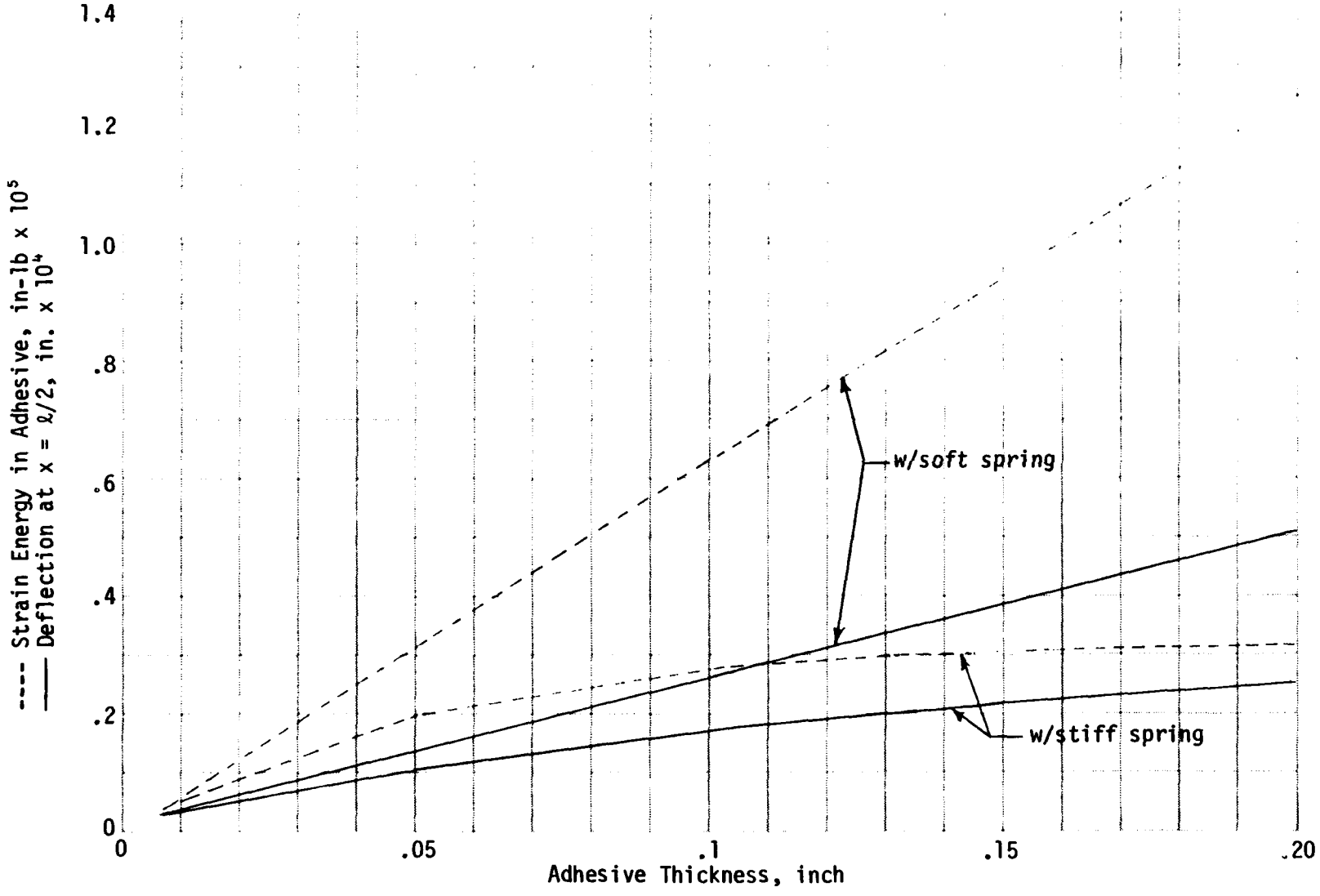

Figure 3. Strain Energy in One Adhesive Layer and Deflection vs. Adhesive Thickness

Figure 4 shows adhesive strain energy and joint deflection vs. adhesive shear modulus. Increase in shear modulus reduces the joint flexibility and hence the overall joint deflection incurred by the unit load. Little effect is observed due to the substitution of a soft spring for a stiff spring or vice versa once the shear modulus has exceeded 5 KSI. Again the trends evidenced appear correct.

REFERENCES

1. Goland, M. and E. Reissner. The Stresses in Cemented Joints. J. Appl. Mech. II, A17-A27 (1944).

2. L. J. Hart-Smith. Adhesive-Bonded Single-Lap Joints. NASA CR-112236, Jan. 1973.

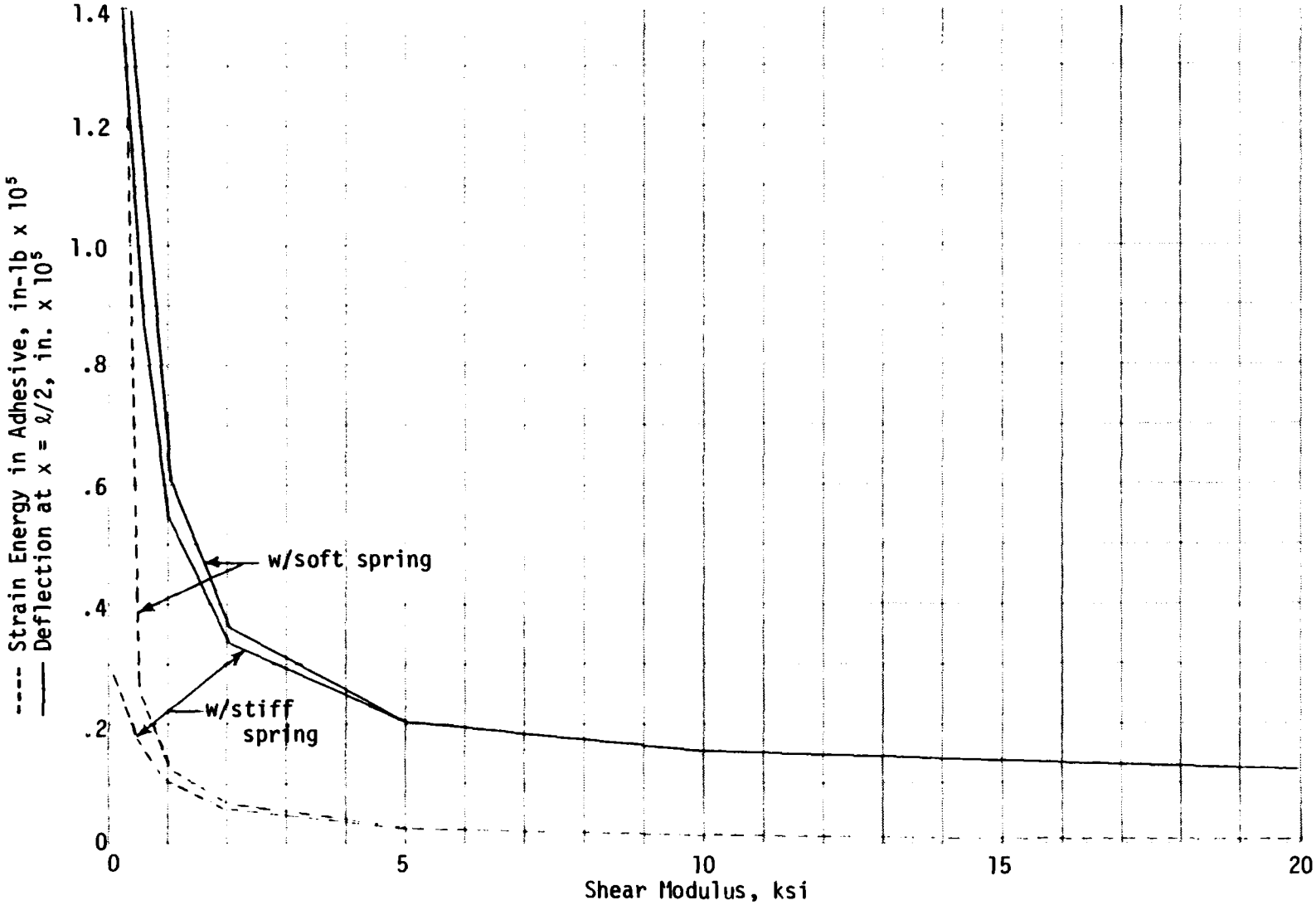

Figure 4. Strain Energy in One Adhesive Layer and Deflection vs. Shear Modulus

To run the program, the file shown should be obtained and compiled in FORTRAN. Input for the model should be arranged in the following order, substituting a 0.0 for the parameter to be varied.

(1) Length of overlap

(2) Thickness of outer adherend

(3) Thickness of inner adherend

(4) Thickness of adhesive layer

(5) Modulus of outer adherend

(6) Modulus of inner adherend

(7) Shear modulus of adhesive

(8) EA of spring material

(9) Length of gap(spring length)

After these parameters are input, the values to be used in the space of the parameter omitted should be listed in the same fashion, followed by a -1.0 to flag end data. This should be input to the program.

```
DJ          09:36 JUN 22,"84

      PROGRAM DAMP(INPUT,OUTPUT,TAPE5=INPUT,TAPE6=OUTPUT)
      DIMENSION D(9),A(4,4),B(4),X(4),V(20)
C     D(1)=L, LENGTH OF OVERLAP
C     D(2)=TO, THICKNESS OF OUTER ADHEREND
C     D(3)=TI, THICKNESS OF INNER ADHEREND
C     D(4)=NU, THICKNESS OF ADHESIVE
C     D(5)=EO, MODULUS OF OUTER ADHEREND
C     D(6)=EI, MODULUS OF INNER ADHEREND
C     D(7)=G, SHEAR MODULUS OF ADHESIVE
C     D(8)=EAS, SPRING STIFFNESS PER LENGTH
C     D(9)=LG, LENGTH OF GAP(SPRING LENGTH)
      DO 10 I=1,9
      READ(5,*) D(I)
10    IF(D(I).EQ.0.0) NO=I
      DO 30 I=1,20
      READ(5,*) V(I)
30    IF(V(I).EQ.-1.00) GOTO 50
50    NSTOP=I-1
      DO 700 I=1,NSTOP
      PRINT 7777
7777  FORMAT(6H      )
      D(NQ)=V(I)
      P=1.0
C     ELEMENTS OF A,B MATRICES
      ETO=D(5)*D(2)
      ETI=D(6)*D(3)
C     PRINT 4000,D(7),D(4),ETO,XLM
      XLM=SQRT((D(7)/D(4))*((1.0/ETO)+(2.0/ETI)))
C     PRINT 4000,ETO,ETI,XLM
      XK=D(8)/D(9)
C     DO 44 IX=1,9
C     PRINT 3000,D(IX)
C4    CONTINUE
      CLM=COSH(XLM*D(1)/2.0)
      SLM=SINH(XLM*D(1)/2.0)
      CLN=COSH(-XLM*D(1)/2.0)
      SLN=SINH(-XLM*D(1)/2.0)
      A(1,1)=-(D(7)/2.0*D(4))*XLM*ETO)*(SLM*CLM)+(CLM*SLM))
      A(1,2)=1.0
      A(1,3)=0.0
      A(1,4)=(D(7)/(2.0*D(4)))*XLM*ETI))*((SLM*CLM)+(CLM*SLM))
      A(2,1)=-(D(9)/ETO)
      A(2,2)=-(D(4)/D(7))
      A(2,3)=+1.0
      A(2,4)=0.0
C     GC=(2.0*D(7))/(D(4)*XLM)
      A(3,1)=2.0
      A(3,2)=0.0
      A(3,3)=0.0
      A(3,4)=1.0
      A(4,1)=0.0
      A(4,2)=0.0
      A(4,3)=-XK
      A(4,4)=1.0
      B(1)=(D(7)/(2.0*D(4)*XLM*ETI))*((CLM/SLM)-(SLM/CLM))
      B(2)=0.0
      B(3)=P
      B(4)=0.0
      N=4
C     PRINT 4000,A(1,1),A(1,2),A(1,3),A(1,4)
C     PRINT 4000,A(2,1),A(2,2),A(2,3),A(2,4)
C     PRINT 4000,A(3,1),A(3,2),A(3,3),A(3,4)
C     PRINT 4000,A(4,1),A(4,2),A(4,3),A(4,4)
```

```
C       PRINT 4000,B(1),B(2),B(3),B(4)
C       SOLUTION
        CALL GAUSS(N,A,B,X)
C       X(1)=TO(-L/2)
C       X(2)=TAU(-L/2)
C       X(3)=DELTA(-L/2)
C       X(4)=TI(-L/2)
C       PRINT 4000,X(1),X(2),X(3),X(4)
C       CALCULATE COEFFICIENTS IN GENERAL SOLUTION
4000    FORMAT(4G12.5)
C       PRINT 4000,GC,D(7),D(4),XLM
        GC=(D(7)/(2.0*D(4)*XLM))
        AA=GC*((P+X(4))/ETI-(X(1)/ETO))/CLM
        BB=GC*((P-X(4))/ETI+(X(1)/ETO))/SLM
C       PRINT 4000,AA,BB,XLM,D(1)
C       CALCULATE STRAIN ENERGY IN ADHESIVE
        S2L=SINH(XLM*D(1))/(2.0*XLM)
        C2=1.0/(D(7)*2.0)
        CL2=D(1)/2.0
        U=C2*((AA**2)*(S2L-CL2)+(BB**2)*(S2L+CL2))
        U=U*D(4)
        PRINT 6000,D(NQ)
6000    FORMAT(11H  VAR=      ,G12.5)
        PRINT 3000,U
3000    FORMAT(11H    U=      ,G12.5)
C       CALCULATE DISPLACEMENT AT X=L/2
        DL1=(2.0*AA*SINH(XLM*D(1)/2.0))/(XLM**2)
        DL2=(AA*D(1)*COSH(XLM*D(1)/2.0))/(XLM)
        DL3=(BB*D(1)*SINH(XLM*D(1)/2.0))/(XLM)
        DL=(1.0/ETO)*(DL1-DL2+DL3)
        PRINT 555,DL
555     FORMAT(11H     DL=     ,G12.5)
        PRINT 666,X(3)
666     FORMAT(11H    X(3)=    ,G12.5)
        DL=DL+X(3)
        PRINT 5000,DL
5000    FORMAT(11H DEL(L 2)= ,G12.5)
700     CONTINUE
        STOP
        END
C
C
C
C
C
C
C
C
C
C
C
        FUNCTION SINH(Q)
        SINH=0.5*(EXP(Q)-EXP(-Q))
        RETURN
        END
        FUNCTION COSH(Q)
        COSH=0.5*(EXP(Q)+EXP(-Q))
        RETURN
        END
        SUBROUTINE GAUSS(N,A,B,DISP)
        REAL A(N,N),B(N),DISP(N)
        NM=N-1
        DO 10 K=1,NM
        L=K
        P=A(K,K)
        DO 20 I=K,NM
        IP=I+1
```

```
      IF(ABS(P).GE.ABS(A(IP,K))) GOTO 20
      P=A(IP,K)
      L=IP
20    CONTINUE
      DO 30 J=1,N
      DUM=A(K,J)
      A(K,J)=A(L,J)
      A(L,J)=DUM
30    CONTINUE
      DUM=B(K)
      B(K)=B(L)
      B(L)=DUM
      KP=K+1
      DO 40 I=KP,N
      A(I,K)=A(I,K)/A(K,K)
      DO 50 J=KP,N
      A(I,J)=A(I,J)-A(I,K)*A(K,J)
50    CONTINUE
      B(I)=B(I)-A(I,K)*B(K)
      A(I,K)=0.0
40    CONTINUE
10    CONTINUE
      DISP(N)=B(N)/A(N,N)
      DO 80 K=1,NM
      SUM=0.0
      NMK=N-K
      DO 60 J=NMK,NM
      JP=J+1
      SUM=SUM+A(NMK,JP)*DISP(JP)
60    CONTINUE
      DISP(NMK)=(B(NMK)-SUM)/A(NMK,NMK)
80    CONTINUE
      RETURN
      END
```

APPENDIX III

GEORGIA INSTITUTE OF TECHNOLOGY

INTERIM REPORT #1

A NEW APPROACH TO DAMPING MEASUREMENTS IN STRUCTURAL JOINTS

Jacky Prucz and Ambur D. Reddy
School of Aerospace Engineering
Georgia Institute of Technology
Atlanta, Georgia 30332

Interim Report 1
McDonnell Douglas Contract 83025032
AFOSR Contract F49620-83-C-0017

December 1983

TABLE OF CONTENTS

Abstract

A new technique for measuring damping and the stiffness of structural joints is being developed. Preliminary experiments on joints made of aluminum specimens have provided promising results.

Damping information is extracted from the changes that occur in certain characteristics of a sine-pulse stress wave as a result of its passage through the joint. For practical set-ups at low frequencies, a preliminary processing of the test data is carried out in order to remove end reflection effects.

The new technique provides realistic and general results that are suitable for direct integration into the overall structural design. The results do not depend on the particular characteristics of the test fixture used for their measurement.

I. INTRODUCTION

Background

The dynamic behavior of the joints in a structure depends on the general structural configuration and properties, as well as on their own characteristics. Since the mass of a joint is usually very small as compared with that of the structural members, its vibration will be governed by the modal characteristics of the entire structure. Moreover, the boundary conditions of each joint are determined by the properties of the connected members, its location in the structure and the joint-member interface. Therefore, the joint characteristics should be evaluated like a homogeneous, equivalent material, rather than like system characteristics of a self-contained structure. The determined properties of the joints can be subsequently combined with those of the structural members in order to synthesize the system characteristics of the whole structure.

The major problem related to the experimental evaluation of dynamic properties is the limited accuracy of the generated damping data. Since reasonably accurate damping information is needed for proper design of a system for vibratory loadings, many measurement techniques have been developed. The basic approaches are reviewed in References 1-3, 13 and 16, along with discussions about the different effects that may degrade the accuracy of the damping data. Two important conclusions may be drawn from a state-of-the-art review on damping measurements:

1. The problem of determination of damping is not yet resolved [13].
2. The main deteriorating effect is the vibratory energy loss in the testing apparatus through the specimen's boundaries [1, 3, 4].

Pulse Propagation Approach

The most popular methods for extracting the damping properties from test data rely upon modal analysis techniques [1-3, 5]. They are suitable mainly for system damping characterization, where the structural configuration and the real boundary conditions may be known in advance [13].

The foregoing discussion about structural joints indicates that their dynamic characterization should be performed by other experimental approaches rather than the modal techniques. Different "non-modal" methods have been reported [2, 5] although the pulse propagation approach has been cited to be one of the most promising [2]. Its main advantage lies in the possibility to eliminate the specimen - fixture interaction effects from the test data, which will improve the damping measurements. Furthermore, general dynamic properties can be measured, that characterize the test specimen alone and do not depend on the particular boundary conditions at the specimen's end. The pulse propagation approach is particularly well suited to structural joints in large space structures, whose dynamic behavior seems to be better described by a travelling wave approach rather than a vibration approach.

A stress pulse is both attenuated and dispersed during its propagation through a viscoelastic medium. The dynamic properties of the medium can be deduced from the development of the propagating pulse [6 , 9]. So far, this approach has been experimentally applied mostly in connection with axial excitation of long and slender rods [2, 3, 6-10]. In this case, it permits a complete dynamic-stiffness characterization of the test specimen, since its axial stiffness is determined by the phase velocity, whereas its damping capability is measured by the pulse attenuation.

The major drawback of the available techniques is that the stress pulse is always generated by an axial impact on one end of the specimen. These tests are

confined, therefore, to extremely high loading rates and do not permit any control on the pulse frequency. However, the pulse propagation approach can be extended to low-frequency tests if a sine pulse, rather than an impact pulse, is applied on the specimen. The excitation frequency can be thus controlled and the frequency-dependence of the dynamic properties can be experimentally investigated. The longer wavelengths associated with low-frequency pulses allow the use of shorter an "less slender" specimens without introducing geometric dispersion effects. Since a perfect sine-pulse contains just one frequency, no significant dispersion is likely to occur, either of geometric or viscoelastic nature.

Since the conventional definitions of damping are related to cyclic oscillations [1, 11, 12], the sine pulse will usually contain one full cycle so that its length will depend on the tested frequency. When the damping effect of the joint is very high, it is possible to deduce the stiffness and damping information by analyzing only the pulse-front rather than its whole length [9]. If, instead of its conventional measures, the damping in the joint is rather expressed in terms of the energy dissipation over a preselected time interval, only the corresponding length of the pulse needs to be generated or analyzed [10, 15].

II. EXPERIMENTAL SET-UP AND PROCEDURE

Electronic Equipment

A block diagram of the experimental set-up is given in Figure 1.

The excitation signal is provided and fully controlled by a Gated Pulse Generator that includes two basic units:

1. a Tektronix FG 501A function generator that controls the signal shape, frequency and amplitude; and
2. a Tektronix PG 501 pulse generator that provides the desired gating of the main signal and controls both the pulse length and its repetition rate.

The Gated Pulse Generator serves also as a trigger unit for the two oscilloscopes included in the set-up.

The four-channel Tektronix 5440 Analog Oscilloscope allows real time monitoring of all the input and output signals, facilitating the adjustment of the excitation signal to the proper amplitude, frequency and pulse length. The excitation pulse is transmitted to the vibration generator through a B&K Power Amplifier Type 2706. Due to the nonavailability of the high stiffness piezoelectric motion transducer to be custom built and supplied by Wilcoxon Research, a readily available electromagnetic B&K Mini-Shaker Type 4810, has been used to excite the specimen. Proper axial excitation cannot be achieved in this case if the longitudinal displacement is restrained at the non-excited end.

The response of the specimen to each excitation pulse is picked up by two accelerometers - one just before the test joint and the other just after it. The accelerometer signals are identically amplified and displayed on two separate channels of the two oscilloscopes.

The NICOLET 4094 Digital Oscilloscope displays the two responses at an adjustable sampling rate, such that its resolution and sweep length can match a

wide range of frequencies and pulse lengths. The specimen responses to consecutive identical pulses can be easily averaged by using the digital oscilloscope's capability to perform automatic averaging between consecutive sweeps. The pulse repetition rate is kept low enough to allow sufficient time for the disturbances due to the previous pulse to die down before the next pulse is applied to the specimen.

The data displayed on the digital oscilloscope and stored in its display memory contains the damping and stiffness contributions fo the test joint for the particular excitation parameters of each test. When a test is completed, its data can be stored on a disk to be processed and analyzed later.

Test Fixture

A schematic of the test fixture with a specimen is shown in Figure 2. The fixture is designed to fit into the environmental chamber with the electric cables drawn out through the port. Since any source of backlash causes a significant distortion of the response signals, all the mechanical attachments must be rigid and free of clearances. For the same reason, the specimen cannot rest on rigid vertical supports, and hence, was suspended by a long, flexible, massless string. Signal distortion also occurs as a result of improper alignment between the directions of the excitation load, the specimen and the accelerometers axes, or as a result of non-uniform or eccentric load distribution over the specimen's cross-section. Sufficient care was exercised in attaching the specimen to the vibration generator and mounting the accelerometers on the specimen to minimize the above possibilities and thus reduce the external noise.

III. DATA ANALYSIS

Since all the experimental data are recorded on disks in a digital form, they can be readily transferred to a computer for numerical analysis. Details of the data analysis and dynamic characteristics determination are discussed below.

Stiffness Evaluation

The axial stiffness of the test joint can be evaluated directly from the "raw" experimental data. It is determined by the propagation time of the pulse front between the first and the second accelerometers (see Figs. 1 or 2). The time delay Δt between the starting points of the outputs of the two acelerometers can be measured directly on the digital oscilloscope (Fig. 3). The use of "sharp" excitation signals, like an impact, along with proper display resolution and pre-triggering mode of the oscilloscope, if necessary, facilitate the Δt measurement and improve its accuracy. An accuracy of ± 1 μsec can be readily achieved under these conditions.

The propagation velocity through the joint is given by:

$$c_j = \frac{\Delta d}{\Delta t} \tag{1}$$

where Δd is the distance between the two accelerometers and it is only slightly bigger than the joint length.

Assuming that the joint may be modeled as a homogeneous element of the same material like the connected members and of identical geometrical configuration, its equivalent stiffness is approximated as follows [2, 7]:

$$E_j = \rho c_j^2 \tag{2}$$

where "ρ" denotes the density of the connected members.

Damping Evaluation

Conventional Measures

The damping capability of the joint can be determined by comparing the response signals picked up by the two accelerometers. The exact analysis procedure depends upon the measure of damping chosen for evaluation [1, 11, 12]. Most measures are defined in the context of a material which can be modeled by the complex-modulus approach, i.e., at any one frequency it behaves like a Voigt solid [8]. Their definitions are usually associated with cyclic or near cyclic oscillations and homogeneous materials.

The new testing technique offers the following three different ways of data analysis for the evaluation of the joint equivalent loss factor, η_j:

1. The specific damping capacity is determined by the ratio of energy dissipated in a unit volume of joint per cycle to the maximum potential energy stored in a unit volume of joint during that cycle. This is probably the most useful form of presenting damping properties for the designer [1]. In the case of longitudinal stress waves, the axial stress at any point is proportional to the corresponding particle velocity [14]. The strain energy associated with the wave is, in turn, proportional to the square of the axial stress. Therefore, if the response signals of the two accelerometers are integrated with respect to time and then squared, the resulting signals, $W_1(t)$ and $W_2(t)$ are proportional to both the potential energy and the kinetic energy associated with the pulse. The proportionality constants depend on the impedance, i.e., on the density and stiffness, of the propagation medium. The specific damping energy is calculated as follows:

$$D = \frac{\sum_{t_i=0}^{T} W_1(t_i) - \sum_{t_i=0}^{T} W_2(t_i)}{(W_1)_{max}} \qquad (3)$$

where "T" denotes the pulse length, i.e. the duration of one cycle. The corresponding loss factor can subsequently be determined from the fundamental definition of damping [4, 11]:

$$\eta_j = \frac{1}{2\pi} D \qquad (4)$$

2. The attenuation coefficient, α_j, of a sine-pulse travelling through the joint may be related to its equivalent loss factor, η_j, according to 6, 7 :

$$\alpha_j = \frac{p}{4\pi c_j} D = \frac{p}{2c_j} \eta_j \qquad (5)$$

where "p" denotes the circular frequency of the pulse. This damping measure is based on the assumption that the pulse amplitude decays exponentially along the joint, i.e. the joint behaves like a homogeneous viscoelastic material of equivalent loss factor η_j. Therefore, if the pulse amplitude before the joint is $(V_1)_{max}$ whereas after the joint it is $(V_2)_{max}$, the attenuation factor can be determined from the relationship

$$(V_2)_{max} = (V_1)_{max} e^{-\alpha_j(\Delta d)} \qquad (6)$$

where $V_1(t)$ and $V_2(t)$ are obtained by time integration of the signals picked up by the first and the second accelerometer, respectively (see Fig. 4)

3. The equivalent loss angle, γ_j, associated with the joint damping, can be directly evaluated by measuring the phase lag, $\Delta\phi$, between the signals picked up by the two accelerometers (see Fig. 4). The

corresponding loss factor is then given by [11, 12]:

$$\eta_j = \tan \gamma_j \tag{7}$$

where

$$\gamma_j = \frac{2\pi}{T} \Delta\phi \tag{8}$$

Energy Balance

The main source of error in the above ways of analysis is, probably, the modeling of the joint as a homogeneous viscoelastic material characterized by some equivalent loss factor, η_j, and axial stiffness, E_j. However, such a modeling is required if the damping capability of the joint is to be expressed in terms of the conventional definitions of material damping measures.

An alternative way of describing the damping in joints is based upon a direct energy balance between any type of input and output signals [10, 15]. A modified loss factor, β_j, can be defined as the ratio between the energy dissipated inside the joint over a certain period of time and the total energy entering the joint over the same period of time.

The data analysis is similar to that for the evaluation of the specific damping energy with the only exception that relations (3) and (4) are now replaced by:

$$\beta_j = \frac{\sum_{t_i=0}^{\tau} W_1(t_i) - \sum_{t_i=0}^{\tau} W_2(t_i)}{\sum_{t_i=0}^{\tau} W_1(t_i)} \tag{9}$$

where $W_1(t_i)$ and $W_2(t_i)$ need not be confined to cyclic excitation and the summation limit "τ" is not restricted to a full cycle.

The use of "β_j" allows a more realistic treatment of the joints as discontinuities in the way of disturbances propagation along a structure. It may be

interpreted as the joints "efficiency" in dissipating the energy associated with these disturbances. However, " β_j" cannot be directly related to the conventional loss factor, η_j. Although it is a more general definition of damping, it introduces two new variables into consideration, namely the shape of the excitation signal and the time interval over which the energy balance is considered.

Effect of Reflections

Any data analysis procedure must be carried out on response signals that include only the joint contribution, without interference with reflections from the specimen's end. If this requirement is not fulfilled, the results will be inaccurate and dependent on the particular boundary conditions at the end of the test specimen.

For high-frequency tests, the far end of the specimen may be sufficiently distanced from the second transducer to enable the recording of the entire pulse length without any interference from the reflections. At low frequencies, however, a similar approach cannot be taken considering the practical limitations and the size of the specimen, especially when the set-up has to fit in an environmental chamber. A special signal analysis algorithm has been developed in order to eliminate most of the effects due to end reflections in the low-frequency tests. The algorithm is based on the assumption that, at any instant of time, the response measured by a transducer is a resultant superposition of different effects at its location. The response signals must be manipulated according to this algorithm before any damping information can be extracted from them.

Suppose that a low frequency sine pulse, s(t), is applied by the vibration generator on a reference continuous specimen made of the same material and geometrically identical with the members of the test specimen (Fig. 5). The end conditions of the reference specimen and the locations of the two accelerometers

are exactly the same like those of the test specimen. During its propagation from the first to the second accelerometer, the pulse is not likely to be significantly affected by the material damping, so that the two transducers would pick-up the same response, s(t), if the specimen was sufficiently long to avoid interference with end reflections. Instead, the transducers mounted on the reference specimen will pick up "modulated" signals

$$S_{R1}(t) = s(t) + r_1(t) \tag{10}$$

$$S_{R2}(t) = s(t) + r_1(t) + r_2(t) \tag{11}$$

where $r_1(t)$ and $r_2(t)$ represent the effects of end reflections at the locations of the first and second transducers, respectively.

When the same sine pulse, s(t), is applied on the test specimen, the responses of the two transducers will include additional effects, introduced by the existence of the joint

$$S_1(t) = s(t) + r_1(t) + R_1(t) + \Delta r_1(t) \tag{12}$$

$$S_2(t) = S_1(t) + r_2(t) + R_2(t) + \Delta r_2(t) + D(t) \tag{13}$$

where

a. $R_1(t)$ and $R_2(t)$ represent direct reflections from the joint at the locations of the first and the second transducers, respectively.

b. $\Delta r_1(t)$ and $\Delta r_2(t)$ represent variations caused by the joint in the end reflections effects $r_1(t)$ and $r_2(t)$, respectively. These variations are due both to the joint damping effect on signals reflected from the end and to the fact that the signals incident to the end are slightly different from the corresponding ones in the reference specimen.

c. D(t) represents the direct effect of the joint damping on the pulse propagated from the first to the second transducer.

When the signals $S_2(t)$ and $S_{R2}(t)$ are horizontally shifted such that all the four signals given in relations (10) - (13) have the same time base, they can be processed in order to yield the direct damping contribution, D(t). The corresponding algorithm is composed of the following manipulations of these four signals:

$$r_2(t) = S_{R2}(t) - S_{R1}(t) \tag{14}$$

$$R_1(t) + \Delta r_1(t) = S_1(t) - S_{R1}(t) \tag{15}$$

$$D(t) + r_2(t) + R_2(t) + \Delta r_2(t) = S_2(t) - S_1(t) \tag{16}$$

Since the two accelerometers are located symmetrically on the two sides of the joint, the following assumption is reasonable for low excitation frequencies:

$$R_2(t) + \Delta r_2(t) = R_1(t) + \Delta r_1(t) \tag{17}$$

Actually, $R_1(t)$ is expected to be higher than $R_2(t)$, but $\Delta r_2(t)$ is expected to be higher than $\Delta r_1(t)$, so that the total reflections effect of the joint may be assumed to be approximately the same at the locations of the two transducers. The validity of this assumption probably deteriorates as the excitation frequency increases, since the higher gradients of the incident and reflected signals enhance the overall reflections effect.

The assumption (17) allows the calculation of D(t) from relation (16):

$$D(t) = S_2(t) - S_1(t) - R_1(t) + \Delta r_1(t) - r_2(t) \tag{18}$$

The damping signal D(t) can be directly integrated with respect to time and squared to yield a signal proportional with the amount of pulse energy dissipated by the joint:

$$\Delta W(t) = W_1(t) - W_2(t) \tag{19}$$

Alternatively, the damping signal D(t) can be added to the input signal $S_1(t)$ in order to obtain a modified output signal, $S_2^*(t)$, "modulated" only by the damping effect of the joint

$$S_2^*(t) = S_1(t) + D(t) \tag{20}$$

The time signals $S_1(t)$ and $S_2^*(t)$ can be subsequently analyzed according to any of the previously mentioned procedures for damping evaluation.

IV. PRELIMINARY TESTS AND DISCUSSION

The feasibility of the new technique has been checked through a series of preliminary tests on five different aluminum specimens:

1. Specimen A - a reference continuous beam
2. Specimeh B - a first riveted joint
3. Specimen C - a second riveted joint, similar to the first.
4. Specimen D - Specimen B filled up with silicone rubber with a constraining steel shim
5. Specimen E - Specimen C filled up with silicone rubber with a constraining steel shim.

The geometrical configuration of the specimens is given in Fig. 6

Dynamic Tests

The test procedure outlined in Section II was adopted for performing the preliminary tests on the specimens. Three different types of excitation pulses were applied, in turn, on each specimen. Their main characteristics are given in Table 1.

Since the software required for the data transfer from the NICOLET 4094 Digital Oscilloscope to the HP 9845B Mini Computer of our facility has not been developed yet, a standard set of disk programs available with the digital oscilloscope was used for the analysis of the preliminary test data.

The damping information was extracted from the sine-type excitations after "preparatory" processing of the corresponding response signals, for removal of the end reflection effects. The impact-type excitation was used only for the stiffness evaluation of the test specimens. The damping capability of the tested joints was evaluated in terms of the energy dissipated over a time interval corresponding to the pulse length, i.e., over a full excitation cycle. As mentioned earlier in Section III, if the dissipated energy is divided by the total input energy,

Table 1. Excitation Pulses

Excitation Type	Generating Function	Frequency Setting (Hz)	Pulse Length (msec)	Initial Amplitude (Volts)	Response Gain Factor	Display Resolution	
						Time Axis (μsec)	Amplitude Axis (+ Volts full scale)
1	Sine (∿)	100	10	5	10	2	1
2	Sine (∿)	500	2	5	10	0.5	1
3	Impact Simulation (∩)	150	2.5	5	1	0.5	1

rather than the maximum strain energy, a "modified" loss factor " β_j " is obtained. The values of " β_j " for the four joints tested at the two frequencies during the preliminary tests, are given in Table 2. All the response signals were automatically averaged during the tests in order to reject possible noise effects.

Table 2. "Modified" Loss Factor From Preliminary Tests

Tested Specimen	First Joint		Second Joint	
	Without VEM*	With VEM*	Without VEM*	With VEM*
Frequency (Hz)	(Specimen B)	(Specimen D)	(Specimen C)	(Specimen E)
100	0.0161	0.1052	0.0275	0.1359
500	0.0276	0.5359	0.1479	0.5017

*VEM - Viscoelastic Material

The order of magnitude of these results and the damping effect of the silicone rubber seem to be accurate at the lower frequency, 100 Hz. The damping enhancement associated with the use of silicone rubber is slightly higher for the first joint (6.5 times as compared with 4.9 times for the second joint). This is probably because its initial loss factor (without VEM) is lower so that it is more sensitive to the viscoelastic treatment. Also, these manually riveted joints have built-in nonuniformities which directly influence their characteristics. The results obtained for the higher frequency, 500 Hz, seem to be less accurate, especially for the second joint. The initial loss factors of the two joints (without VEM) are higher at 500 Hz than at 100 Hz, but the difference is much higher for the second joint. The slip and backlash effects associated with the mechanical clearances about the

rivets seem to be more pronounced in the second joint and at higher frequencies. This is a reasonable explanation to the results given in Table 2. The data analysis algorithm for the elimination of the end reflections effect is expected to be more accurate at low frequencies than at high frequencies. Therefore, the results obtained at 500 Hz may include some end reflections effects which are affecting their accuracy.

Static Tests

Static tension tests were carried out on specimens A, B, and C in order to measure their axial stiffness between the locations of the two accelerometers. No static tests were performed on specimens D and E since the silicone rubber only filled up a gap in the joints and it was not expected to change their axial stiffness. The loading was provided by a Baldwin screw type testing machine and the extension of the specimen between the above two locations was measured using an extensometer with a built-in LVDT unit.

The axial stiffness of each specimen was determined from the linear fitting of the corresponding load vs. strain data. The static test results are given in Table 3 along with the corresponding values from the dynamic tests.

Table 3. Ratios of Extensional Moduli Relative to the Continuous Beam (Specimen A)

Specimen	Static Value	Dynamic Value
First Joint (B)	0.423	0.436
Second Joint (C)	0.540	0.420

Both the dynamic and the static techniques predict similar ratios between the extensional moduli of Specimens A and B. The dynamic result for the second joint (Specimen C) does not agree well with its static correspondent, perhaps because of the higher mechanical clearance existent in this specimen.

V. REFERENCES

1. Plunkett, R., "Measurement of Damping," Section Five, Structural Damping, Ruzicka, J.E., ed., ASME Annual Meeting in Atlantic City, N.J., 1959.

2. Bert, C. W. and Clary, R.R., "Evaluation of Experimental Methods for Determining Dynamic Stiffness and Damping of Composite Materials," Composite Materials: Testing and Design (3rd Conference), ASTM STP 546, 1974, pp. 250-265.

3. Gibson, R.F. and Plunkett, R., "Dynamic Stiffness and Damping of Fiber-Reinforced Composite Materials," The Shock and Vibration Digest, Vol. 9, No. 2, February 1977.

4. Crandall, S. H., "The Role of Damping in Vibration Theory," Journal of Sound and Vibration, Vol. 11, No. 1, 1970, pp. 3-18.

5. Smith, S., and Yee, R.C., "A New Technique for the Characterization of Structural Materials Under Dynamic Loading," AIAA Paper No. 78-510.

6. Kolsky, H., "The Propagation of Stress Pulses in Viscoelastic Solids," Philosophical Magazine, Vol. 1, Series 8, No. 8, 1956, pp. 693-710.

7. Tauchert, T. R., and Moon, F.C., "Propagation of Stress Waves in Fiber-Reinforced Composite Rods," AIAA Journal, Vol. 9, No. 8, 1971, pp. 1492-1498.

8. Lifshitz, J. M., "Specimen Preparation and Preliminary Results in the Study of Mechanical Properties of Fiber Reinforced Materials," AFML-TR-69-89, Part I, Air Force Materials Laboratory, Wright-Patterson Air Force Base, Ohio, 1969.

9. Blanc, R.H. and Champomier, F.P., "A Wave-Front Method for Determining the Dynamic Properties of High Damping Materials," Journal of Sound and Vibration, Vol. 49, No. 1, 1976, pp. 37-44.

10. Gupta, R., "Optimum Design of Wave Transmitting Joints," Wave Motion 4, North-Holland Publishing Company, 1982, pp. 75-83.

11. Bert, C. W., "Material Damping: An Introductory Review of Mathematical Models, Measures and Experimental Techniques," Journal of Sound and Vibration, Vol. 29, No. 2, 1973, pp. 129-153.

12. Bert, C.W., "Composite Materials: A Survey of the Damping Capacity of Fiber Reinforced Composites," Damping Applications for Vibration Control, Torvik, P.J., ed., ASME Winter Annual Meeting, Chicago, 1980, pp. 53-63.

13. Chu, F.H. and Wang, B.P., "Experimental Determination of Damping in Materials and Structures," Damping Applications for Vibration Control, Torvik, P.J., ed., ASME Winter Annual Meeting, Chicago, 1980.

14. Timoshenko, S. P. and Goodier, J. N., Theory of Elasticity, 3rd Edition, McGraw-Hill Book Company, 1970, pp. 485-513.

15. Lundberg, B., Gupta, R. and Andersson, L. E., "Optimum Transmission of Elastic Waves through Joints," Wave Motion 1, North-Holland Publishing Company, 1979, pp. 193-200.

16. Read, B.E. and Dean, G.D., The Determination of Dynamic Properties of Polymers and Composites, John Wiley and Sons, New York, 1978.

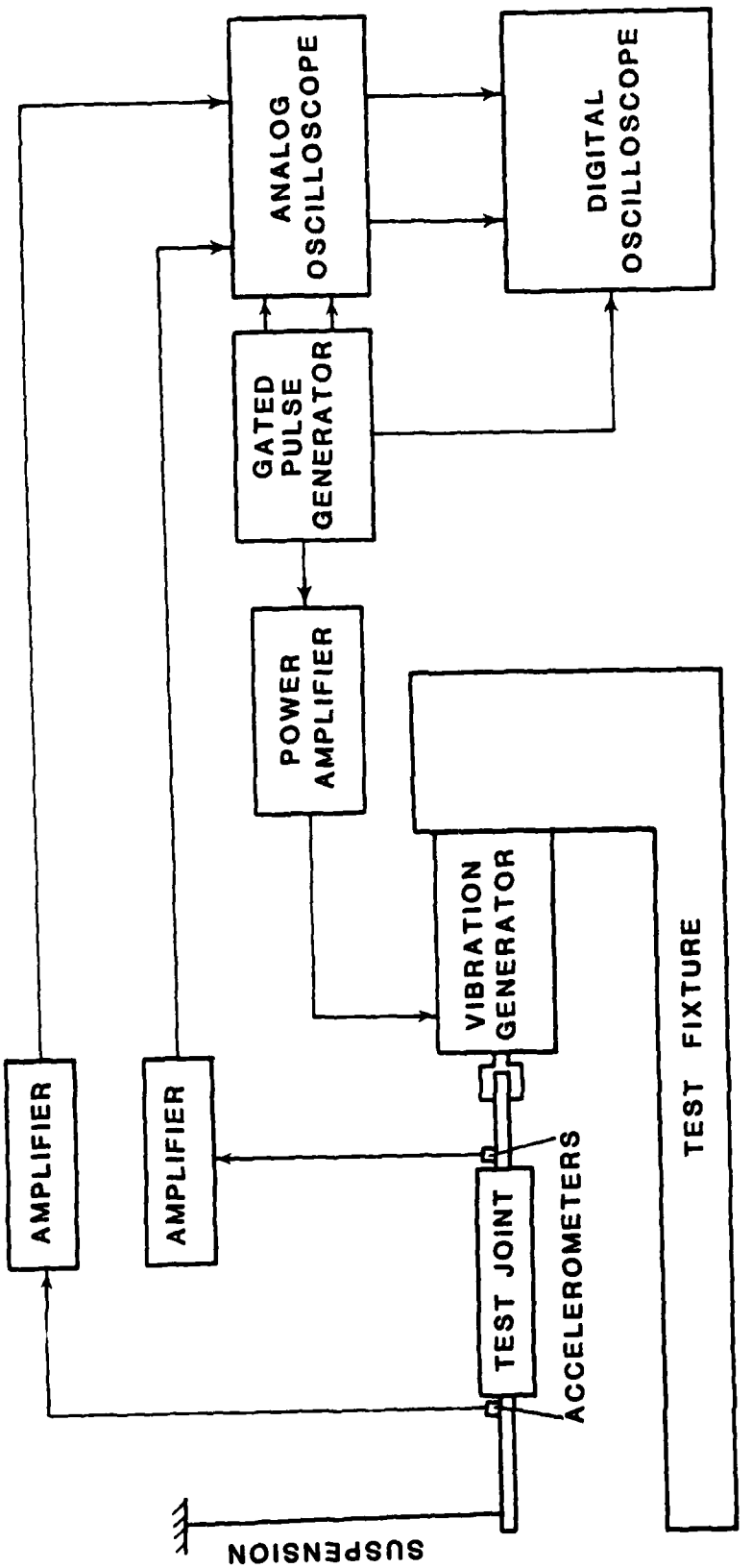

Fig.1- EXPERIMENTAL SET-UP

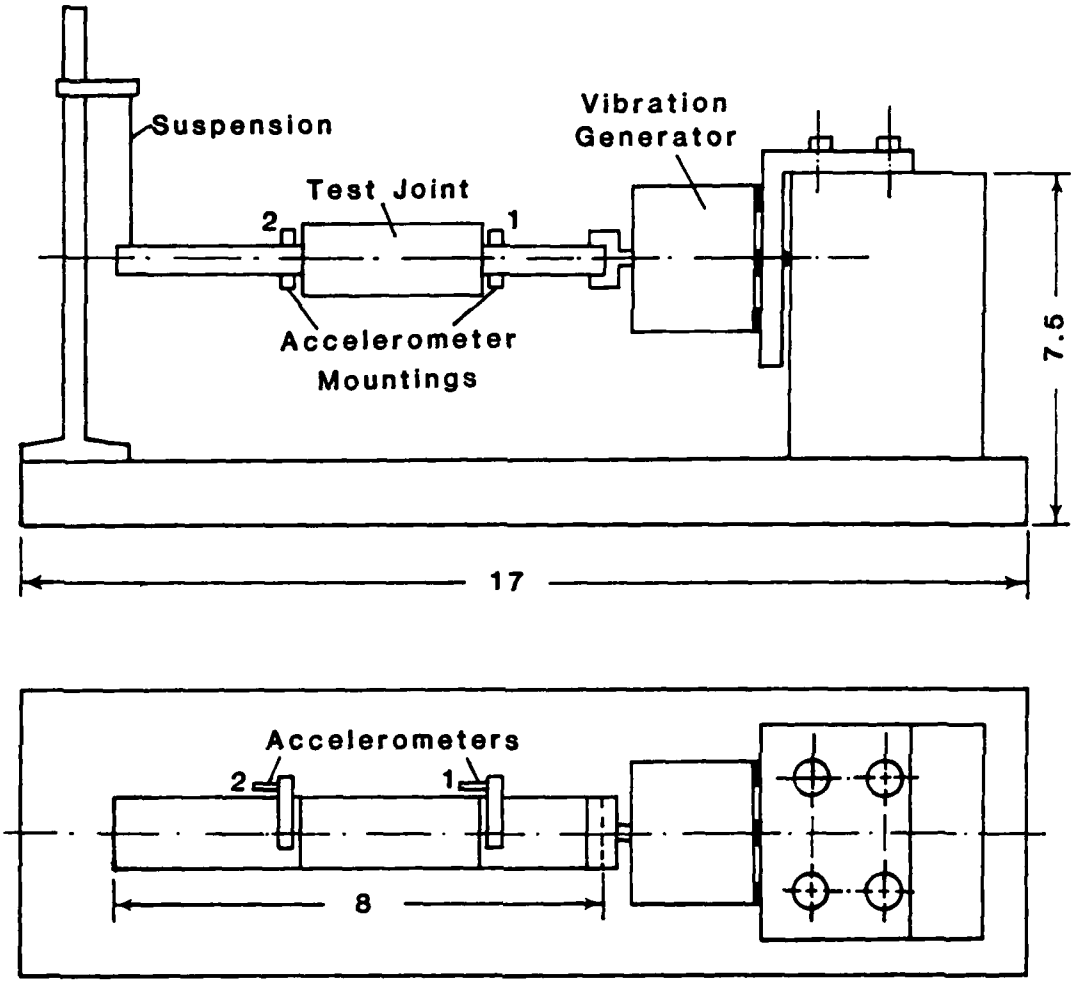

(Dimonsions in Inches)

Fig.2- TEST FIXTURE

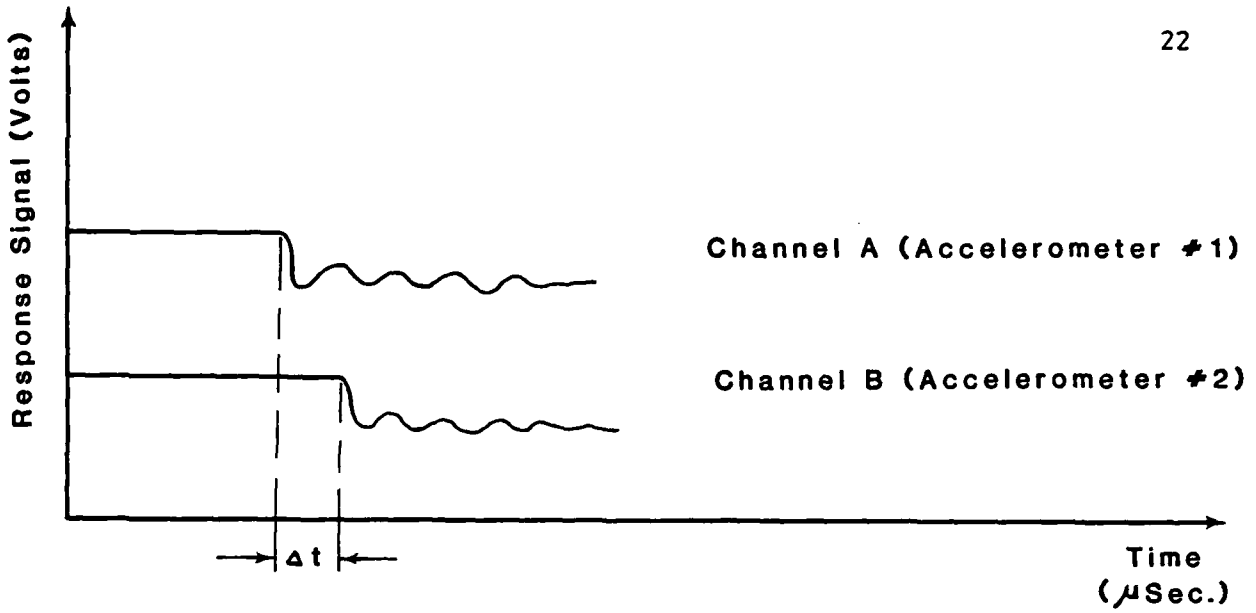

Fig.3- EXAMPLE OF DISPLAY FOR STIFFNESS MEASUREMENT

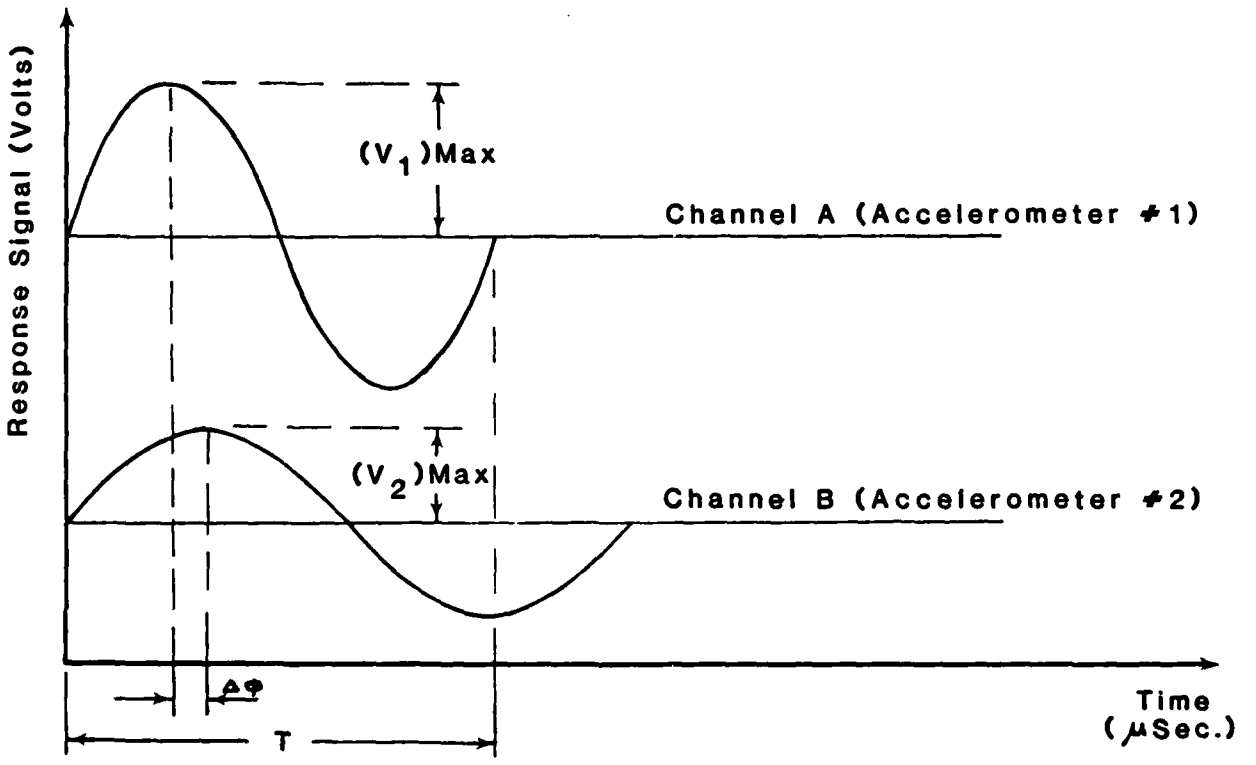

Fig.4- EXAMPLE OF DISPLAY FOR DAMPING MEASUREMENT

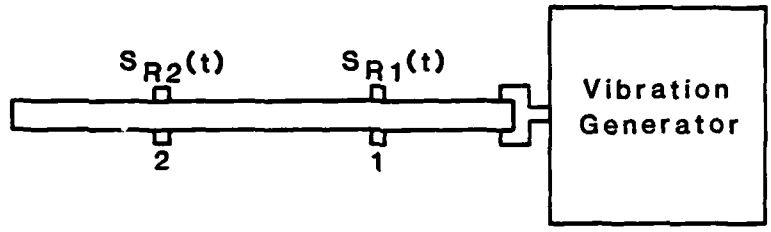

REFERENCE SPECIMEN

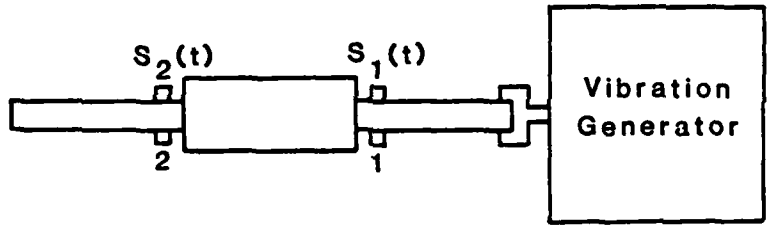

TEST SPECIMEN

Fig.5- AUXILIARY SKETCH FOR REFLECTIONS ELIMINATION

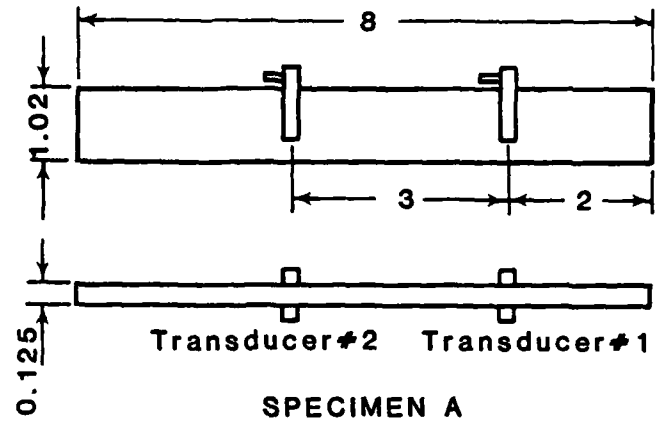

SPECIMEN A

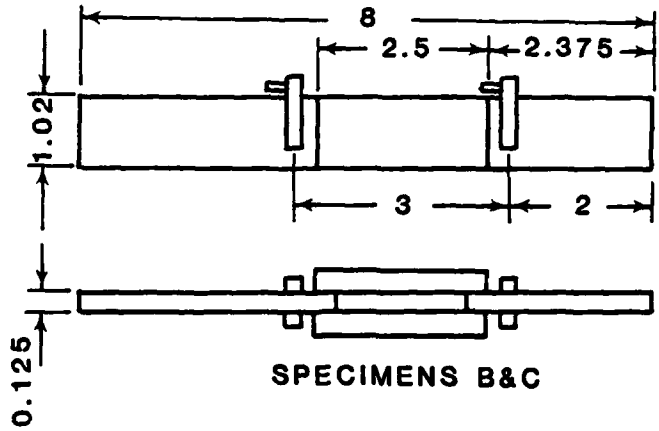

SPECIMENS B&C

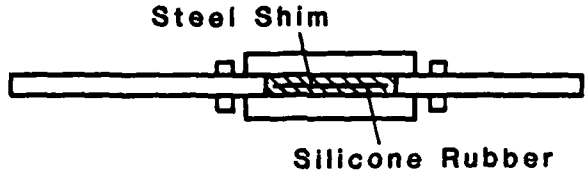

SPECIMENS D&E

(Dimensions in inches)

Fig.6- SPECIMENS WITH MOUNTED TRANSDUCERS FOR PRELIMINARY TESTS

APPENDIX IV

GEORGIA INSTITUTE OF TECHNOLOGY

INTERIM REPORT #2

ADVANCED AEROSPACE STRUCTURES

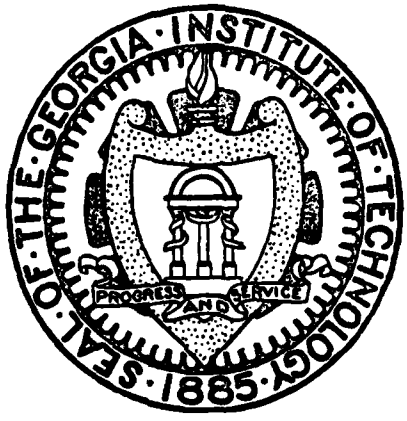

FACILITY AND SOFTWARE DEVELOPMENT FOR THE EXPERIMENTAL EVALUATION OF PASSIVELY DAMPED JOINTS FOR SPACE STRUCTURES

Jacky Prucz
School of Aerospace Engineering
Georgia Institute of Technology
Atlanta, Georgia 30332

Interim Report 2
McDonnell Douglas Contract 83025032
AFOSR Contract F49620-83-C-0017

June 1984

TABLE OF CONTENTS

NOMENCLATURE

a	Propagation time from the loaded end to the input location
A_{1R}	Reflection factor at the member-joint interface
A_{1T}	Transmission factor at the member-joint interface
A_{2T}	Transmission factor at the joint-member interface
A_o	Reflection factor at the loaded end
A	Reflection factor at the opposite end
A_m, A_j	Cross-sectional area of member and joint, respectively
b	Propagation time from the input to the output locations
c	Propagation time from the output location to the unloaded end
d	Attenuation coefficient
$D(t)$	Damping effect time signal
C_m, C_j	Wave propagation velocities in member and joint, respectively
E_m, E_j	Equivalent extensional modulus of member and joint, respectively
$I(t)$	Incident time signal
m_m, m_j	Equivalent mass per unit length of member and joint, respectively
m, n, p	Time control parameters
$R_1(t)$	Reflected signal at the member-joint interface
$R_2(t)$	Reflected signal at the joint-member interface
$S_{R1}(t)$, $S_{R2}(t)$	Input and output measured signals, respectively, for the reference continuous bar specimen
$S_1(t)$, $S_2(t)$	Input and output measured signals, respectively, for the joint specimen
$T_1(t)$	Transmitted signal at the member-joint interface
$T_2(t)$	Transmitted signal at the joint-member interface
t	Time variable
t_1, t_2	Reflection times at the input and output locations, respectively.
α_1, α_2	Reflection and transmission parameters at the member-joint and joint-member interfaces, respectively.

1. INTRODUCTION

This report covers the research work carried out at GIT during the period 2 January - 31 May 1984 in regard to the project of new passively damped joining concepts for space structures, AFOSR Contract No. F49620-83-C-0017. The foregoing activities since the starting date of the contract (May 1983) were focussed on potential design configurations (presentation outlined as Ref. [10]) and the development of the new sine-pulse propagation approach in accordance with the particular requirements of this project (Refs. [1] and [2]). In this testing technique, a sine-pulse of the desired frequency is applied at one end of the specimen and the corresponding longitudinal response is measured at two fixed locations, before and after the joint section. The damping information is extracted from the changes that occur in certain characteristics of this stress wave as a result of its passage through the joint.

Detailed information regarding this method has been presented in Ref. [2]. However, the associated data processing algorithm is described in depth in this report, since it has been improved, generalized and organized in a systematic fashion by taking advantage of the more powerful computerized procedures enabled by the transfer of the test data from the digital oscilloscope to the computer. In addition, dispersion of extensional waves because of lateral inertia effects, which is mentioned only briefly in Ref. [2], is discussed in more detail here in Chapter 5.

Because of the unexpected delay in the development of the piezoelectric vibration generator by Wilcoxon Research Inc., only a few preliminary experiments have been conducted on the composite joint specimens recently supplied by MDAC. Nevertheless, the time period covered in this report has been used efficiently by accomplishing all the preparatory tasks necessary for facilitating the experiments once the piezoelectric vibration generator is acquired without any further delays.

These tasks have included both research activities, mainly related to the preparation of the computer software for data processing and analysis, and development work related to the experimental facilities and equipment. The environmental chamber that provides the required temperature range has been received already, whereas the signal generator and power amplifier that will activate the piezoelectric transducer are presently assembled in our instrumentation laboratory. The Blue-M LN-270C-I is a mechanical convection horizontal airflow constant temperature environmental chamber. It uses LN_2 as the cooling medium. It can provide a temperature range from -120°C to +300°C. It is a front opening chamber with one lead-in port and has inside dimensions of 25 x 20 x 20 inches. A versatile test fixture, that may be used for all the scheduled tests, has been designed and manufactured in our mechanical shop. Its basic design considerations are brought up in Chapter 2.

Most of the research work reported in this document is focussed on the development of two different packages of computer software:

1. A versatile set of programs for data transfer, processing and analysis based on the two new testing techniques selected for this project - the sine-pulse propagation approach and the simplified steady state approach (Refs. [1] and [2]). The main algorithms of this software are described in Chapter 3.
2. A complete computer simulation of the wave system generated in a joint specimen as the result of an arbitrarily shaped pulse applied at one of its ends. Such a simulation is needed in connection with the pulse propagation approach in order to justify the data processing algorithm on one hand and provide a tool for checking its range of validity on the other hand. A full description of this program is presented in Chapter 4.

2. TEST FIXTURE DESIGN

A new test fixture has been designed and manufactured for the experimental evaluation of the passively damped joint specimens. Because of the corrosive action of liquid nitrogen, the cryogenic agent used in low temperature tests, stainless steel AISI 304 is the material selected for the fixture.

Three major considerations have guided the design of the test fixture:

1. Geometric compatibility with the BLUE M environmental chamber, Model No. LN-270C-1 whose inside dimensions are 25 x 20 x 20 inches.
2. Maximum versatility, such that the fixture can accommodate specimens of different lengths and it can be used without major changes for the two selected testing techniques: the pulse propagation approach and the simplified steady state approach (Ref. [1]).
3. Maximum possible stiffness within reasonable weight limits. The upper weight limit has been chosen to be about 80-85 lb, so that two people can handle the assembled fixture.

These considerations have led to a fixture of modular construction, whose basic configuration includes four rectangular plates interconnected by four bolts and a system of four threaded rods with 12 nuts as shown in Fig. 1. This allows a continuous variation in the position of the right-hand plate, so that specimens with lengths between approximately 6 to 11 inches can be tested in this fixture by the simplified steady state technique (see Fig. 2). When the pulse propagation technique is used, a suitable slot in the top-plate is provided, along which the vertical suspension string can be slid horizontally according to the specimen length (Fig. 3).

The design process involved two main steps:

1. The dimensions of all the components have been first established based on the restrictions imposed by the environmental chamber and strength considerations. Design data and methods given in Refs. 5-7 have provided the basis for the stress analysis of the fixture. Assuming that, when the simplified steady state technique is used, the piezoelectric vibration generator can apply a cyclic load whose maximum amplitude is 500 lb, the critical design criterion turns out to be the fatigue strength of the connection bolts. The minimum screw diameter imposed by this criterion for a factor of safety equal to 2 is 0.287 inches, that led to the 3/8 inches size selected for the connecting bolts and threaded rods.

2. The second part of the design dealt with the stiffness evaluation of the fixture in the axial direction, since this parameter is usually included in the model equations of the simplified steady state approach [1]. For this purpose, the fixture has been modeled as a system of linear elastic springs interconnected in series or in parallel, according to the contribution of the individual elements to its overall stiffness. Basic, strength of materials formulas have been used in order to assess the relevant stiffness of each component. In the basic configuration of the fixture, its equivalent axial stiffness is about 0.3×10^6 lb/in if the end plates are assumed to be simply supported and about 0.8×10^6 lb/in if they are assumed to be clamped. Since some of the test specimens may be expected to have higher axial stiffness than these figures, several ways to increase the stiffness of the fixture have been evaluated. The most practical approach, which

is also consistent with the weight limitations and the modular construction concept of the fixture, has been found to rely upon the use of additional stiffening rods in the axial direction (Fig. 2). For example, the use of four threaded stiffening rods placed close to the center line of the fixture, may enhance its stiffness to about 3×10^6 lb/in for simply supported end plates or 3.6×10^6 lb/in for clamped end plates.

3. DATA ANALYSIS SOFTWARE

The computer software necessary for data processing and analysis has been developed and debugged. The programming language is "BASIC" and it is adapted for use on a HP 9845B minicomputer. In order to enhance its versatility, the software includes several analysis options, so that it can be used essentially without changes for different testing techniques, as long as the experimental data can be stored and recorded on the NICOLET 4094 Digital Oscilloscope (see the "Experimental Set-up" in Ref. [2]).

The software package consists of three major parts, according to the three main phases of data transformation from raw measured data to final experimental results. The parts are

1. Digital data transfer from the NICOLET 4094 Digital Oscilloscope to the HP 9845 B minicomputer.
2. Data processing for removing the effect of reflections from the test joint and the specimen's end - this step is required only in the pulse propagation approach.
3. Data analysis in accordance with the particular testing technique and the parameters selected to yield the final results.

3.1 Digital Data Transfer

The NICOLET 4094-HP 9845B interface program performs the transfer of digital data stored in the memory of the oscilloscope to the computer memory. The transfer is carried out in ASCII characters (American Standard Code for Information Interchange) through the GPIB (General Purpose Interface Bus) interface system. A HP 98034A Interface Card is used to connect the HP 9845B Computer to the GPIB system.

The data transfer is usually performed in three successive steps:

1. Transfer of descriptive wave information on all the data waveforms stored in the oscilloscope memory.
2. Transfer of normalization data for each waveform separately, one at a time. The normalization set is necessary in order to convert data point values into absolute time and voltage measurements, according to the control settings on the NICOLET control panel during the real time data acquisition.
3. Data points transfer for each waveform separately, one at a time. The starting point, the total number of transmitted points and the count spacing between them can be selected arbitrarily, so that only the relevant portions of each waveform will be transferred.

When the normalization set is applied on the corresponding waveform, each data point value is translated into the correct time and voltage. Therefore, each time signal measured in the test is finally stored in the computer memory as a time vector and a voltage vector corresponding to the number of the transferred data points. This information can be subsequently recorded on a magnetic tape. In addition to the interface error messages, a plotting routine has been included in the program in order to verify the accuracy of the transferred data by comparison with the original waveform, as displayed by the oscilloscope. An example of measured time signals plotted by the computer is shown in Fig. 4. A schematic block diagram of the data transfer procedure is given in Fig. 5.

3.2 Data Processing

Any time delay between the acquired signals can be accounted for by suitable horizontal shifting of the corresponding time vectors, so that all the waveforms have the same time base before their processing.

The reflections effect included in these data can be separated in two components, according to its source:

1. Direct reflections of the propagating signal from the test joint itself.
2. Multiple reflections of the foregoing portions of the signal at the ends of the specimen and the member-joint interfaces.

3.2.1 Direct Joint Reflections. If a longitudinal wave is propagating along a bar, it is partly reflected and partly transmitted when it reaches a discontinuity interface either in the geometrical or the mechanical properties of the bar (see Fig. 6). The extent of this reflection depends on the nature of the discontinuities themselves and it is governed by stress equilibrium and displacement continuity conditions at the interface [8]. Therefore, if the joint is modeled as an homogeneous bar element, whose equivalent geometrical and mechanical properties differ from those of the connected members, the direct reflections at its two interfaces are given by (see Nomenclature list and Fig. 6 for notations)

$$R_1(t) = - I(t)\frac{\alpha_1 - 1}{\alpha_1 + 1} \tag{1}$$

$$R_2(t) = - T_1(t)\frac{\alpha_2 - 1}{\alpha_2 + 1} \tag{2}$$

whereas the corresponding transmissions are

$$T_1(t) = I(t)\frac{2}{\alpha_1 + 1} \tag{3}$$

$$T_2(t) = T_1(t)\frac{2}{\alpha_2 + 1} \tag{4}$$

It is seen that the extent of the reflections and transmissions is determined by the non-dimensional parameters α_1 and α_2, that are given by

$$\alpha_1 = \frac{c_m}{c_j}\frac{A_j E_j}{A_m E_m} = \sqrt{\frac{m_j E_j A_j}{m_m E_m A_m}} \tag{5}$$

$$\alpha_2 = \frac{1}{\alpha_1} \tag{6}$$

Therefore, two major observations can be made with regard to the time signals measured before and after the joint:

1. The input signal is mainly a superposition between the incident wave, I(t), and its direct reflection from the joint, $R_1(t)$.
2. The output signal is mainly the transmitted wave $T_2(t)$ and it includes the damping effect of the joint on the transmitted wave $T_1(t)$, rather than on the originally propagating wave, I(t) like in the absence of the joint.

If all the properties included in expression (5) are known, the coefficients α_1 and α_2 can be directly calculated from the relations (5) and (6). However, they can also be evaluated experimentally by separation of the reflected signal $R_1(t)$ from the total input signal measured in the test. This is accomplished by comparison of the input signal measured in the presence of the joint with the corresponding input signal measured on a reference continuous specimen [2]. The basic equation of this step is

$$-R_1(t) = \text{FIT}\left[S_{R1}(t) - S_1(t)\right] \tag{7}$$

where the operator "FIT" denotes a curve fitting procedure applied on the difference of the two signals in order to eliminate the multiple reflections effect (see Section 3.2.2). The measured reflected signal $R_1(t)$ is subsequently used for the evaluation of the coefficient α_1 according to relation (1), where the incident signal

I(t) is supposed to be identical with that of the reference continuous bar, $S_{R1}(t)$. The experimental value of α_1 can be either correlated with its theoretical value from relation (S), or it can be used for the evaluation of an unknown property in this relation, which is most likely to be the equivalent axial stiffness of the joint, E_j.

The major advantage of this data processing algorithm lies in the realistic treatment of disturbance propagation along a structure that will always include direct reflections from the joints, in addition to the damping effects of the structural members and joints. Moreover, if all the other properties in Equation (5) are known, this algorithm provides an additional approach for the experimental evaluation of the equivalent elastic modulus of the test joint. The data processing algorithm that accounts for the direct reflections from the joints is schematically described in Fig. 7.

3.2.2 Multiple Reflections

The data processing algorithm for the elimination of the multiple reflections effect relies upon the basic characteristics of this effect in the case of a reference continuous bar. If such a bar were infinitely long and with no material damping, the measured time signals $S_{R1}(t)$ and $S_{R2}(t)$ would be identical (assuming equal sensitivity of the corresponding transducers). If, however, the length of the bar is finite, multiple reflections occur at its ends and their effect is included in the measured signals $S_{R1}(t)$ and $S_{R2}(t)$. Therefore, even in the absence of material damping, the difference between these two signals is not a perfect zero line. There is a difference between the multiple reflection effects due to the different locations of the two transducers. This difference is mainly the result of the time delays associated with the propagation of the reflected waves from one location to the other. Considering the small values of these delays, along with the relatively small gradients associated with low frequency signals, the difference between the

multiple reflection effects at the locations of the two transducers is expected to be very small. At a particular time, this difference can be either positive or negative, depending on the sign and the relative magnitude of the reflected waves whose superposition determines the multiple reflection effects at that time.

In conclusion, in the absence of material damping, the difference between the multiple reflection effects at the locations of the two transducers is expected to resemble a low-amplitude, high-frequency random noise about the horizontal time axis. A complete computer simulation of longitudinal waves propagation along a finite-length bar verifies this conclusion (see Chapter 4).

In the test of a real bar specimen, the effect of material damping is also included in the difference between the measured signals $S_{R1}(t)$ and $S_{R2}(t)$, in addition to the multiple reflections effect. Unlike the last one, however, the damping effect is expected to be characterized by a monotonic decrease in the signal amplitude during its propagation from the first to the second transducer location. The difference between the real measured signals $S_{R1}(t)$ and $S_{R2}(t)$ is, therefore, expected to be described by a high-frequency "modulation noise" about a smooth, continuous curve, which would represent the damping effect in the absence of multiple reflections. The experimental data shown in Fig. 8 is in good agreement with this conclusion. One may notice that the multiple reflections effect is more pronounced at the start of the pulse, but it diminishes with time, probably because of the attenuation of the reflected waves by the material damping in the specimen.

A special routine has been included in the data processing algorithm in order to separate the damping and the multiple reflection effects from each other. This is a least-square, polynomial, curve fitting procedure between all the data points obtained by subtraction of the input and output signals from each other [9].

It is essentially equivalent to a high frequency noise filtering, but it is carried out on a digital computer rather than an analog filter. The smooth curve labeled as "Damping Effect" in Fig. 8 is the 5th order polynom that, according to this routine, represents the best fit of the corresponding data points.

It can be therefore concluded that for a continuous bar specimen, the damping information is separated from the two measured time signals according to the equation:

$$D(t) = FIT\left[S_{R2}(t) - S_{R1}(t)\right] \tag{8}$$

where the operator "FIT" denotes the curve fitting procedure applied on the test data.

If the above discussion is extended from a continuous bar to a real joint specimen, the same conclusions will hold as to the basic differences between the damping and the multiple reflection effects. In this case, however, it is more difficult to extract the damping information from the measured time signals $S_1(t)$ and $S_2(t)$ because they also include the effect of direct reflections from the joint itself that has been discussed in Section 3.2.1. That is why Equation (8) cannot be extended directly to a joint specimen, but it has to be slightly modified in order to account for this effect. A detailed analysis of the various effects that are superposed in each measured time signal leads to the following basic equation for this part of the algorithm:

$$D(t) = \frac{\alpha_1 + 1}{2\alpha_1}\left[FIT(S_2(t) - S_1(t)) - FIT(S_{R1}(t) - S_1(t))\right] \tag{9}$$

where D(t) represents the damping effect of the joint on the part of the pulse that is transmitted through it. The purpose of the "FIT" operators that appear in Equation (9) is the elimination of multiple reflection effects, both from the ends and from the member-joint interfaces of the specimen. It can be readily checked

that in the absence of direct reflections from the joint, Equation (9) is reduced to Equation (8) since in this case $\alpha_1 = 1$ and the result of the second "FIT" operator is zero (see Equation 7).

The basic steps for extracting damping information from the measured test data are schematically shown in Fig. 9.

3.3. Data Analysis

Whatever testing technique is used, as long as the experimental data is acquired in the form of voltage time histories, they can be recorded by the digital oscilloscope and subsequently transferred to the computer according to the procedure outlined in Section 3.1. The "raw" data is then converted into final experimental results by an appropriate computer routine, that is selected in accordance with the technique used for its acquisition.

A previous evaluation of potential experimental methods has shown that two new approaches are the most suitable for the testing of passively damped joints [1]. They are

1. The new sine-pulse propagation technique
2. The new simplified steady-state technique

When the second technique is used, the corresponding analysis program can be applied directly on the measured test data. Not so in the case of the first technique, where the test data undergoes the "clean-up" procedure described in Section 3.2 before it is subject to the analysis algorithm. In spite of this additional processing routine, the pulse propagation technique is expected to yield improved results over a wide frequency range. That is because this technique enables a more realistic testing of the joint specimens under transient excitation, in which the real, direct reflections from the joint are taken into account, but the particular dynamic characteristics of the test fixture do not affect the experimental results.

A general flow diagram of the data analysis procedures for the two selected testing methods is given in Fig.10. Their underlying assumptions and features are described in Refs. [1] and [2] for the pulse propagation approach and in Ref. [1] for the simplified steady state approach. Both methods yield, at the end, the equivalent complex modulus of the test joint, no matter what its design configuration is. Any correlation between the test results and the complex moduli of the viscoelastic materials used in the joint can be performed only through an appropriate analytical model of its particular configuration. It is interesting to note that if the joint is modeled as an homogeneous bar element with different properties than those of the members, the sine-pulse propagation approach provides two separate evaluation ways for both the elastic and the viscous components of the equivalent complex modulus. Therefore, some kind of "internal" correlation is possible with this technique, in addition to the correlations between basically different testing methods, or between experimental and theoretical predictions.

4. WAVE SYSTEM SIMULATION

A complete simulation of longitudinal pulse waves propagation within a finite joint specimen has been developed on the HP 9845B computer for two main purposes:

1. To provide a theoretical basis for the data processing algorithm described in Section 3.2.
2. To enable a quantitative assessment of its accuracy and its range of applicability.

The simulation is based upon the fundamental theory of axial-wave-propagation, according to which a stress, or a displacement wave travels without distortion along an elastic bar and only its sign, but not its shape or amplitude, can be changed when it is reflected at the ends of the bar [8]. The reflections that occur at the discontinuity interfaces between the joint and the members differ from this observation only by the fact that uniform amplitude changes over all the length of the pulse are also possible (see Section 3.2.1 and Ref. [8]). The damping effect of the joint is included in the simulation by means of an exponential decay factor that multiplies the waves transmitted through the joint. This is equivalent to the amplitude decay associated with the wave propagation through homogeneous viscoelastic media, where the corresponding attenuation coefficient is a measure of the material damping effect [2].

The multiple reflections that occur during the pulse length are simulated as a sequence of new waves "radiation" from four possible "sources" - the ends of the bar and the two member-joint interfaces. Every time a wave-front reaches one of these "sources", at least one new wave of the same shape is generated, its sign and amplitude depending on the relevant boundary conditions for that "source". When the "source" is a member-joint interface, two new waves are generated, a reflected and a transmitted one, according to the equations given in Section 3.2.1. This is

obviously a highly divergent accounting process, that ends when either one of the following two criteria is fulfilled:

1. The control time variable becomes equal to the pulse length.
2. The amplitude of the reflected waves is below a preset limit (in the case of weak reflections and/or high damping).

The resultant effect of the linear superposition between the main propagating signal and the growing system of reflected and transmitted waves is continuously tracked and updated by the program at two fixed locations. These correspond to the locations of the data acquisition transducers on the test specimen, i.e., one before the joint and one after it [1, 2]. Schematic flow charts of the simulation model, along with the basic recurrence formulas are given in Fig. 11 for the input position and in Fig. 12 for the output position (see Nomenclature list for notations). These charts describe one run of the simulation program, starting with the initially applied signal and tracking its propagation way through the specimen. To complete the simulation, such a separate run is required also for each new signal generated by reflection from a member-joint interface. The only differences consist of the initial time shift and the smaller starting amplitude of this type of signal.

Fig. 13 brings up an example of simulation results that provide a solid theoretical support for the data processing algorithm presented in Section 3.2. The figure displays the predicted difference between the resultant output and input signals when a 100 Hz pulse is propagating through two aluminum specimens with no damping effects. The continuous bar results include only the multiple reflections effect, that looks like a high frequency random noise about the time axis. In the case of the joint specimen, however, the direct reflections from the joint are dominant and their effect evidently is a smaller output than the input signal, although there is no damping in the joint.

5. LATERAL INERTIA EFFECTS

Unlike the propagation of flexural waves, that is always associated with significant frequency dispersions, the propagation of extensional waves in bars is affected by such dispersions only in certain conditions [ ]. It has been shown that the dispersion effect in longitudinal waves becomes significant only when their wavelength is of the same order of magnitude or shorter than the largest cross-sectional dimension of the specimen, so that the lateral inertia effect can no longer be neglected [3, 4]. The commonly accepted criterion for neglecting this effect is that the wavelength of the signal should be at least 10 times greater than the largest cross-sectional dimension [3]. This condition imposes the use of very thin and long specimens whenever a testing technique based on impact pulses is applied [4]. Nevertheless, it becomes much less restrictive if a sine-pulse, rather than an impact pulse is used in the tests, especially in the low frequency range as in the case of this project [1]. Even when the upper frequency limit of 100 Hz is considered, the corresponding wavelength for a graphite-epoxy composite specimen will be about 700 in., which is about 450 times higher than the 1.5 in. largest cross-sectional dimension of the present specimens.

However, the major reason for choosing a sine-shaped pulse as excitation signal is the associated frequency control capability rather than the elimination of undesired dispersion effects. Even in conditions that are favorable to such effects, they are expected to be greatly reduced in the case of a sine-pulse as compared with the commonly used impact pulse because of the obvious difference in the frequency content of these two types of pulses.

Finally, it should be emphasized that the sine pulse approach is based so far on a time domain analysis of the test data and if any dispersion occurred, it would affect the results only through the associated distortion in the shape of the pulse. Given the short propagation distance between the two response pick-up locations

and the narrow frequency spectrum of a sine pulse, such a distortion, if it existed, would be very small. However, it might alter the results when a damping parameter dependent on the shape of the pulse, like the attenuation coefficient, is used, but no significant errors should be expected when a more global parameter, like the energy dissipation per cycle, is used as a measure of damping in the specimen.

6. REFERENCES

1. Trudell, R.W., Rehfield, L.W., Reddy, A.D., Prucz, J. and Peebles, J., "Passively Damped Joints for Advanced Space Structures," presented at the "Vibration Damping Workshop" sponsored by the Air Force Flight Dynamics Laboratory, Long Beach, California, February 27-29, 1984.

2. Prucz, J. and Reddy, A.D., "A New Approach to Damping Measurements in Structural Joints," Interim Report 1, AFOSR Contract F49620-83-C-0017, December 1983.

3. Kolsky, H., Stress Waves in Solids, 1953.

4. Bert, C.W., and Clary, R.R., "Evaluation of Experimental Methods for Determining Dynamic Stiffness and Damping of Composite Materials," Composite Materials: Testing and Design (3rd Conference), ASTM STP 546, 1974, pp. 250-265.

5. Baumeister, T. and Marks, L.S., editors, Standard Handbook for Mechanical Engineers, Seventh Edition, McGraw-Hill, 1967.

6. Spotts, M.F., Design of Machine Elements, Fourth Edition, Prentice-Hall, Inc., 1971.

7. Faupel, J. H. and Fisher, F.E., Engineering Design, Second Edition, John Wiley and Sons, 1981.

8. Clough, R.W.and Benzien, J., Dynamics of Structures, McGraw-Hill, Inc., 1975.

9. Harnett, D.L., Introduction to Statistical Methods, Second Edition, Addison-Wesley Publishing Company, 1975

10. Reddy, A.D., Prucz, J. and Rehfield, L.W., "Preliminary Thoughts on Joints with Passive Damping," presented to MDAC in June 1983.

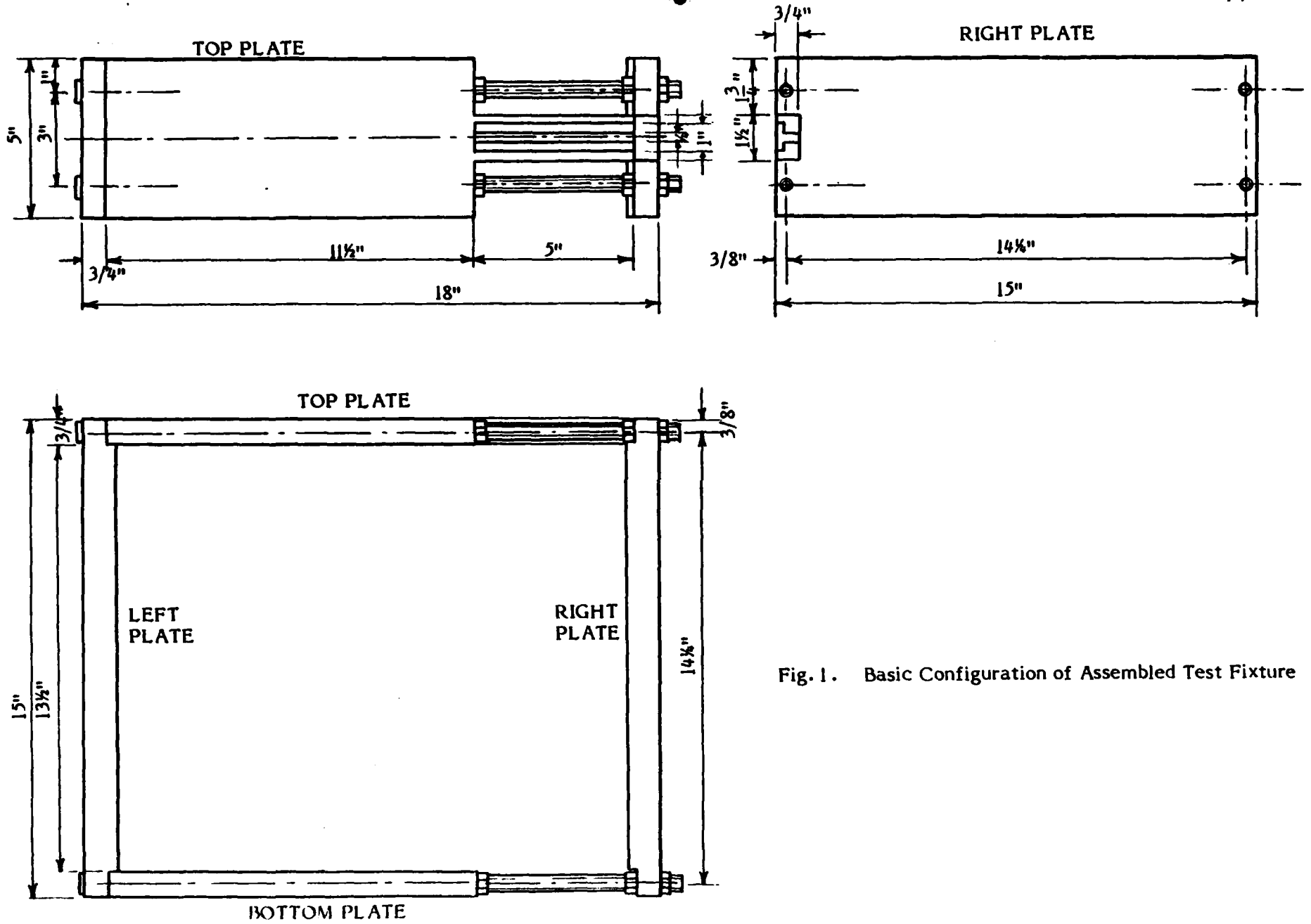

Fig. 1. Basic Configuration of Assembled Test Fixture

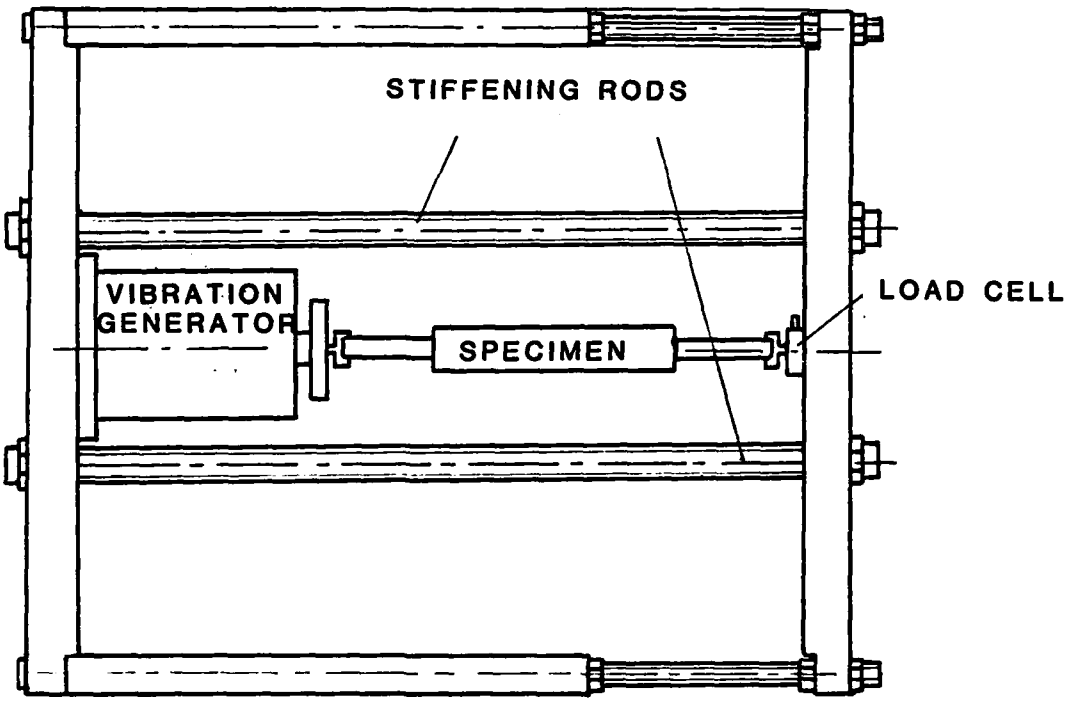

Fig. 2. Test Fixture Configuration for Simplified Steady State Technique

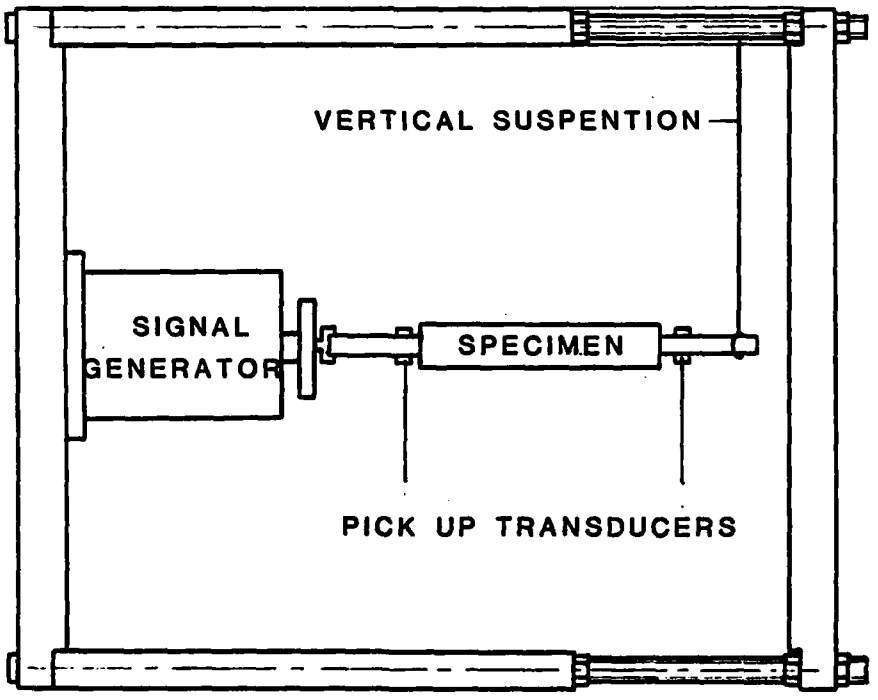

Fig. 3. Test Fixture Configuration for Sine-Pulse Propagation Technique

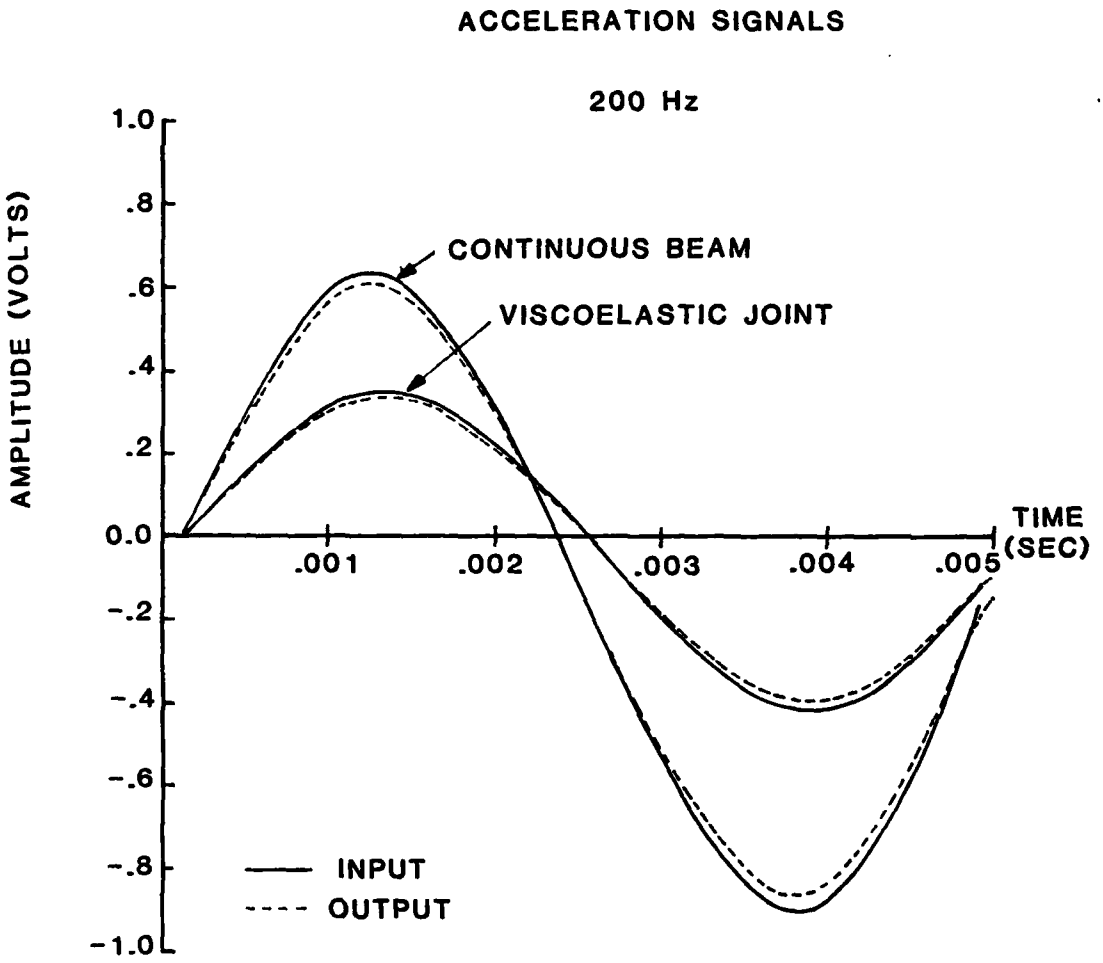

Fig. 4. Computer Plot of Measured Signals

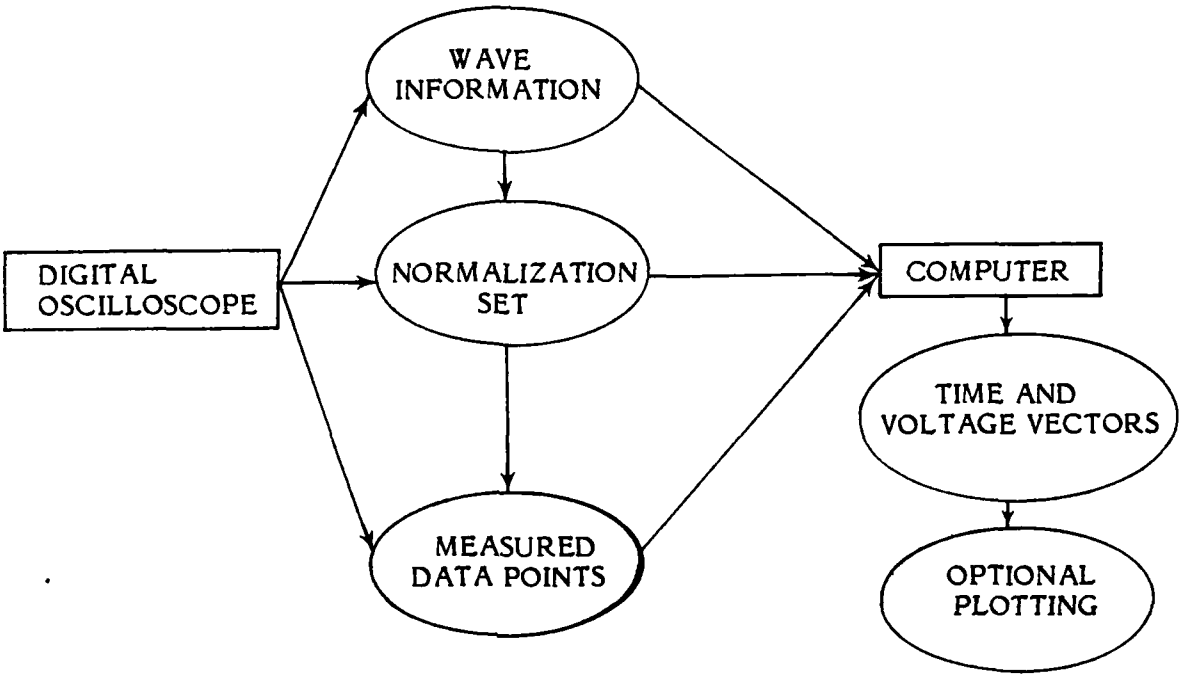

Fig. 5 Data Transfer Flow Chart

WAVE PROPAGATION THROUGH A JOINT

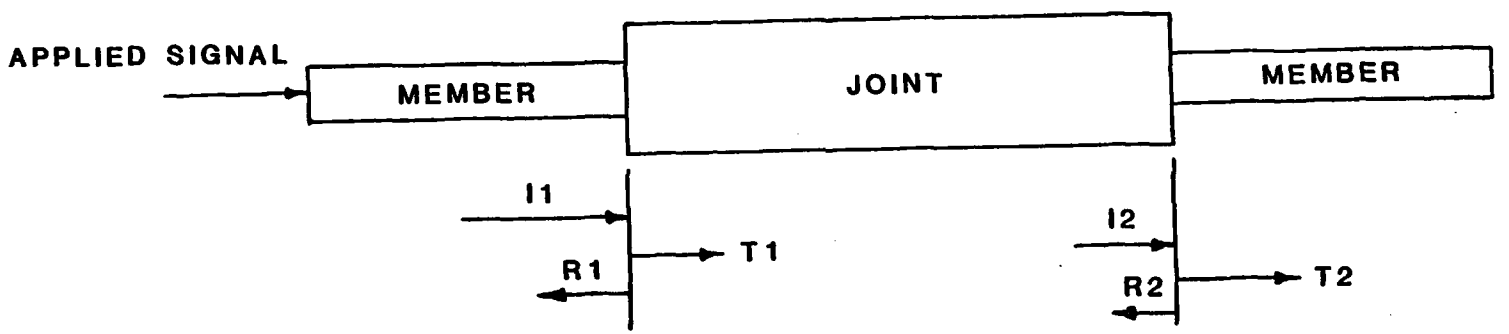

I1,2-INCIDENT WAVES

T1,2-TRANSMITTED WAVES

R1,2-REFLECTED WAVES

FIG. 6 WAVE PROPAGATION THROUGH A JOINT

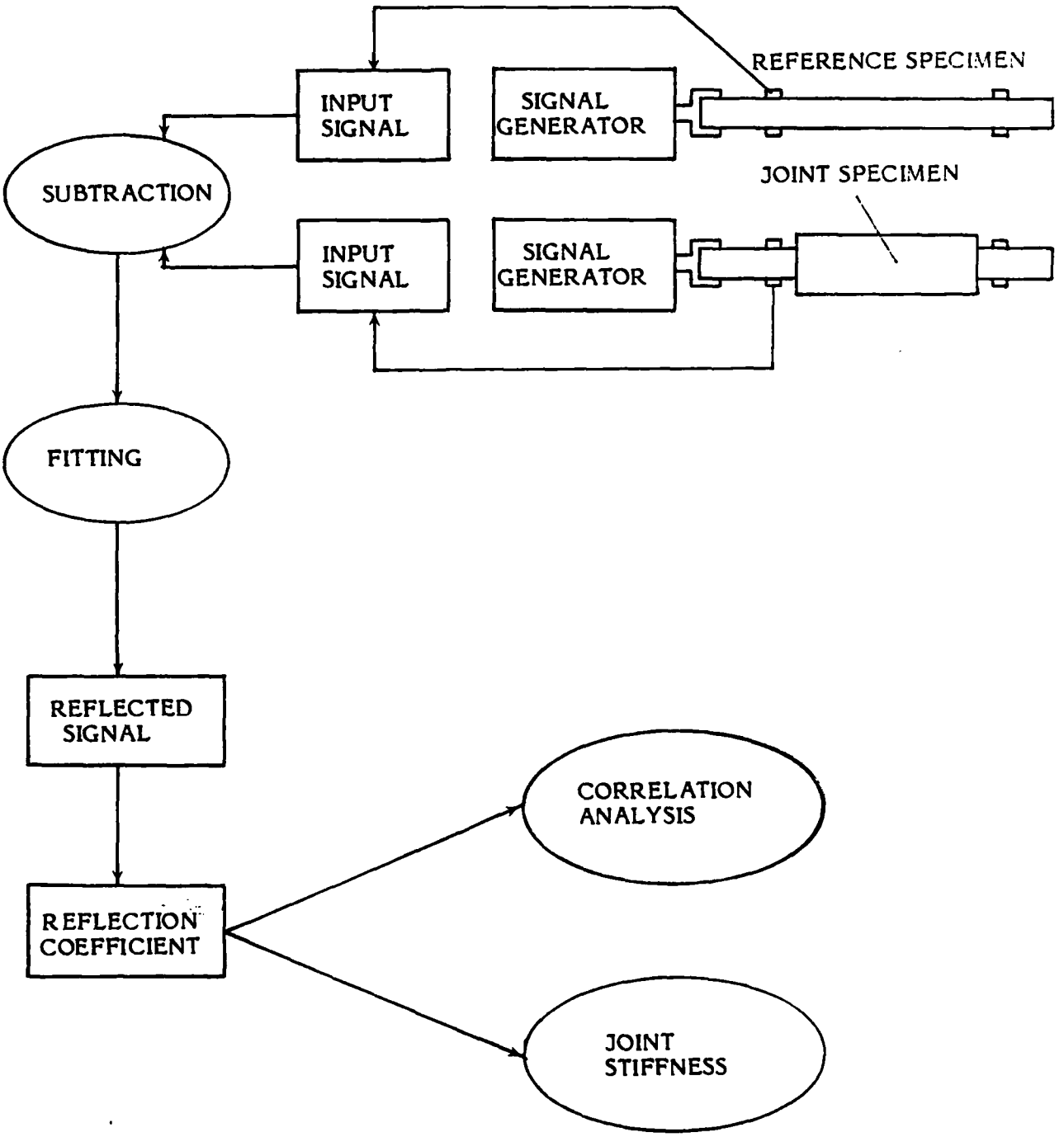

Fig. 7. Analysis of Direct Joint Reflections

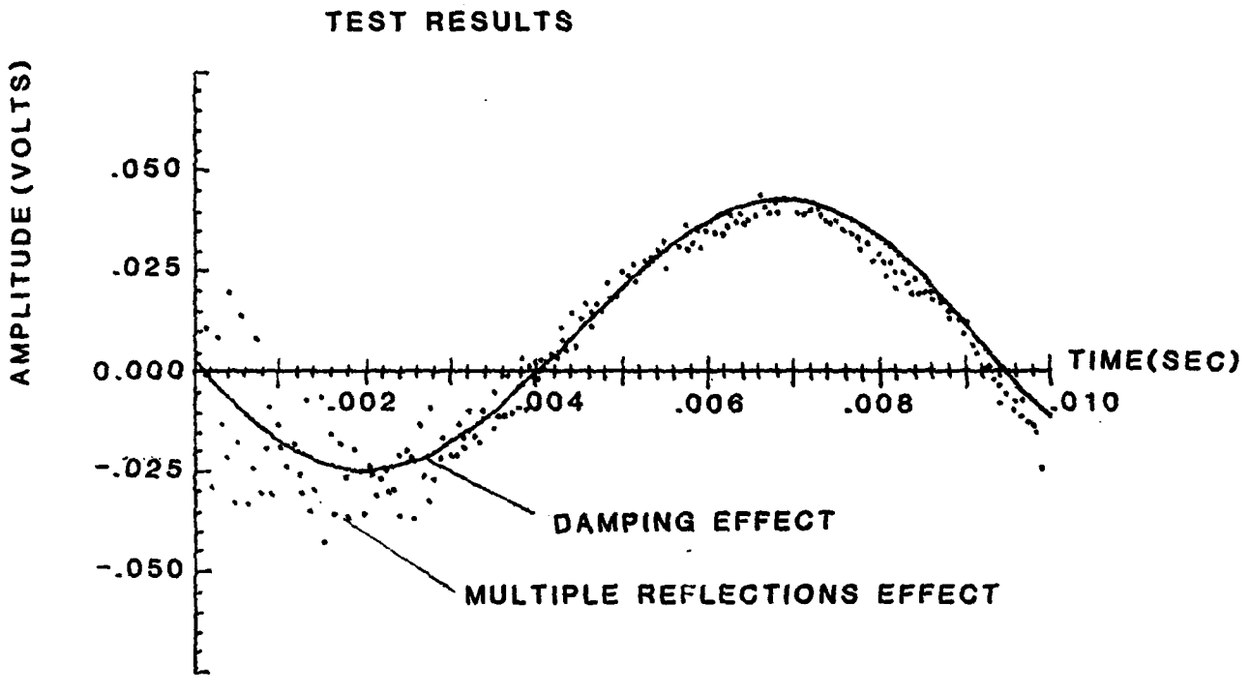

Fig. 8. Difference Signal Between Output and Input Test Data

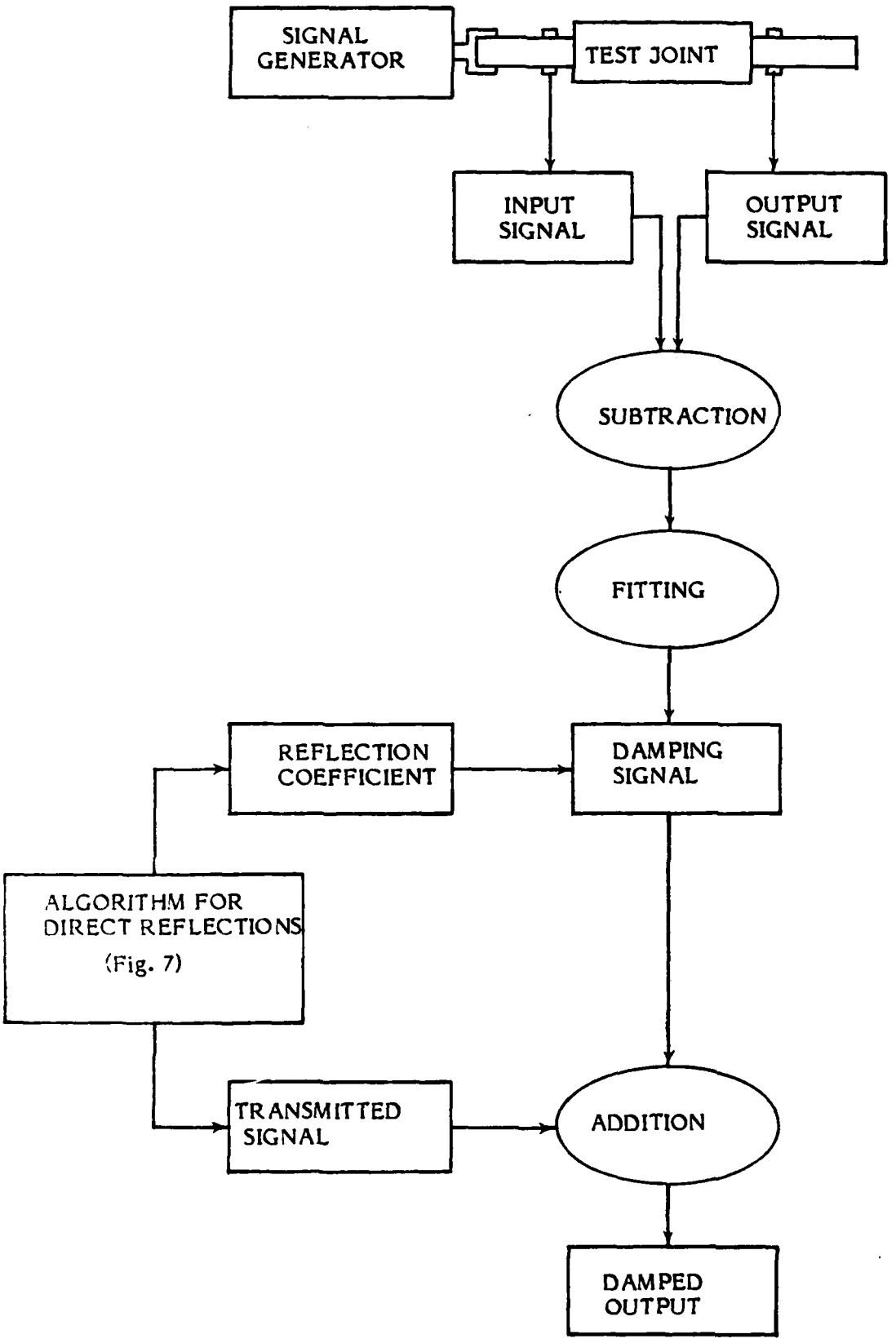

Fig. 9. Separation of Damping Effect

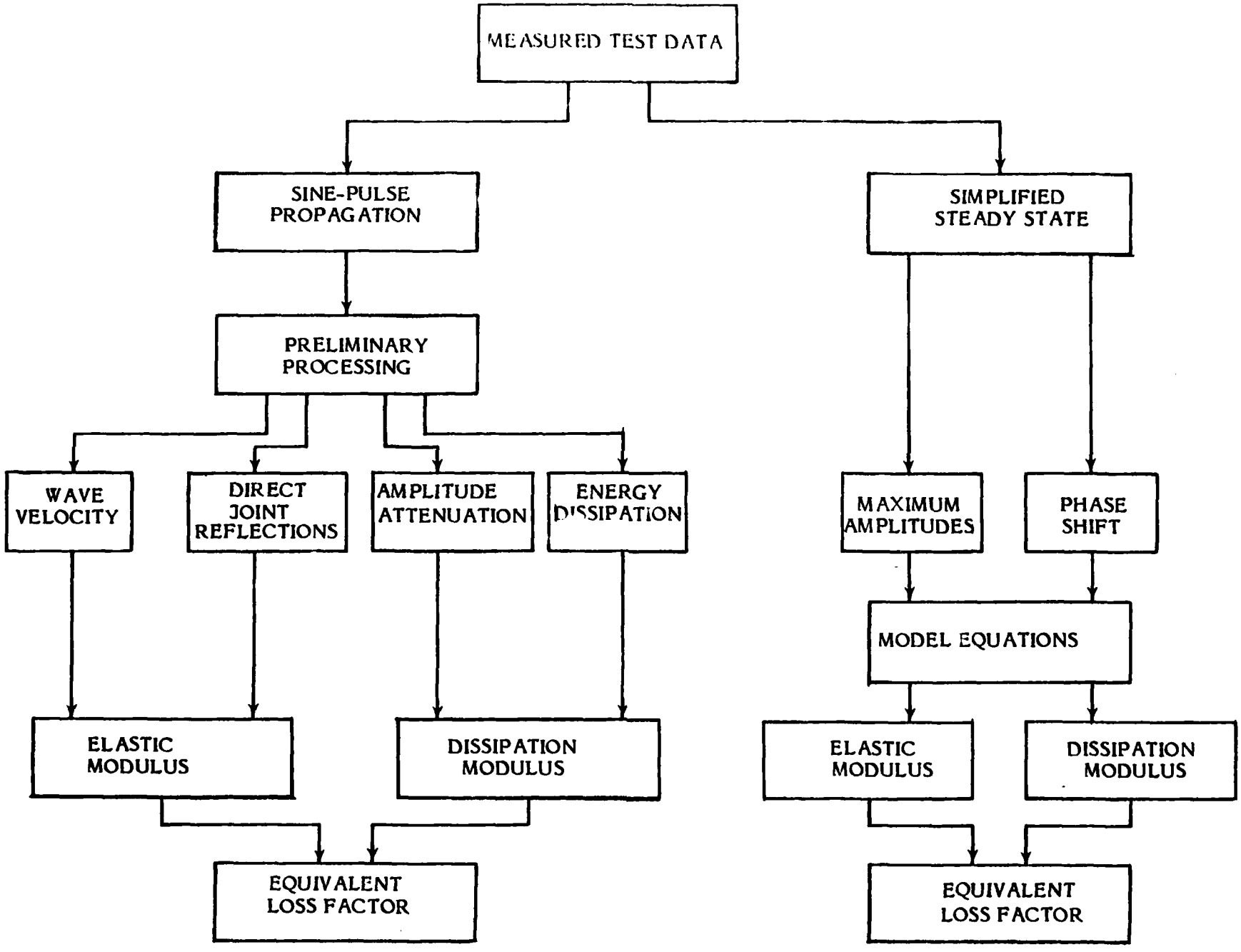

Fig. 10. General Data Analysis Diagram

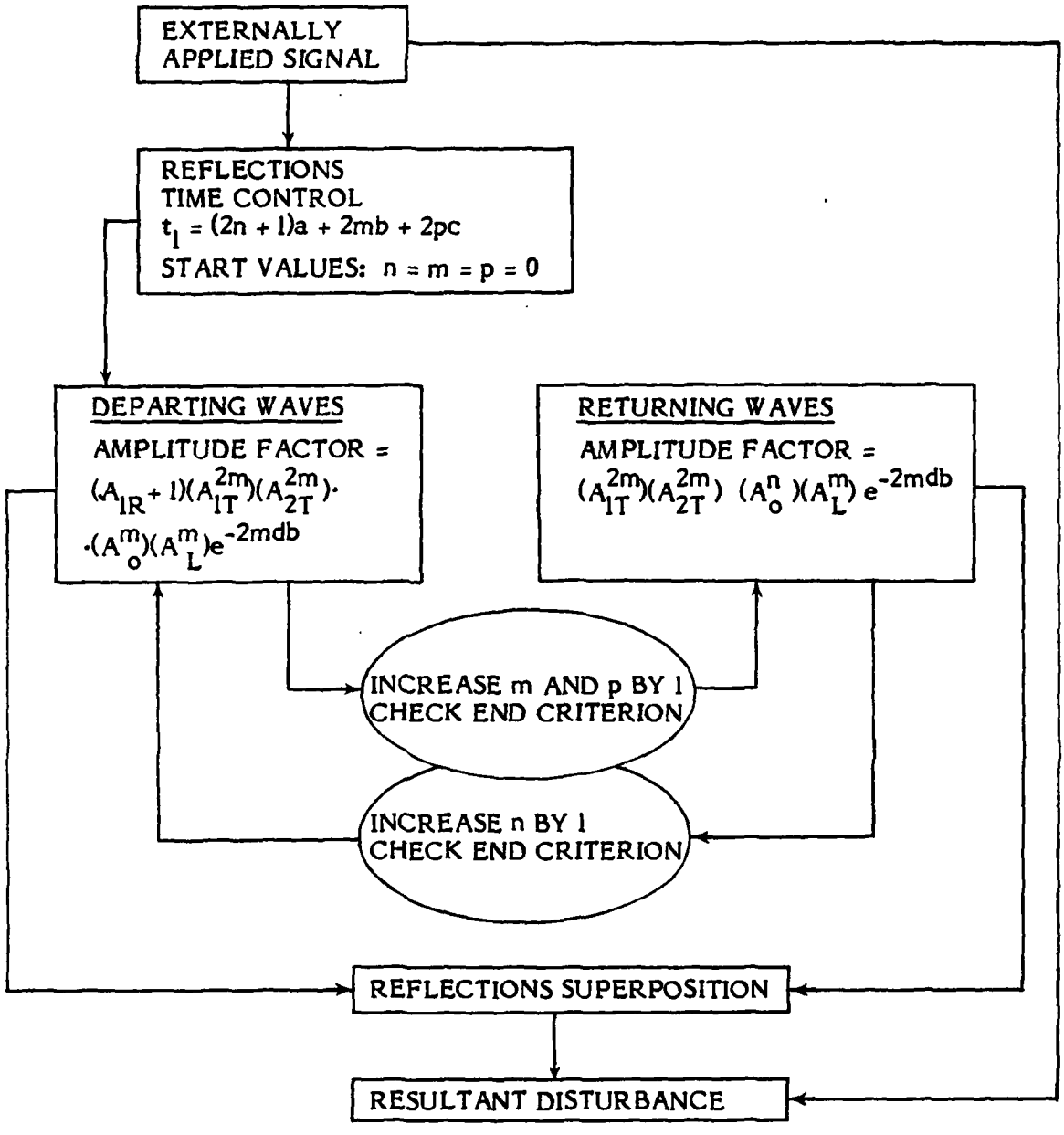

Fig. 11. Simulation Flow Chart for Input Location

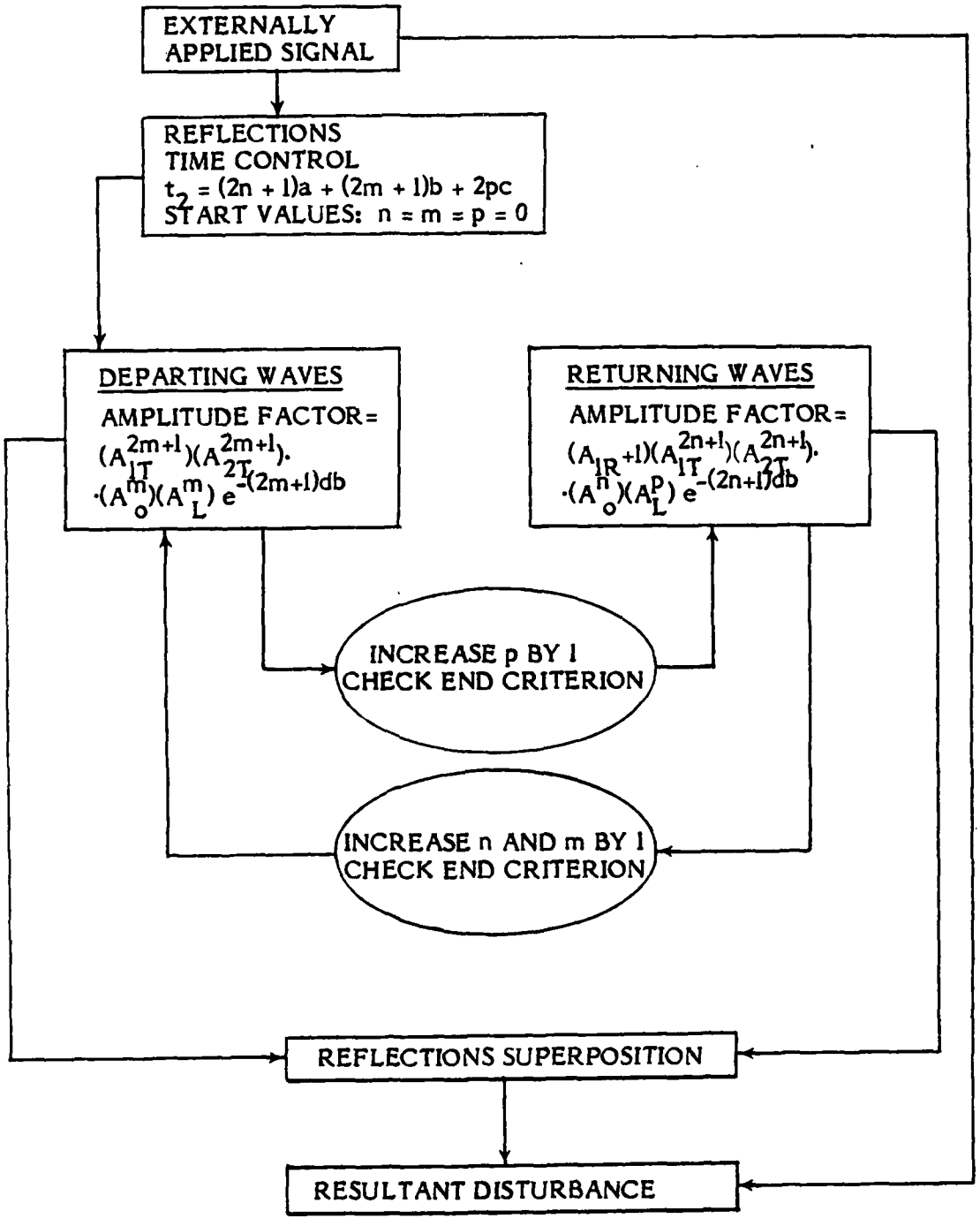

Fig. 12. Simulation Flow Chart for Output Location

REFLECTIONS EFFECT

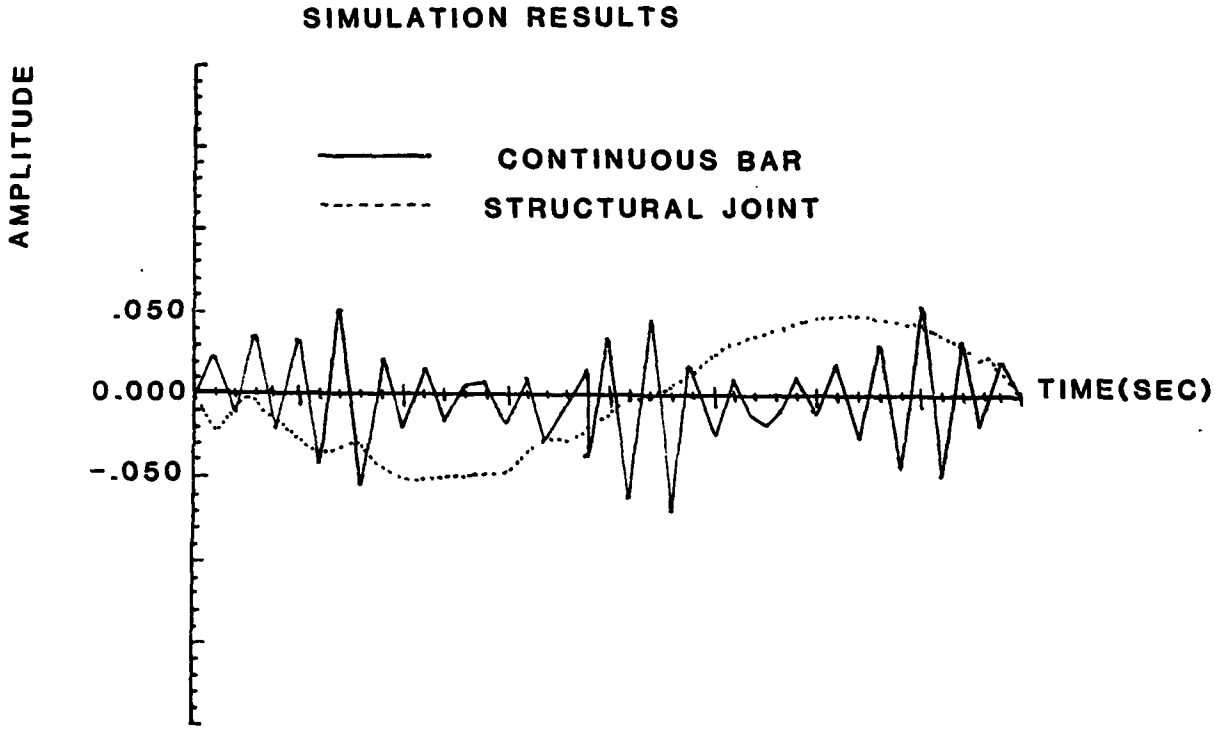

Fig. 13. Difference Signals Between Output and Input Simulation Results

APPENDIX V

A SIMPLIFIED STEADY STATE DAMPING MEASUREMENT TECHNIQUE

A SIMPLIFIED STEADY STATE DAMPING MEASUREMENT TECHNIQUE

The most popular methods for extracting the damping properties from test data rely upon modal analysis techniques [1]. All the collected data is associated with specific modes of vibration and it may be analyzed either in the time domain (transient methods) or the frequency domain (steady state methods). The modal techniques are suitable mainly for system damping characterization where the structural configuration and the real boundary conditions may be known in advance [2]. They provide both stiffness and damping properties, but are confined to linear systems and natural frequencies of vibration.

Non-resonant forced vibration techniques [3-5] seem to be more suitable than the modal methods for the experimental investigation of passively damped joints, since their results can cover a continuous frequency spectrum. The test specimen is subjected to cyclic loading at the desired frequency and the damping is measured by the amount of energy dissipated per cycle. This can be evaluated by different ways, like direct measurement of storage and dissipation moduli, phase angle measurement between excitation and response, or measurement of the area enclosed inside the corresponding hysteresis loop. The last approach is the most common one, but it is restricted to low frequencies [6, 7]. The hysteresis loop approach also has been used for energy dissipation measurements in structural joints [8], since it can be applied to non-linear and non-homogeneous systems. The non-resonant forced vibration methods are more appropriate than the modal techniques to material damping characterization.

A simplified steady state test technique has been developed to determine the complex modulus of viscoelastic materials at arbitrary frequencies and displacement. As discussed previously, the complex modulus of viscoelastic materials is presently determined by existing resonant test techniques or by measurement of the hysteresis loop in a physical test machine providing force and displacement data. However, these conventional resonant and non-resonant forced vibration test methods have some significant limitations which can be overcome by this new measurement approach.

Resonant techniques provide data only at specific frequencies and, therefore, require a new test setup for each new set of frequencies desired. Conventional physical test machines provide data at arbitrary frequencies and amplitudes, but operate well only at very low frequencies. Accurate, independent measurements of both the relative displacement of the specimen ends and the applied force are required in addition to the control functions of the test machine. The test apparatus shown in Figure 1 will determine the complex modulus of the test specimen without an independent relative displacement measurement. Vectors of the applied voltage and the measured force are the only data required, thereby greatly simplifying test setup and conduct. Because the viscoelastic joints being considered for large space structures have high stiffness and, therefore, very low displacement, the lack of a requirement for measuring relative displacement is a very attractive feature of this test method.

The physical arrangement and structural schematic identifying the relevant stiffness characteristics of the test setup are shown in Figure 1. A harmonic voltage applied to the piezoelectric exciter L_1 generates a small harmonic motion at X_1. This motion is transmitted through the test specimen, resulting in measured forces at the piezoelectric load cell L_2. As shown in Figure 2, the complex stiffness of the specimen can be calculated from the harmonic transducer inputs and outputs just described. When the specimen is much more flexible than the test apparatus, the approximate relationships on the left-hand side of Figure 2 apply. When the specimen stiffness approaches that of any other element, the exact relationships on the right-hand side must be used.

The non-resonant steady state technique, which does not require relative displacement measurements, seems to be well suited to the task of characterizing damped joints for large space structures. In the near future this approach will be applied to some representative joint specimens.

Physical Arrangement

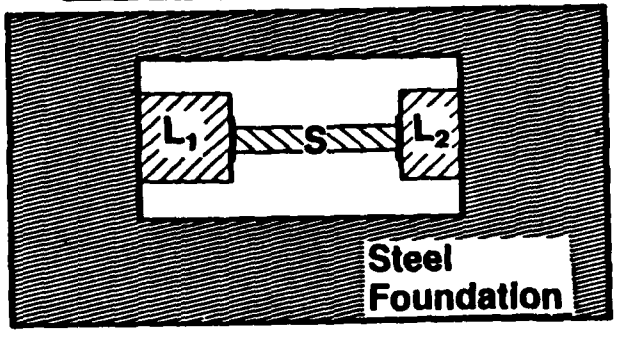

Structural Schematic

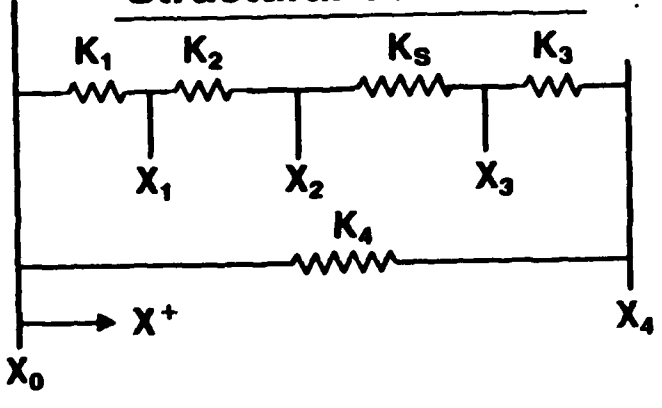

Figure 1. Steady-State Test Apparatus

Structural Parameters

L_1 = Piezoelectric Exciter
- K_1 = Exciter Stiffness
- K_2 = Cell Case Stiffness

L_2 = Piezoelectric Load Cell
- K_3 = Load Cell Stiffness

S = Test Specimen
- K_S = Specimen Stiffness

Steel Foundation
- K_4 = Foundation Stiffness

$\hat{X}_1$ = Unloaded Motion Applied

F_3 = Load Measured

The Method to Determine the Complex Stiffness from Transducer Inputs and Outputs is:

$$\hat{X}_1 = A \cos \omega t \text{ Where } A = (\mu\text{in./V}) \text{ (Volts Applied)}$$

$$F_3 = B \cos (\omega t + \theta) \text{ Where } B = (\text{l b/V}) \text{ (Volts Output)}$$

If $k_s << $ Any k_l, Then

$$k_s \simeq F_3/\hat{X}_1$$

$$re\,(k_s) \simeq \frac{B}{A} \cos \theta$$

$$imag\,(k_s) \simeq \frac{B}{A} \sin \theta$$

$$\eta k_s \simeq \tan \theta$$

If $k_s \Rightarrow$ Any k_l Then the Exact Relations Must Be Used

$$k_s \equiv \left[\frac{\hat{X}_1}{F_3} - \Delta\right]^{-1} \text{ Where } \Delta = \sum_{l=1}^{4} \frac{1}{k_l}$$

$$re\,(k_s) \equiv \frac{\frac{B}{A} \cos \theta - \frac{B^2}{A^2} \Delta}{1 - 2\Delta \frac{B}{A} \cos \theta + \frac{B^2 \Delta^2}{A^2}}$$

$$imag\,(k_s) \equiv \frac{l \frac{B}{A} \sin \theta}{1 - 2\Delta \frac{B}{A} \cos \theta + \frac{B^2 \Delta^2}{A^2}}$$

$$\eta k_s \equiv \frac{imag\,(k_s)}{re\,(k_s)}$$

Figure 2. Steady-State Equations

REFERENCES

1. Ramsey, K. A. Effective Measurements for Structural Dynamics Testing, Part I. Sound and Vibration, November 1975, pp 24-35.

2. Chu, F. H. and B. P. Wang. Experimental Determination of Damping in Materials and Structures. Damping Applications for Vibration Control, P. J. Torvik, ed. ASME Winter Annual Meeting, Chicago, 1980.

3. Read, B. E. and G. D. Dean. The Determination of Dynamic Properties of Polymers and Composites. John Wiley and Sons, New York, 1978.

4. Plunkett, R. Measurement of Damping. Section 5, Structural Damping, J. E. Rizicka, ed. ASME Annual Meeting in Atlantic City, NJ, 1959.

5. Bert, C. W. and R. R. Clary. Evaluation of Experimental Methods for Determining Dynamic Stiffness and Damping of Composite Materials. Composite Materials: Testing and Design (3rd Conference), ASTM STP 546, 1974, pp 250-265.

6. Mentel, T. J. and S. H. Chi. Experimental Study of Dilatational- versus Distortional-Straining Action in Material-Damping Production. The Journal of the Acoustical Society of America, Vol. 36, No. 2, February 1964.

7. Smith, S. and R. C. Yee. A New Technique for the Characterization of Structural Materials under Dynamic Loading. AIAA Paper No. 78-510.

8. Richardson, R. S. H. and H. Nolle. Energy Dissipation in Rotary Structural Joints. Journal of Sound and Vibration, Vol. 54, No. 4, 1977, pp 577-588.